

INVESTIGATION OF PROCESS PARAMETERS ON PROPERTIES OF
EPOXY BASED CATAPHORETIC COATINGS

A THESIS SUBMITTED TO
THE GRADUATE SCHOOL OF NATURAL AND APPLIED SCIENCES
OF
MIDDLE EAST TECHNICAL UNIVERSITY

BY

NALAN GÜLÇİN KAYKAÇ

IN PARTIAL FULFILLMENT OF THE REQUIREMENTS
FOR
THE DEGREE OF DOCTOR OF PHILOSOPHY
IN
POLYMER SCIENCE AND TECHNOLOGY

AUGUST 2022

Approval of the thesis:

**INVESTIGATION OF PROCESS PARAMETERS ON PROPERTIES OF
EPOXY BASED CATAPHORETIC COATINGS**

submitted by **NALAN GÜLÇİN KAYKAÇ** in partial fulfillment of the requirements for the degree of **Doctor of Philosophy in Polymer Science and Technology, Middle East Technical University** by,

Prof. Dr. Halil Kalıpçılar
Dean, Graduate School of **Natural and Applied Sciences** _____

Prof. Dr. Necati Özkan
Head of the Department, **Polymer Science and Technology** _____

Assoc. Prof. Dr. Erhan Bat
Supervisor, **Chemical Engineering, METU** _____

Prof. Dr. Ali Çırpan
Co-Supervisor, **Chemistry, METU** _____

Examining Committee Members:

Prof. Dr. Necati Özkan
Polymer Science and Technology, METU _____

Assoc. Prof. Dr. Erhan Bat
Chemical Engineering, METU _____

Prof. Dr. Göknur Bayram
Chemical Engineering, METU _____

Prof. Dr. Bora Maviş
Mechanical Engineering, Hacettepe University _____

Assist. Prof. Dr. Salih Ertan
Chemical Engineering, Atılım University _____

Date: 12.08.2022

I hereby declare that all information in this document has been obtained and presented in accordance with academic rules and ethical conduct. I also declare that, as required by these rules and conduct, I have fully cited and referenced all material and results that are not original to this work.

Name Last name : Nalan Gülçin Kaykaç

Signature :

ABSTRACT

INVESTIGATION OF PROCESS PARAMETERS ON PROPERTIES OF EPOXY BASED CATAPHORETIC COATINGS

Kaykaç, Nalan Gülçin
Doctor of Philosophy, Polymer Science and Technology
Supervisor : Assoc. Prof. Dr. Erhan Bat
Co-Supervisor: Prof. Dr. Ali Çırpan

August 2022, 146 pages

Cataphoresis is the process of applying high-performance epoxy resins to metal surfaces in order to increase the corrosion resistance of metal materials by using electrochemistry principles. This process is widely used in automotive industry to ensure long time corrosion durability of the vehicles. The cataphoresis process proceeds in two main steps followed by baking. These processes can be roughly summarized as zinc phosphating and electrocoating. A multiple number of degreasing, washing and rinsing steps occur during the mass production between these main steps to ensure best performance of the coating. A typical cataphoresis line has fifteen baths to carry out these two basic operations prior to baking. In order to ensure the quality of the coating, all baths should be prepared and monitored regularly in the light of certain parameters.

Within the scope of this study, in the first chapter, the effect of some operational parameters on surface quality such as roughness and some physical properties such as stone chip resistance, corrosion resistance and adhesion are evaluated.

SEM, FTIR, DSC and TGA are performed to the coatings in order to understand the effectiveness of the parameters and to determine optimum operation parameters.

In the first chapter, it is found that; the increase in parameters such as voltage, application time, application temperature and solvent ratio, which directly affect the film thickness, adversely affect the surface quality and mechanical properties. Pigment and resin ratios directly affect the crater problem and gloss on the surface. Crater formation is seen on the surface at low pigment ratios, while a dullness occurs on the surface at high pigment ratios. It has been observed that parameters that directly affect the viscosity and mobility of the coating solution, such as solid matter, pigment ratio, solvent ratio and bath temperature, directly affect the thickness and mechanical strength of the coating.

In the second chapter of this thesis study, a DOE study is conducted to find optimum physical properties of the coating according to the results based on the preliminary analysis obtained at previous chapter and a regression equation is defined.

In the third chapter of the study, to find optimum operation conditions of the zinc phosphating process prior to electrocoating, another DOE study is investigated for phosphate conversion layer. Zinc phosphate bath temperature and duration of the process are changed to reach optimum conversion layer structure to promote corrosion resistance behavior.

In the fourth chapter, performance tests are applied on the zinc phosphate coatings to validate DOE results. It is obtained that uniform and fine-grained crystal structure with lower coating weight gives the best physical performance after electrocoating. In this study 180 sec immersion time at a temperature of 45 °C is found as optimum condition in terms of crystal morphology, coating weight and performance results such as corrosion, adhesion, stone chip and water immersion resistance.

In the last chapter, a cross comparison of optimum conditions with a reference condition is performed. It is found that optimum condition of phosphate and electrocoating provides a better surface quality together with better physical properties while providing material, energy and cost savings as well.

Keywords: Cataphoresis, Electrocoating, Zinc Phosphating, Roughness, Corrosion Resistance

ÖZ

PROSES PARAMETRELERİNİN EPOKSİ ESASLI KATAFORETİK KAPLAMALARIN ÖZELLİKLERİNE ETKİLERİNİN ARAŞTIRILMASI

Kaykaç, Nalan Gülçin
Doktora, Polimer Bilim ve Teknolojisi
Tez Yöneticisi: Doç Dr. Erhan Bat
Ortak Tez Yöneticisi: Prof. Dr. Ali Çırpan

Ağustos 2022, 146 sayfa

Kataforez, metal malzemelerin korozyon direncini arttırmak için bir takım elektrokimya ilkelerini kullanarak bazı yüksek performanslı epoksi reçinelerin metal yüzeylere uygulanması işlemidir. Bu işlem, araçların uzun süre korozyona dayanıklı olmasını sağlamak için otomotivde yaygın olarak kullanılmaktadır. Kataforez işlemi iki ana adımda ilerler ve bunu pişirme işlemi takip eder. Bu işlemler kabaca Çinko-Fosfatlama ve Elektro-kaplama olarak özetlenebilir. Kaplamanın en iyi performansını sağlamak için bu ana adımlar arasında seri üretim sırasında çok sayıda yağdan arındırma, yıkama ve durulama adımları da gerçekleştirilir. Tipik bir kataforez hattında, pişirme öncesinde bu iki temel işlemi gerçekleştirmek için on beş banyo bulunur. Kaplama kalitesinin sağlanması için tüm banyolar belirli parametreler ışığında düzenli olarak hazırlanmalı ve izlenmelidir.

Bu doktora çalışması kapsamında, pürüzlülük gibi bazı operasyonel parametrelerin yüzey kalitesine etkisi ve taş çarpma direnci, korozyon direnci ve yapışma gibi bazı mekanik özellikler incelenmiştir.

Parametrelerin etkinliğini anlamak ve optimum çalışma parametrelerini belirlemek için kaplamalara SEM, FTIR, DSC ve TGA gibi karakterizasyon yöntemleri uygulanmıştır.

Bu tez çalışmasının ilk bölümünde, film kalınlığını doğrudan etkileyen voltaj, uygulama süresi, uygulama sıcaklığı ve solvent oranı gibi parametrelerin artmasının yüzey kalitesini ve mekanik özelliklerini olumsuz etkilediği, pigment ve reçine oranının yüzeydeki krater problemini ve parlaklığını doğrudan etkilediği görülmüştür. Düşük pigment oranlarında yüzeyde krater oluşumu gözlemlenirken, yüksek pigment oranlarında yüzeyde matlık oluştuğu gözlemlenmiştir. Katı madde, pigment oranı, solvent oranı ve banyo sıcaklığı gibi kaplama çözeltisinin viskozitesini ve hareketliliğini doğrudan etkileyen parametrelerin, kaplamanın kalınlığını ve mekanik mukavemetini doğrudan etkilediği gözlemlenmiştir.

Bu tez çalışmasının ikinci bölümünde, birinci bölümde elde edilen ön analizlere dayalı sonuçlara göre kaplamanın optimum fiziksel özelliklerini bulmak için bir DOE çalışması yapılmıştır.

Çalışmanın üçüncü bölümünde, Elektro-kaplama öncesi Çinko-Fosfatlama işleminin optimum çalışma koşullarını bulmak için, fosfat dönüşüm tabakası için başka bir DOE çalışması incelenmiştir. Çinko Fosfat banyosu sıcaklığı ve işlemin süresi, korozyon direnci davranışını iyileştirerek optimum çalışma koşullarına ulaşmak için değiştirilmiştir.

Çalışmanın dördüncü bölümünde DOE sonuçlarının doğrulanması için çinko fosfatlı yüzeylere bir takım performans testleri yapılmıştır. Elektrokaplama sonrası en iyi fiziksel performansı düşük kaplama ağırlığına sahip düzgün ve ince taneli kristal yapının verdiği tespit edilmiştir. Bu çalışmada kristal morfolojisi, kaplama ağırlığı ve korozyon, yapışma, taş çarpma dayanımı ve suya daldırma direnci gibi

performans sonuçları açısından 45 °C'de 180 sn optimum fosfatlama koşulu olarak bulunmuştur.

Çalışmanın son bölümünde çalışma kapsamında bulunan optimum koşullar referans bir koşul ile çapraz olarak karşılaştırılmıştır. Fosfat ve elektrokaplamanın optimum koşulunun, daha iyi fiziksel özelliklerle birlikte daha iyi bir yüzey kalitesi sağladığı ve aynı zamanda malzeme, enerji ve maliyet tasarrufu sağladığı bulunmuştur.

Anahtar Kelimeler: Kataforez, Elektrokot, Çinko-Fosfatlama, Pürüzlülük, Korozyon Direnci

To my missed father

ACKNOWLEDGMENTS

I would like to express my deepest gratitude to my supervisor Assoc. Prof. Dr. Erhan Bat, who accepted me as a doctoral student at a time when I was extremely hopeless about the future of my doctoral studies. Throughout my entire study, he has made a very valuable contribution to my thesis by being an endless guide and supporter. I am also grateful to my thesis monitoring committee members Prof. Dr. Gökür Bayram and Prof. Dr. Bora Maviş for their invaluable guidance and support.

I would like to thank my esteemed company Ford Otosan, who gave me the opportunity to use all kinds of test materials and laboratory facilities throughout my doctoral study. I also want to thank my laboratory team especially to İlker Kar who never made me feel my absence throughout the process and helped me with my thesis studies. I would like to express my special thanks to Murat Çakır, Sadi Özel, Ergün Başdemir and Ali Kiremitçi the valuable representatives of PPG, BASF-Chemetall and Akafor companies who did not spare their valuable technical knowledge and guidance with the test materials and infrastructure support I benefited from throughout my studies.

Special thanks to; My husband Ahmet Ali Baydağ to be there whenever I needed. My beloved family who always believed in me; my dear father Remzi Kaykaç who didn't have the chance to see these days, my dear mother Nimet Kaykaç, my dear siblings Nazan İlçin, Zeynep Burçin and Meltem Aylin Kaykaç, my dear uncles Hikmet and İsmail Sığlam, my deceased grandfather Cemil Sığlam and my grandmother Cemenur Sığlam who never stops praying for my good sake. To my colleagues Ferda Yıldırım and Muharrem Altıoğlu, who always supported and encouraged me whenever I fell into despair throughout my work. To my lab mate Öznur Kavak who didn't spare her support even a moment.

TABLE OF CONTENTS

ABSTRACT.....	v
ÖZ	viii
ACKNOWLEDGMENTS	xii
TABLE OF CONTENTS.....	xiii
LIST OF TABLES.....	xvi
LIST OF FIGURES	xviii
LIST OF ABBREVIATIONS.....	xxiii
LIST OF SYMBOLS	xxv
CHAPTERS	
1 INTRODUCTION	1
1.1 Motivation and Scope of the Study.....	2
2 BACKGROUND INFORMATION AND LITERATURE REVIEW	5
2.1 Cathodic Electrodeposition	6
2.1.1 Cataphoresis Process.....	7
2.2 Literature Survey.....	20
2.2.1 Literature Review on Electrocoating Process	20
2.2.2 Literature Review on Phosphating Process.....	24
3 EXPERIMENTAL WORK.....	29
3.1 Experimental Procedures Used in Electrocoating.....	29
3.1.1 Materials Used	29
3.1.2 Electrocoating of the Panels.....	29
3.1.3 Structural and Morphological Characterization.....	32

3.1.4	Performance Analysis.....	33
3.1.5	Thermal Analysis.....	34
3.1.6	Surface Characterization	35
3.2	Statistical Methods Used in Parameter Sifting	35
3.2.1	Correlation analysis	35
3.2.2	Regression Analysis	36
3.3	Design of Experiment (DOE)	37
3.4	Experimental Procedures Used in Phosphating	37
3.4.1	Materials Used.....	37
3.4.2	Phosphating of the Panels.....	37
3.4.3	Structural and Morphological Analysis.....	38
4	RESULTS AND DISCUSSION.....	41
4.1	Preliminary Assessment of Operational Parameters on Electrocoating Process.....	41
4.1.1	Effect of Deposition Voltage.....	45
4.1.2	Effect of Induction Time	51
4.1.3	Effect of Bath Temperature	58
4.1.4	Effect of Pigment over Binder Ratio	66
4.1.5	Effect of Solid Content Ratio	73
4.1.6	Effect of Organic Solvent Content Ratio.....	78
4.1.7	Effect of Baking Temperature	84
4.1.8	Overall Evaluation of Preliminary Assessment.....	90
4.2	Determination of Optimum Electrocoating Parameters by Using DOE...	93
4.3	Determination of Optimum Phosphating Parameters by Using DOE	103

4.4	Physical Performance Tests for Phosphating	108
4.4.1	Morphological Analysis.....	112
4.4.2	Dimensional Analysis of Zinc Phosphate Crystals.....	121
4.5	Cross Comparison of Optimized Phosphating and Electrocoating Conditions with Reference Conditions	125
5	CONCLUSIONS.....	129
	REFERENCES	131
	APPENDICES	136
A.	Summary of Physical and Mechanical Properties of Preliminary Assessments	136
B.	Summary of Thermal Properties of Preliminary Assessments.....	138
C.	Minitab™ 17 Software Outputs for DOE Studies.....	140
D.	Ford Laboratory Material Specifications and Test Methods.....	143
	CURRICULUM VITAE.....	145

LIST OF TABLES

TABLES

Table 1.1 Electrocoating parameters vs performance tests.	3
Table 1.2 Phosphating parameters vs performance tests.....	4
Table 1.3 Cross comparison tests for optimum conditions.	4
Table 2.1 Analysis of a typical phosphate coating [7].	12
Table 2.2 Worldwide specifications on zinc phosphate conversion layer [7].	13
Table 4.1 Preliminary test conditions of electrocoating parameters.	42
Table 4.2 Process parameters to understand the effect of deposition voltage.....	45
Table 4.3 Process parameters to understand the effect of induction time.	51
Table 4.4 Process parameters to understand the effect of bath temperature.	58
Table 4.5 Process parameters to understand the effect of pigment over binder ratio.	67
Table 4.6 Process parameters to understand the effect of solid content ratio.	73
Table 4.7 Process parameters to understand the effect of organic solvent content ratio.....	78
Table 4.8 Process parameters to understand the effect of baking temperature.	84
Table 4.9 Statistical analysis results of ED parameters vs roughness and stone chip resistance.	95
Table 4.10 Parameter limits for DOE study.	97
Table 4.11 The 2 level full factorial experiment design with 4 factors and 3 repeating.	98
Table 4.12 Response variables of the DOE study.	100
Table 4.13 Optimum parameters according to the DOE response optimizer.....	102
Table 4.14 Measurement results at optimum parameters.....	102
Table 4.15 DOE limits for phosphating parameter optimization.	104
Table 4.16 Measurement results for phosphating DOE study.....	106
Table 4.17 Coating weights at all conditions.	107

Table 4.18 Measurement results for performance tests at all conditions.....	109
Table 4.19 Phosphating process parameters of all conditions including “Reference”.....	112
Table 4.20 Crystal size dimensional distribution results for all conditions.....	123
Table 4.21 Optimum and reference parameters for phosphating and electrocoating steps for the pilot test setup.....	125
Table 4.22 Cross comparison of performance results.....	126
Table A.1 Physical and mechanical properties at different deposition voltages. .	136
Table A.2 Physical and mechanical properties at different induction times.....	136
Table A.3 Physical and mechanical properties at different bath temperatures.....	136
Table A.4 Physical and mechanical properties at different pigment/binder ratios.	137
Table A.5 Physical and mechanical properties at different solid content ratios...	137
Table A.6 Physical and mechanical properties at different organic solvent ratios.	137
Table A.7 Physical and mechanical properties at different baking temperatures.	137
Table A.8 Glass transition temperature and residue percentage obtained by DSC and TGA at different deposition voltages.....	138
Table A.9 Glass transition temperature and residue percentage obtained by DSC and TGA at different induction times.	138
Table A.10 Glass transition temperature and residue percentage obtained by DSC and TGA at different bath temperatures.	138
Table A.11 Glass transition temperature and residue percentage obtained by DSC and TGA at different pigment/binder ratios.....	138
Table A.12 Glass transition temperature and residue percentage obtained by DSC and TGA at different solid content ratios.	139
Table A.13 Glass transition temperature and residue percentage obtained by DSC and TGA at different organic solvent ratios.	139
Table A.14 Glass transition temperature and residue percentage obtained by DSC and TGA at different baking temperatures.	139

LIST OF FIGURES

FIGURES

Figure 2.1 Principles of anodic and cathodic electrodeposition [2].	6
Figure 2.2 Major steps in electrocoating process [6].	8
Figure 2.3 2.0 kx SEM Images of Phosphophyllite (Sample A) and Hopeite (Sample B) Crystals [37].	27
Figure 2.4 SEM Images of Hopeite (Sample 1A Spray and 1B Immersion), Phosphophyllite apart from Hopeite (Sample 2A Spray and 2B Immersion), Predominant Phosphophyllite (Sample 3A Spray and 3B Immersion) Crystals [38].	28
Figure 3.1 Test Setup; a) Reaction Bath; Anode and Cathode b) Rectifier 0-400V c) Oven 250 °C	30
Figure 3.2 Schematic illustration of paint micel movement in the dispersion.	31
Figure 3.3 Schematic illustration of electrodeposition process.	32
Figure 3.4 Schematic illustration of “r” correlation coefficient.	36
Figure 3.5 Phosphating Test Setup.	38
Figure 4.1 FTIR Spectra for Resin and Pigment Paste.	43
Figure 4.2 SEM images of phosphated steel panels at different magnifications. a) 2.50 kx b) 5.00 kx c) 10.0 kx.	44
Figure 4.3 Surface measurements according to voltage levels. (a) Film Thickness (b) Gloss (c) Roughness	46
Figure 4.4 Mechanical properties according to voltage levels. (a) Hardness (b) Impact Resistance (c) Stone Chip Resistance	47
Figure 4.5 SEM images (5.00 kx) of coated panels at different deposition voltages. (a) 200V (b) 300V (c) 400V	48
Figure 4.6 Glass Transition Temperature vs Deposition Voltage, Obtained by DSC Analysis.	49
Figure 4.7 Residual weight vs deposition voltage, obtained by TGA analysis.	50

Figure 4.8 Surface Properties according to induction times. (a) Film Thickness (b) Gloss (c) Roughness	53
Figure 4.9 Mechanical Properties according to induction times. (a) Hardness (b) Impact Resistance (c) Stone Chip Resistance	54
Figure 4.10 SEM images (10.0 kx) of coated panels at different induction times. (a) 100 sec (b) 135 sec (c) 170 sec (d) 200 sec	56
Figure 4.11 Glass transition temperature vs induction time, obtained by DSC analysis.....	57
Figure 4.12 Residual weight vs induction time, obtained by TGA analysis.....	58
Figure 4.13 Surface Properties according to bath temperatures. (a) Film Thickness (b) Gloss (c) Roughness.....	60
Figure 4.14 Mechanical Properties according to bath temperatures. (a) Hardness (b) Impact Resistance (c) Stone Chip Resistance	62
Figure 4.15 SEM images (10.0 k.x) of coated panels at different bath temperatures. a) 17.5 °C b) 25 °C c) 30 °C d) 35 °C e) 40 °C.....	64
Figure 4.16 Macroscopic images of a) insufficient coating at low bath temperature 17.5 °C and b) pinholes at high bath temperature 40 °C.....	64
Figure 4.17 Glass transition temperature vs bath temperatures, obtained by DSC analysis.....	65
Figure 4.18 Residual weight vs bath temperature, obtained by TGA analysis.....	66
Figure 4.19 Surface Properties according to Pigment/Binder Ratio. (a) Film Thickness (b) Gloss (c) Roughness.....	68
Figure 4.20 Mechanical properties according to pigment/binder ratio. (a) Hardness (b) Impact Resistance (c) Stone Chip Resistance	69
Figure 4.21 SEM images (10.0 kx) of coated panels at different pigment over binder ratios. a) 0.05 b) 0.15 c) 0.25	70
Figure 4.22 Macroscopic image of craters and pinholes that are seen at low p/b ratio (0.05). a) Craters b) Pinholes.....	71
Figure 4.23 Glass transition temperature vs pigment/binder ratios, obtained by DSC analysis.....	72

Figure 4.24 Residual weight vs pigment/binder ratios, obtained by TGA analysis.	72
Figure 4.25 Surface Properties according to solid content ratio. (a) Film Thickness (b) Gloss (c) Roughness	74
Figure 4.26 Mechanical properties according to solid content ratio. (a) Hardness (b) Impact Resistance (c) Stone Chip Resistance	75
Figure 4.27 SEM images (2.5 kx) of coated panels at different solid content ratios. a) 15% b) 21% c) 27%.....	76
Figure 4.28 Glass transition temperature vs solid content ratios, obtained by DSC analysis.	77
Figure 4.29 Residual weight vs solid content ratios, obtained by TGA analysis....	78
Figure 4.30 Surface Properties according to Organic Solvent Ratio. (a) Film Thickness (b) Gloss (c) Roughness	80
Figure 4.31 Mechanical properties according to organic solvent ratio. (a) Hardness (b) Impact Resistance (c) Stone Chip Resistance.....	81
Figure 4.32 SEM images (2.5 kx) of coated panels at different organic solvent ratios. a) 2.47% b) 4.85% c) 7.11%.....	82
Figure 4.33 Glass transition temperature vs organic solvent ratios, obtained by DSC analysis.	83
Figure 4.34 Residual weight vs organic solvent ratios, obtained by TGA analysis.	83
Figure 4.35 Surface Properties according to baking temperatures. (a) Film Thickness (b) Gloss (c) Roughness	85
Figure 4.36 Mechanical properties according to baking temperatures. (a) Hardness (b) Impact Resistance (c) Stone Chip Resistance.....	86
Figure 4.37 SEM images (10.0 kx) of coated panels at different baking temperatures. a) 135 °C b) 175 °C c) 195 °C	87
Figure 4.38 SEM images of 135 °C baking condition at different magnifications. a) 500x b) 2.50 kx c) 5.00 kx d) 10.00 kx	88
Figure 4.39 Glass transition temperature vs baking temperatures, obtained by DSC analysis.	89

Figure 4.40 Residual weight vs baking temperatures, obtained by TGA analysis.	90
Figure 4.41 Correlation Analysis of Stone Chip Resistance vs Film Thickness. ...	96
Figure 4.42 Regression equation for roughness.....	102
Figure 4.43 Minitab predictions versus measurements for roughness value.	103
Figure 4.44 Salt spray test results at all conditions.....	110
Figure 4.45 Stone chip test results at all conditions.....	111
Figure 4.46 10.0 kx SEM images of all conditions of pretreatments.	113
Figure 4.47 Average coating weight per unit surface area for all test conditions.	114
Figure 4.48 SEM images of phosphated steel panels at A, B, C and Reference conditions with different magnifications. a) 2.50 kx b) 5.00 kx c)10.0 kx.....	117
Figure 4.49 SEM images of phosphated steel panels at C, D and Reference conditions with different magnifications. a) 2.50 kx b) 5.00 kx c)10.0 kx.....	119
Figure 4.50 SEM images of phosphated steel panels at E, F, G, H and I Conditions with different magnifications. a) 2.50 kx b) 5.00 kx c)10.0 kx	120
Figure 4.51 Crystal length Box and Whisker plot diagrams of all test conditions.	121
Figure 4.52 Crystal thickness Box and Whisker plot diagrams of all test conditions.	122
Figure 4.53 Crystal length/thickness for all test conditions.....	124
Figure 4.54 Salt spray test results. I) P-OPT and E-OPT II) P-OPT and E-S III) P-S and E-OPT IV) P-S and E-S	128
Figure A.1 Response Optimizer Interface of Minitab™ 17.	140
Figure A.2 Model Summary.	140
Figure A.3 Response optimizer output of Minitab™ 17 software.....	141
Figure A.4 Model summary and regression equation of coating weight versus temperature and time.....	142
Figure A.5 Measurement vs Minitab Prediction for Coating Weight.....	142
Figure A.6 Response Optimizer Output for Coating Weight versus Temperature and Time.	143

Figure A.7 Ford Motor Company material specification and test methods for
electrocoat material. 143

LIST OF ABBREVIATIONS

ABBREVIATIONS

AC	Alternating Current
ATR	Attenuated Total Reflectance
CED	Cataphoretic Electrodeposition
DC	Direct Current
DI	Deionized
DMTA	Dynamic Mechanical Thermal Analysis
DOE	Design of Experiment
DSC	Differential Scanning Calorimetry
DTA	Differential Thermal Analysis
ED	Electrodeposition
EDXS	Energy-Dispersive X-ray Spectroscopy
EEWs	Epoxy Equivalent Weights
EIS	Electro Impedance Spectroscopy
E-OPT	Optimum Electrocoating Bath Parameters Obtained in the Studies
E-S	Reference Electrocoating Bath Parameters
FE-SEM	Field Emission Scanning Electron Microscopy
FLTM	FORD Laboratory Test Method
FTIR	Fourier Transform Infrared
PCC	Phosphate Chemical Conversion

P-OPT	Optimum Phosphating Bath Parameters Obtained in the Studies
P-S	Reference Phosphating Bath Parameters
RMS	Root Mean Square
SEM	Scanning Electron Microscopy
TGA	Thermo-Gravimetric Analysis
ToF-Sims	Time-of-Flight Secondary Ion Mass Spectrometry
VIF	Variance Inflation Factor

LIST OF SYMBOLS

SYMBOLS

r	Pearson's Correlation Coefficient
$R-Sq$	Amount of Variation
ρ	Correlation Coefficient
T_g	Glass Transition Temperature

CHAPTER 1

INTRODUCTION

To form a protective layer against corrosion on metal surfaces that have complex shapes, the most effective way is electrodeposition. Electrodeposition (also called E-coat, electrocoat, or electrophoretic coating) is a widely used coating technology that has provided superior levels of performance on a vast array of industrial metal objects for over 60 years. By automotive manufacturers, cathodic electrodeposition has been widely used since the 1960s and the electrocoat technology has evolved dramatically since then. Today, over 98% of all car bodies produced globally utilize an electrocoat primer. New fields of application for electrocoat continue to be found continually. With the electrodeposition method, it is possible to provide a uniform and smooth corrosion protection coating regardless of the shape and complexity of metal surfaces [1, 2].

Stone impact damage to painted automotive exteriors is one of the significant concerns for both to the automobile manufacturer and the paint supplier. Damage occurs by stones that are either launched by rear tires of heavy-duty trucks or stones dropped from moving gravel trucks. Stone impact can result in removal of one or more paint layers and in some cases can lead to delamination at the metal–polymer boundary. Removal of paint layers referred to as chipping is a cosmetic issue while delamination at the metal–polymer interface can lead to corrosion [3]. Most of the scientific studies covers anti-corrosion behavior of the electrocoatings. There are much less studies concerning stone chip resistance of the electrocoatings that is also very important as well as anti-corrosive behavior in the automotive sector.

Surface quality of the electrocoating is also crucial, since the electrocoat layer is the first layer of the automotive paint, all surface problems that occur in this layer are also visible in the following paint layers. Therefore any surface quality problems need to be repaired. This leads to increased inefficiencies in production and possible customer complaints. Not only the stone chip resistance, but also surface quality problems of the electrocoats including roughness, dirt, crater and pinhole have a limited amount of studies in the literature.

Therefore this study covers the effects of certain operational parameters on coating materials' surface quality (roughness, dust, dirt, crater, pinholes etc) together with physical and mechanical properties (stone chip resistance, adhesion, hardness, thickness etc).

1.1 Scope of the Study

In the first chapter of the study some preliminary tests were conducted to understand which parameters are mostly affecting the overall quality of the coatings. The main purpose of this study was to investigate influences of seven parameters on the physical, thermal and surface quality properties of the epoxy based cataphoretic coatings and to investigate statistically if there is a correlation between those parameters and surface roughness or not. The parameters examined for this are; voltage, bath temperature, coating time, curing temperature, pigment/binder ratio, organic solvent ratio and solids ratio. Characterization methods and statistical correlation analysis are used to sift some of the parameters. Operational parameters that are investigated and the examined properties due to those parameters are listed below in Table 1.1.

Table 1.1 Electrocoating parameters vs performance tests.

<i>Changed Parameters</i>	<i>Performance Tests</i>	<i>Characterizations</i>
Voltages	Stone Chip Resistance	TGA
Baking Temperatures	Adhesion (Crosscut)	DSC
Induction Time	Hardness	SEM
Induction Temperature	Thickness	FTIR
P/B Ratio	Surface Quality	
Organic Solvent Ratio	Surface Roughness	
Solid Content	Gloss	
	Impact Resistance	

According to the results of preliminary studies in the second chapter of the study, statistical methods are used to sift some of the parameters. A DOE approach is used to investigate the best possible parameters to provide both surface quality and mechanical properties such as stone chip resistance. After the DOE study, the optimum electrocoating condition is determined by statistical methods provided by Minitab™ 17 program. This condition is also confirmed with physical testing and measurements. Since phosphating is the most critical step of pretreatment which is applied prior to electrocoating process, in the third chapter of the study, optimum operation parameters of the phosphating bath in terms of temperature and time are determined to achieve better corrosion resistance of the coating. Another DOE design is created for the pretreatment bath to determine optimum conditions for the physical and mechanical properties of the final product by arranging coating weight and crystal size. Operational parameters that are investigated and the examined properties due to those parameters are listed below in Table 1.2.

Table 1.2 Phosphating parameters vs performance tests.

<i>Changed Parameters</i>	<i>Performance Tests</i>	<i>Characterizations</i>
Time	Stone Chip Resistance	SEM
Temperature	Adhesion (Crosscut)	
	Salt Spray Resistance	
	Water Immersion	

As the last part of the study, to understand the effect of optimum conditions obtained for both electrocoating and phosphating process, cross comparison tests are conducted between optimum and reference conditions. Cross comparison tests for optimum conditions are given in Table 1.3.

Table 1.3 Cross comparison tests for optimum conditions.

<i>Changed Parameters</i>	<i>Performance Tests</i>	<i>Surface Quality</i>
Phosphating	Stone Chip Resistance	Roughness
Electrocoating	Adhesion (Crosscut)	Film Thickness
	Salt Spray Resistance	Gloss
	Water Immersion	
	Impact Resistance	
	Hardness	

CHAPTER 2

BACKGROUND INFORMATION AND LITERATURE REVIEW

Electrodeposition can be applied either anodic or cathodic indicative of where coating deposition takes place (see Figure 2.1). In the late 1950s and early 1960s, anodic electrocoats were developed. The cathodic system was developed and commercialized later in the appliance industry in the late 60s and early 70s. A negative-charged paint moiety is deposited on a positively-charged metal substrate during anodic electrocoating. These polymer species are acid functional and amine solubilized. Anodic electrocoats provide excellent color and gloss control at an economical cost. Metal ions are dissolved from the parts being coated during anodic deposition. As a result of their ability to interact with moisture, these ions become trapped in the deposition paint film and reduce corrosion performance. As a result of the presence of iron in the anodic films, other undesirable effects can occur, such as staining and discoloration. The cathodic deposition process, in which positively charged paint moieties are attracted to negatively charged parts, incorporates much less iron into the deposition film, thereby improving corrosion resistance significantly. Furthermore, the polymer species are amine functional and acid-soluble, with the alkaline nature of the polymer leading to better corrosion resistance than can be obtained with acid-functional polymers. Cathodic electrocoat systems are generally specified when high coating performance is needed [2].

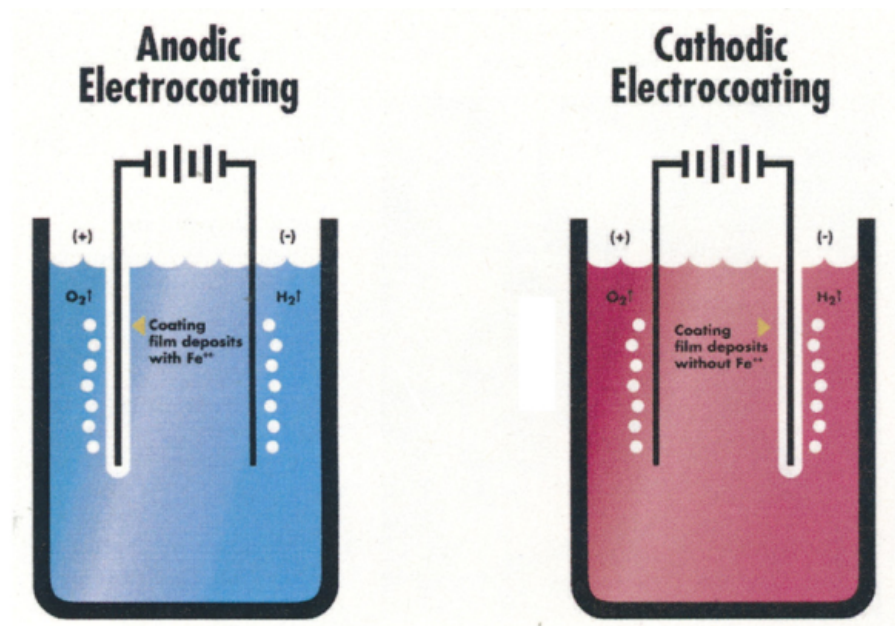


Figure 2.1 Principles of anodic and cathodic electrodeposition [2].

2.1 Cathodic Electrodeposition

Cathodic electrodeposition is an application process whereby the coating of metal substrates is achieved through the application of an electric flux. If the resin moieties are charged positively in the dispersion that makes the electrodeposition process cathodic. Electrolysis of the water is the primary electrochemical reaction that occurs in cathodic electrodeposition systems. The first electrochemical reaction is the reduction of water on the cathode, that increases the local pH near the cathode. The local increase in pH results in deprotonation of the amine groups on the epoxy resin chemically. The deprotonated micelles are no longer stable in solution and deposit on the cathode [1].

It is not the only advantage of this application method to offer superior corrosion performances, but also to offer processes and materials that are environmentally friendly and economically efficient. Today almost every car has this layer on its body

in order to provide a good corrosion protection. Cathodic electrodeposition increases throwing power, uniformity of coats, thickness, and reduces contamination. The electrocoat process has several major advantages, including: complete coverage of complex parts with unsurpassed film uniformity; material transfer efficiency that routinely exceeds 99%; highly automated, closed-loop systems with excellent productivity and low operating costs; fast line speeds and high part racking density; very low air and wastewater emissions that foster environmental compliance; and a totally enclosed system that leaves the paint application area cleaner and safer. In recent decades, this technique has been utilized for applying anticorrosion primers [2, 4, 5].

2.1.1 Cataphoresis Process

A number of electrochemistry principles are used to increase the corrosion resistance of metal materials through cataphoresis, which involves applying epoxy resins to metal surfaces to increase corrosion resistance. To ensure long-term corrosion resistance, this process is widely used in the automotive industry. The cataphoresis process proceeds in two main steps followed by baking. These processes can be roughly summarized as Zinc Phosphating and Electrocoating. A multiple number of degreasing, washing and rinsing steps are also occur during the mass production between these main steps to ensure best performance of the coating. A typical cataphoresis line has fifteen baths to carry out these two basic operations prior to baking. In order to ensure the quality of the coating, all baths should be prepared and monitored regularly in the light of certain parameters.

Main steps of the process can be summarized as degreasing and cleaning prior to phosphating, phosphating as a pretreatment, rinsing prior to electrocoating, electrocoating as the main step, post rinsing of electrocoating and baking as a last step (see Figure 2.2).

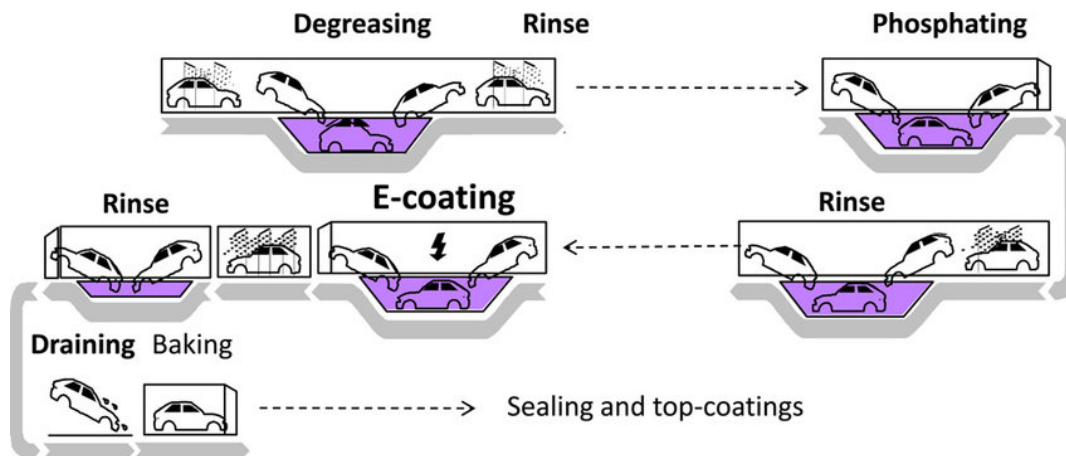


Figure 2.2 Major steps in electrocoating process [6].

2.1.1.1 Steps of Phosphating Process (Pretreatment)

In the pretreatment process of electrocoating, phosphating is the most critical step. To ensure the best corrosion protection, phosphating is mandatory to increase the adhesion of the electrocoating to the steel surface. Physical and mechanical properties of the final product are also affected by the quality of the phosphating process. Phosphating is an established process and used by all automotive manufacturers around the world. The body of an automobile contains various substrates such as cold rolled steel, electrogalvanized steel, and hot dip galvanized steel made of various alloys. Trication zinc phosphate is the world standard pretreatment process for multi-metal car bodies. This process consists of several steps: degreasing, rinsing, activation, phosphating, rinsing, passivation (optional), and final rinsing with degreasing water. The standard body pretreatment process includes four steps to optimally prepare the metal surface without the rinsing step, which are degreasing, activation, phosphating and passivation (optional) respectively [7].

2.1.1.1.1 Degreasing

Solvent degreasing is important for removing all types of contaminants from metal surfaces and creating water-break free surfaces. That is, after the excess degreasing chemicals have been washed away with water, there is a continuous film of water on the surface [8].

In automotive pretreatment processes, degreasers are usually composed of two components: inorganic salts and organic surfactants. Inorganic salts have the role of removing inorganic impurities such as metal particles and weld beads. Organic surfactants are responsible for removing organic contaminants such as oils, lubricants, soaps and other organic contaminants. Solvent degreasing liquid is applied for both spray and dip applications. Conveniently, spray application is followed by dip application. The degreasing tank should be emptied regularly or continuously passed through a filtration system to remove both oil and other contaminants from the solution [7].

2.1.1.1.2 Activation

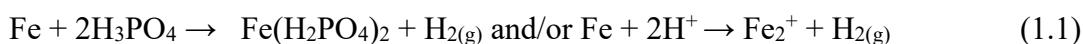
Activation is important to increase the number of nuclei and provide the highest crystallinity on the metal surface [7, 9]. This is necessary to increase the number of phosphate crystals per unit surface area, resulting in a reduction in the coating weight of the conversion layer applied. Aqueous dispersions of titanium ortho phosphates with a pH between 7 and 11 are typically used for activation. The activation bath is discharged at regular intervals, depending on the activator product, how dirty the bath is, and crystal size and coating weight requirements. These time intervals may range from about 1 week to about 6 months [7].

2.1.1.1.3 Phosphating

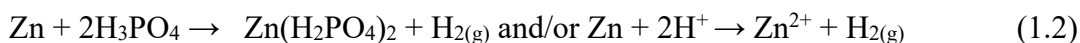
Phosphate pretreatment (iron and zinc) is used to ensure adhesion between the electrocoat and the substrate to improve corrosion protection. Main components of a phosphating bath are phosphoric acid (H_3PO_4), zinc phosphate ($\text{Zn}(\text{H}_2\text{PO}_4)_2$), accelerators (Sodium Nitrite, Sodium Nitrate, Sodium Chlorite, Peroxide etc) and Ni and Mn modifiers.

The first step in any conversion process is a pickling attack on the metal surface with free phosphoric acid. Metal losses in cold-rolled steel sheets, galvanized steel sheets, and aluminum usually fall in the ranges from 0.5 to 2 g/m² [7].

Pickling reaction for steel substrates;



Pickling reaction for zinc-coated substrates;



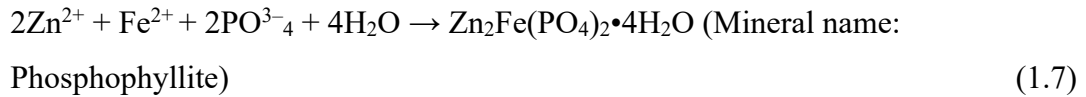
Hydrogen ion consumption leads to a pH shift in the diffusion layer adjacent to the metal surface, exceeding the solubility limits, leading to the formation of PO_4^{3-} and consequent precipitation of zinc (and other metal cations) phosphate [7].

Formation of PO_4^{3-} to provide protolytic equilibria;

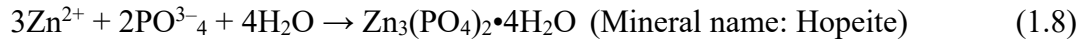


Coating reaction for steel substrates;



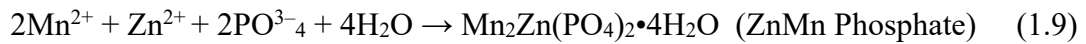


Coating reaction for zinc-coated substrates;

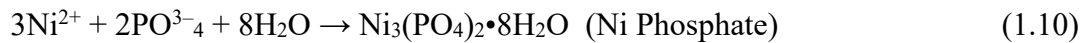


The main crystalline phases produced by low zinc phosphate are Hopeite and Phosphophyllite. Phosphate crystals are electrical insulators, but they contain pores that occupy about 1% of the surface area. This is a very important requirement for electrocoating deposition.

If Mn is used as modifier than additional coating formulation is seen in the crystal structure is as following;



If Ni is also added as a modifier in the trication environment a small amount of $\text{Ni}_3(\text{PO}_4)_2 \cdot 8\text{H}_2\text{O}$ also occurs on the coating formulation.



Typical coating formulation analysis is given in Table 2.1.

Table 2.1 Analysis of a typical phosphate coating [7]

Type of Phosphating Process	Substrate	Zn(%)	Mn(%)	Ni(%)	Fe(%)	P ₂ O ₅ (%)
Low-Zinc	On Steel	32	<0.2	1	6.5	35
Low-Zinc	On Steel	30	4.2	0.8	5.8	35
Manganese Modified						
Low-Zinc	On Zinc Galvanized Steel	48	<0.2	1.4	<0.2	35
Low-Zinc	On Zinc Galvanized Steel	43	6.4	1.2	<0.2	35
Manganese Modified						

When the substrate is steel, the metal ion Fe²⁺ that is dissolved from the pickling reaction is oxidized using the accelerators (e.g., nitrite/nitrate, chlorate or peroxides) and will precipitate out as sludge. If the substrate is galvanized steel, Zinc (Zn²⁺) ions are incorporated into the coating reaction and do not form any sludge. Due to the combination of galvanization and steel on mass production, sludge generated during phosphate treatment must be continuously removed by filtration techniques to keep the conversion layer performance constant [10].

Sludge formulation is as follows [10];



The phosphate bath should never be dumped. According to the literature and examples of commercial applications, the processing time is about 180 seconds and the temperature is 35-55 °C [7]. The requirements and specifications for zinc phosphate conversion layers vary from one vehicle supplier to another. Requirements are different for Korean, European, North American and Japanese car manufacturers. Table 2.2 outlines the crystal size and coating weight technical standards of the

world's automobile manufacturers. The biggest differences between automobile manufacturers can be seen in North America and Japan. The narrowest specifications can be found in several European manufacturers [7].

Table 2.2 Worldwide specifications on zinc phosphate conversion layer [7]

Region	Zn Crystal Size, μm	Coating Weight, g/m^2
North America	2 - 10	1.6 – 4.3
European	< 10	1.5 – 3.5
Japan	< 20	2.0 – 5.0
Korean	2 - 10	2.0 – 4.0

2.1.1.1.4 Passivation

Passivation can be applied in order to improve corrosion resistance of phosphated and coated metal sheet, but it is optional. The conversion layer can be given a passivation post-rinse with chrome (VI), Cr (III) or chrome-free solutions. Japanese, Korean and recently European manufacturers do not use passivation treatment [7].

2.1.1.2 Steps of Electrocoating Process

The electrocoat bath is composed of 80 to 90% deionized water and 10 to 20% paint solids. The deionized water serves as the carrier for paint solids, which consists of resins, pigment, and small amounts of solvents. As the backbone of the paint film, resin provides properties like corrosion resistance and ultraviolet resistance. In addition to providing color and gloss, pigments also protect against corrosion. Using solvents ensures a smooth appearance and application of the film. An electrocoat process involves applying paint to a part with a specific film thickness, which can be controlled by applying voltage. Deposition slows down when the coated part becomes electrically insulated. To provide complete coverage of the counter

electrode, electrocoat solids first deposit in the areas closest to it, and as these areas become insulated from current, they are forced into more recessed, bare metal areas. It is called throwing power and is a crucial aspect of the electrocoat process. A number of components are involved in the electrocoat bath solids deposition process: rectifiers, which supply DC currents to the bath for deposition of ionic species; circulation pumps to maintain proper paint bath uniformity; a heat exchanger and chiller to control the temperature of the bath; filters, which remove dirt particles introduced into the systems; and ultrafilters that produce permeate for rinsing and allow for recovery of excess paint solids [2].

2.1.1.2.1 Post-rinsing

When the part leaves the bath, excess non-electroplated paint solids adhere to the part and need to be washed away to maintain process efficiency and optimal aesthetics. Cleaning items are supplied by an extra filter and are called permeates. Permeates containing low molecular weight organic matter and some solvent are used to wash away residues from the component. Excess solids and permeates are counter currently returned to the bath for excellent transfer efficiency [2].

2.1.1.2.2 Baking

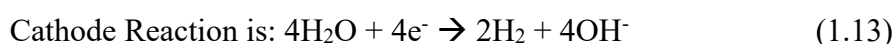
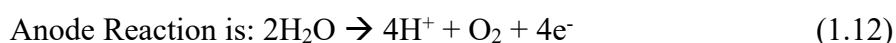
After post-rinsing, the coated parts are placed in a baking oven to cure and crosslinking of the coating. The result is a high quality finish with no flow, dripping or sagging. Bake temperatures range from 180 to 375°F depending on the type of electrocoat applied [2].

2.1.1.2.3 Reaction Mechanism of Cataphoresis Process

There are charged ions and moieties in the aqueous solution. In fact, it is the presence of negatively charged moieties that retain the positively charged resin molecules in the cathodic solution. The solubility of the resin depends on the critical balance between the positively and negatively charged ions. Positively charged ions in solution are cations and negatively charged ions are anions. Thus, cations are drawn to the cathode by the law of attractors of opposites. The cations move in its direction since the cathode is essentially locked in place. That movement is called migration. Cathodic paint refers to paint that deposits at the cathode, whereas cationic paint has positive charges. Consequently, the terms cathodic and cationic denote the location and kind of paint deposition, respectively. Essentially, cathodic electrocoating involves dipping the item to be coated into a tank of water-thinned paint during a paint plating operation. The paint is then exposed to a direct current. The item that will be painted becomes the cathode in a cathodic system. Paint solids which are positively charged are attracted to the cathode [7].

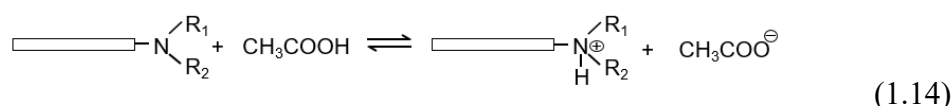
Electrodeposition of paint films simultaneously involves electrolysis, electrophoresis, electrodeposition and electroendosmosis.

- Electrolysis (decomposition): The process of a conductive liquid disintegrating under the influence of an electric current is known as electrolysis. The primary cataphoresis reaction involves the electrolysis of water to produce hydrogen and oxygen.



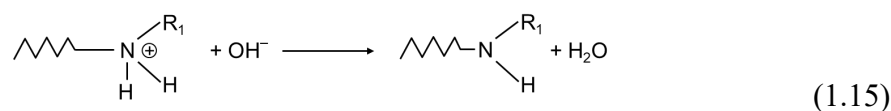
- Electrophoresis (migration): The movement of electrically colloidal moieties in a conductive media as a result of a potential difference is known as electrophoresis. An electrical field causes moieties of pigment and colloidal

resin to move through a process called electrophoresis. Colloidal moieties will acquire a positive charge if the paint vehicle is cationic. As a result of electrophoresis, these moieties move towards the cathode under the influence of an electrical potential. Amino groups in paint become soluble and gain positive charges in cataphoresis reactions when acid is added. Positive charged moieties move toward cathode.

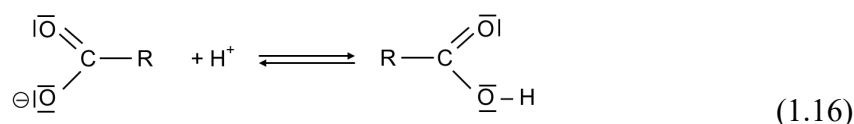


- Electrodeposition (precipitation): The precipitation of paint moieties at an electrode. Moieties with a positive charge will deposit at the cathode, and moieties with a negative charge will deposit at the anode. Anions are negative charged moieties that keep positively charged resin moieties dissolved in solution, which is why they are sometimes called counterions.

Cathode reaction is;



Anode reaction is;



- Electroendosmosis (dehydration): this is the final phase of the process. Paint solids are drawn to the cathode and precipitated, which results in a semi-permeable film, allowing water to pass through it. As a result, the deposited film is dehydrated. Films of this type are relatively resistant to physical distortion. The film can be rinsed with water to remove bath drag-out due to this characteristic and water insolubility. Drag-out is non-deposited paint that

adheres loosely to the coated article after it is removed from the bath. This drag-out must be removed in order to the deposited film to look good.

In summary, an electrical potential applied to two electrodes in a bath containing a conductive solution produces electrolysis of the solution and electrophoresis of the charged moieties. The cathode is the site of precipitation or coagulation. Until an even and continuous film covers the entire surface, this process continues. Since the electrodeposited film has a relatively high electrical resistance at a given voltage, the process ends when the film is nearly equal on all surfaces and edges. The film thickness is directly proportional to the resistance of the deposited coating.

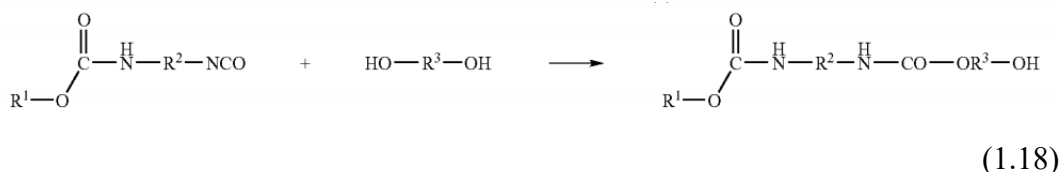
2.1.1.2.4 Reaction Mechanism of Amine-Modified Epoxy Coating

The amine-modified epoxy resin for CED process may be prepared for example, by a method comprising the steps of [11];

1. Providing a half-blocked isocyanate by reaction of an isocyanate compound with a blocking agent,

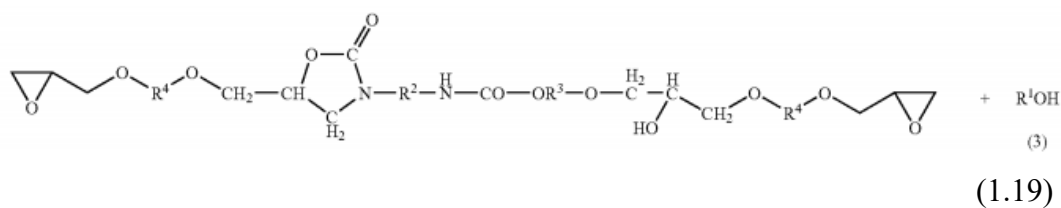


2. Preparing a blocked prepolymer by reaction of the half-blocked isocyanate with a monoalcohol or polyol,

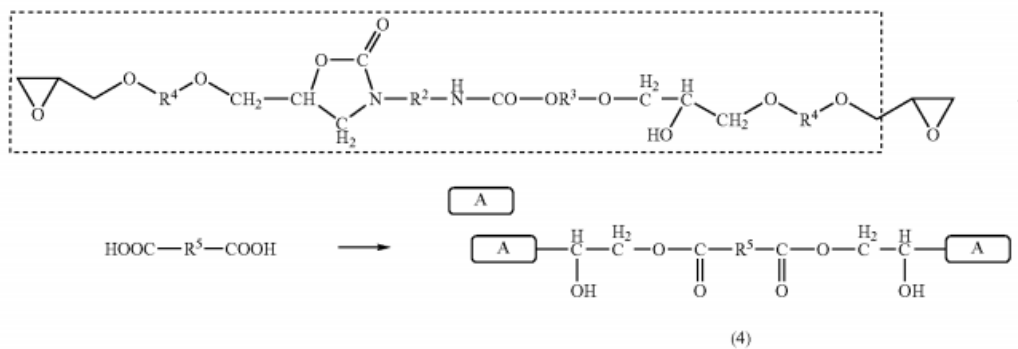


3. Forming an epoxy resin containing oxazolidone ring by reaction of the blocked prepolymer with a diglycidyl ether type epoxy resin,



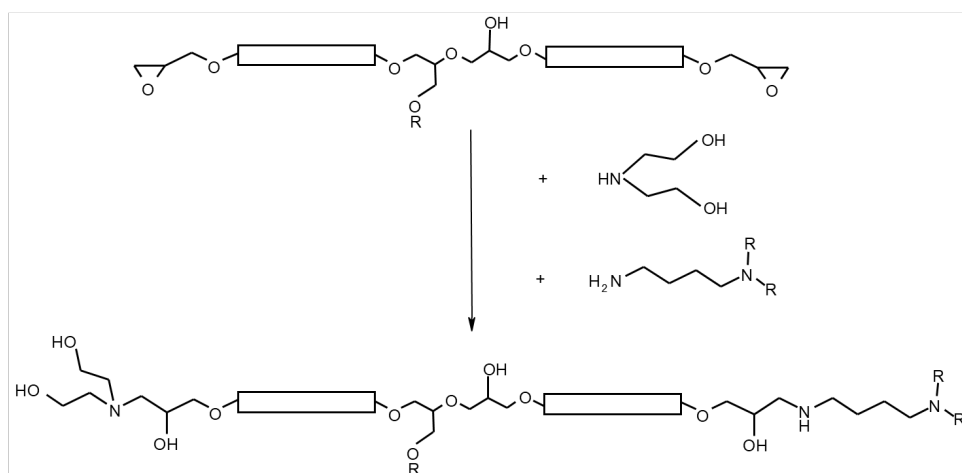


4. Chain-extending the epoxy resin containing oxazolidone ring with at least saturated or non-saturated hydrocarbon group containing dicarboxylic acid,



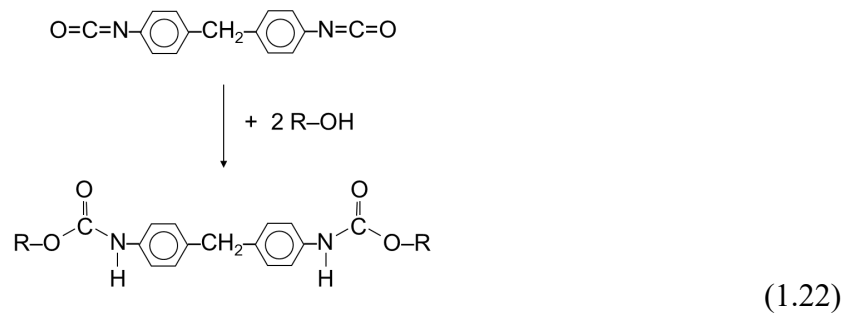
(1.20)

5. Modifying the chain-extended epoxy resin with an amine.

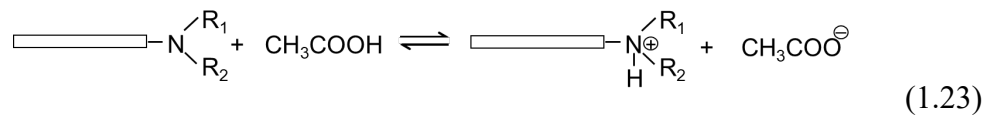


(1.21)

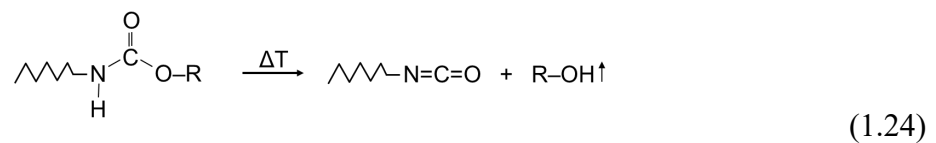
Preparation of crosslinking agents; Reaction of isocyanates with alcohols to block the crosslinker to inhibit the reaction of epoxy and crosslinker without coating to the surface to form capped isocyanates.



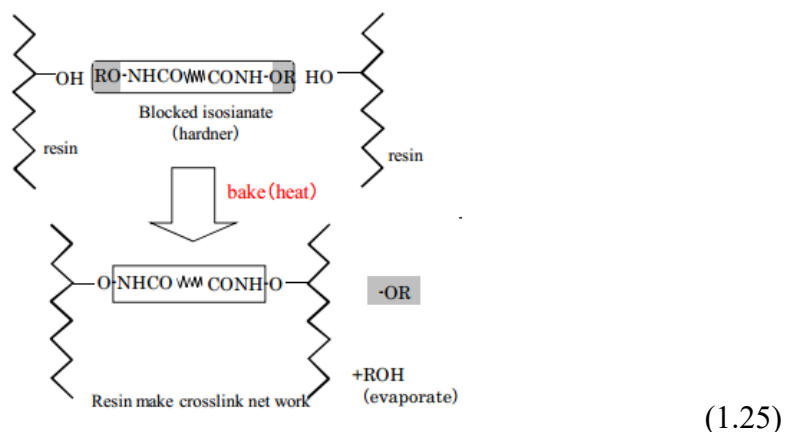
Preparation of epoxy dispersion; Addition of acidic groups to amine modified epoxy resin and crosslinker mixture to provide amine groups to disperse in water and gain positive charge.



Baking; Decapping of isocyanates with heat. Blocking agent (alcohol) is evaporated in the oven, isocyanate is activated.



Crosslinking; Reaction of isocyanate groups with –OH and –NH groups of main epoxy resin.



2.2 Literature Survey

According to the literature review about electrocoating process, it is seen that scientific studies have begun in 90's although the electrocoating process have begun to get used in 60's itself. In the literature it is seen that the studies are mostly related with chemical and physical properties – anticorrosion behavior in particular, surface quality of the coatings and reaction kinetics and formulations respectively. In the scope of this thesis study literature review about phosphating process and electrocoating process is given separately.

2.2.1 Literature Review on Electrocoating Process

In the field of reaction mechanism and kinetics there are 3 studies that take attention. Acamovic *et al.* [11] studied effect of different substrates such as bare steel, phosphated steel, bare-zinc plated steel and phosphated zinc plated steels to reaction kinetics, porosity and corrosion resistance of the coatings. They found that overall corrosion resistance of the phosphated or zinc-plated steel covered with the cathodic electrocoat was much higher than when the substrate was bare steel. It is also understood that, the rather small increase in porosity or conductivity of the deposited layer was over compensated by the protective properties of the phosphate or zinc layers under the electrocoat. Vatistas *et al.* [12] investigated effect of different application voltages to electrokinetic, electrochemical and other mechanisms. They found that at low values of the applied voltage the proposed mechanisms proceed regularly, but as the applied voltage increases, a rather irregular evolution is observed. Padasha *et al.* [1] investigated mechanism of film formation by changing induction time on different substrates such as bare steel, galvanized steel and phosphated steel. They found that the induction time was not due solely to concentration buildup near the cathode. Although the morphology of the initial coatings observed for different substrates varied, the coating preferentially deposited at areas where the local current density was higher.

In the literature limited number of studies have been found related with surface quality of the electrocoatings. Two major surface problems that are studied by the researchers are craters and porosity of the surfaces. Both problems bring additional repairing costs to the coatings. Four significant study have taken attention. Ranjbar *et al.* [13] have investigated the effect of degree of neutralization of the resin to surface porosity. It is found that by increasing the degree of neutralization, the film grows in a porous like manner which can be attributed to the fact that the rate of hydrogen gas evolution is much higher than the rate of electrocoagulate deposition of the moieties on the surface. Vatisas [14] has introduced a resistance between the electric source and the sample to be electrocoated to reduce the sharp initial conditions of electrocoating. It is found that introduction of the control resistance increases the voltage of the film rupture when the phosphated steel is used, while the application of the same technique on the substrates; hot-dipped galvanized and phosphated steel and zinc-electroplated and phosphated steel shows that this technique is a very efficient method of avoiding cratering and improving the quality of the paint. Ranjbar *et al.* [15] have investigated the influence of different substrates such as bare steel, phosphated steel and aluminum to surface porosity. It is concluded that the underlying substrate affects the properties of the deposited film. On the aluminum substrate, because of the cathodic corrosion, films that are more porous and conductive were obtained. In the case of phosphated steel, a less porous film forms on the surface, so the throwing power is greater (current cut-offs at shorter times) and the voltage rise occurs more rapidly. The behavior of the bare steel lies between the aluminum and the phosphated steel. Seraj *et al.* [16] have synthesized an anti-cratering additive which was based on amino-propyl-triethoxy-silane (APTES) to improve anti-cratering behavior of the coatings. Increasing the amount of anti-cratering agent (0.4–0.6 wt.%) decreased the number of craters. The results showed that panels electrocoated with the additive had a better appearance and fewer craters.

Adhesion is one of the most important properties of electrocoats because corrosion protection behavior of the coatings is directly related to the barrier properties of the coatings. Higher adhesion provides higher barrier properties of the coatings and corrosion resistance also increase by increasing adhesion. Only a few studies have been found related with understanding adhesion properties of the electrocoatings under different circumstances. Reddy *et al.* [17] investigated the influence of surface pretreatment and electrocoating parameters on the adhesion of cathodic electrocoat to the Al alloy surfaces. The pretreatments studied were acetone wipe and alkaline cleaning. There was not much effect of acetone cleaning of these alloy surfaces on the adhesion performance of the cathodic electrocoat. It is understood that the conversion coatings could be eliminated by a simple process like alkaline cleaning for improving the adhesion performance of cathodic electrocoat films. Reknens *et al.* [18] evaluated the possibilities to determine the protective properties of unscratched alkyd coatings on steel using the tape test and the blistering tests. The initial induction time is mainly dependent on the pre-existent conductive pathways and non-bonded areas. The undercutting induction time is attributed to the total effect of the barrier, inhibitive and adhesive properties. The comparison of the blistering rates before and after the undercutting induction time allows to evaluate the role of the durability of adhesive bonds. If initial and final blistering rates are of the same order, tape test will be useless to show the adhesion loss. Possibilities of wet adhesion determination of unscratched samples by X-cut tape test are limited to low-performance coatings.

The most important prospect of electrocoatings are their long lasting anti-corrosive behaviors. Most of the scientific studies in the literature are investigating the anti-corrosive behaviors of electrocoatings. Beside overall corrosion improvement, filiform corrosion and edge protection also have great importance. Not only improving anti-corrosive behavior but also finding out some fast and reliable corrosion test methods are also taking attention in the literature. To understand or improve anti-corrosive behavior of electrocoatings, effect of different epoxy

equivalent weights (EEWs), different application voltages, different silane sol-gel pretreatments, different substrates (Steel, Zn-Mn alloys) and different baking conditions and their effects on anti-corrosive behavior are investigated by some researchers [19-24]. Electro Impedance Spectroscopy (EIS) method is commonly used to measure and understand corrosion behavior. This technique is very common and gives reliable, fast, comparable and sensitive results when compared to traditional cycling salt spray tests [20, 24, 25]. Besides some researchers have developed new techniques to have more reliable and faster results even then EIS method, such as AC/DC/AC. Addition to corrosion investigation by EIS method, DSC, TGA and SEM techniques are used to characterize the electrocoatings [20, 23].

Similar to overall corrosion protection, filiform corrosion prevention have great importance especially in the automotive sector. Effect of different baking temperatures, different crosslinking densities and different surface pretreatment methods are investigated to improve filiform corrosion resistance [26-28]. Besides different measurement techniques are compared [29] and improvement of EIS technique is studied by researchers [30]. To characterize the coatings, Image Analyser, DSC, Scanning Kelvin Probe, ToF-Sims, EDXS and SEM techniques are used [26-30].

One major drawback of electrocoat paints is their weak coverage of sharp edges that remain after car body assembling. At the beginning of baking, the paint tends to flow away from edges resulting in low film build. Premature corrosion may consequently start along these relatively unprotected edges [31]. To improve anti corrosive edge-protection of electrocoatings, effect of increasing coating thickness by amount of flow modifiers, adding silica nanoparticles and epoxy-amine microgels are investigated [4, 5, 31]. Different from other characterization methods, FE-SEM, RMS and DMTA analysis are used to characterize the coatings.

Besides anticorrosion behavior, the stone chip resistance of automotive coatings is considered to be one of the important characteristics during service. Moving automobiles are often subjected to impact by lofted stones. The velocity at which the stone hits the automobile is approximately the same as the velocity of the vehicle, i.e. 40–140 km/h. Stone impact onto a painted automobile body can result in paint removal or delamination at the substrate–paint interface, ultimately leading to corrosion of the metal substrate [32, 33]. The chip resistance of automotive paint can be defined as the ability of a multi-layered coating systems applied onto a substrate to withstand impact of foreign particles without damage. Researchers reported that, the glass transition temperature of the primer coating is the key factor in stone chip resistance. The chip resistance has been decreased by increasing the glass transition temperature, such as by increasing the baking temperature and decreasing the oil length [32-34].

2.2.2 Literature Review on Phosphating Process

Fouladi *et al.* [35] examined morphological evolution of magnesium phosphate coating on steel surface as a function of phosphating time and temperature. They have found that increasing the phosphating temperature facilitated the precipitation of coating and increased its thickness. They have also stated that increasing phosphating time enhanced both thickness and uniformity of the coating. It is stated that increasing both temperature and time caused the growth in crystal size. Increase in crystal size and phosphate layer thickness resulted with better corrosion protection. In this study, the magnesium phosphate coating was investigated directly in terms of corrosion resistance, no electrocoat coating was applied on the coating. When the corrosion resistance of the phosphate coating was examined alone, it was seen that the size of the crystal structure and the reduction of the porosity had a positive effect on corrosion protection.

Unlike the study of Fouladi *et al.* [39], some porosity in the phosphating process as a pretreatment of cathodolysis coating is important and necessary for maintaining the conductivity of the surface. Because the surface must be conductive for electrocoating that is applied after zinc phosphate chemical conversion coating.

Jiang *et al.* [36] tried to provide additional insights into the mechanism of formation of a phosphate chemical conversion (PCC) coating on alloy steel. They have stated that PCC coating has a double-layer structure. First an amorphous base layer in contact with the steel substrate occurs, followed by an outer crystalline phosphate layer. According to their investigation, the results indicated that the formation of the PCC coating can be divided into four stages as electrochemical dissolution of the substrate, deposition of an amorphous phase, phosphate crystallization and growth and the dynamic balance between coating dissolution and formation respectively. They have stated that according to the previous studies, it is well known that, when a piece of steel is dipped into an acid conversion bath, many micro primary cells including micro anodes and micro cathodes are formed. If steel is used as a substrate then iron dissolves at micro anodes and the hydrogen evaluates at micro cathodes resulting an increase of pH at the metal/solution interface. Increase in the pH alters dissociation equilibrium, in order to re-adjust the dissociation equilibrium, multistage hydrolysis of soluble primary phosphates (H_3PO_4) results with obtaining phosphate ion (PO_4^{3-}) in the bath. Subsequently phosphate and the cations in the bath (Zn^{2+} , Fe^{2+} etc) are deposited on the surface of the steel and then gradually grow to produce a PCC coating. They have explained that a few researchers had suggested that a very thin base layer is formed first, as soon as the steel makes contact with the conversion bath, and this base layer may contain sub crystalline oxides and phosphates of iron. Jiang *et al.* [36] used advanced characterization methods to provide additional insights to the mentioned amorphous base layer. Their results showed that amorphous base layer contains Fe_2O_3 and FePO_4 , while the crystalline layer is mainly composed of Hopeite $\text{Zn}_3(\text{PO}_4)_2 \cdot 4\text{H}_2\text{O}$ and Phosphophyllite $\text{Zn}_2\text{Fe}(\text{PO}_4)_2 \cdot 4\text{H}_2\text{O}$.

Jiang *et al.* [36] explained the reactions in the bath as follows;

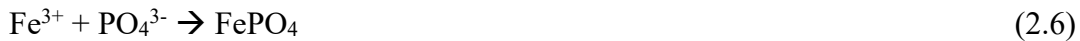
Dissolution of iron at micro anodes and hydrogen evolution at micro cathodes occurs simultaneously via the following reaction;



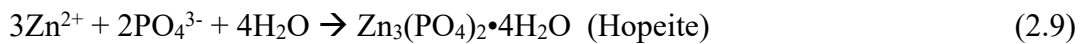
Hydrogen evolution increases pH at the metal/solution interface which then alters the dissociation equilibrium, leading to the formation of PO_4^{3-} ;



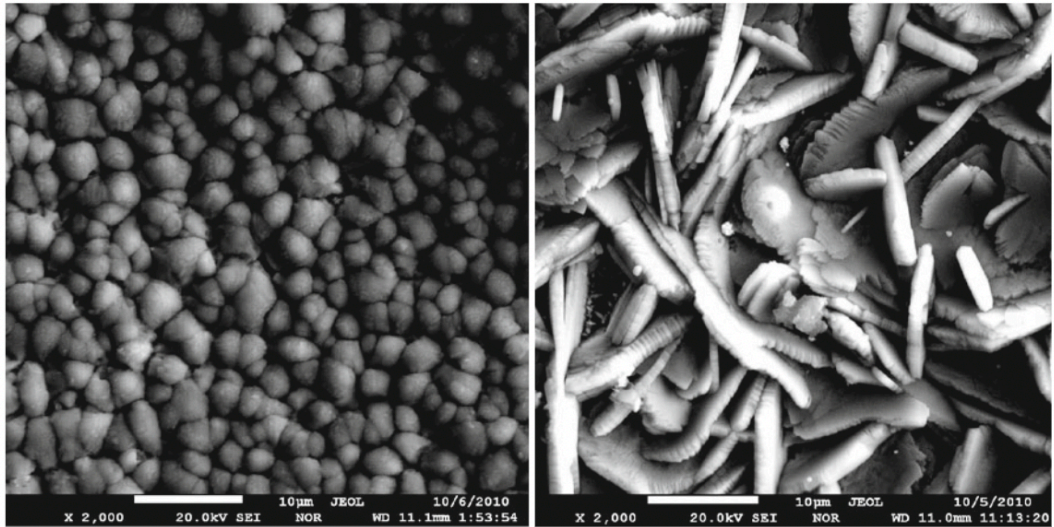
Deposition of an amorphous phase occurs;



Crystallization and crystal growth is given below as mentioned previously;



Rani *et al.* [37] stated that the adhesion of electrodeposition (ED) paint on steel sheets for automotive industry is highly influenced by the properties of the zinc phosphate coating that applied prior to ED process. They applied two different types of zinc phosphate formulations (Hopeite and Phosphophyllite) to a steel surface than coated the panels with the ED material to investigate their corrosion resistance. They stated that the phosphate coating enriched with a Phosphophyllite structure showed a globular crystal structure with less porosity, whereas a Hopeite structure showed a coarse needle-like structure with high porosity. SEM images of Phosphophyllite and Hopeite crystals are given in Figure 2.3 [37].



SEM image of sample A

SEM image of sample B

Figure 2.3 2.0 kx SEM Images of Phosphophyllite (Sample A) and Hopeite (Sample B) Crystals [37]

Bubert *et al.* [38] investigated the crystal structures of Phosphophyllite and Hopeite crystals under spray and immersion conditions. Figure 2.4 gives SEM images for both spray and immersion applications of phosphate crystals according to their Hopeite and Phosphophyllite contents.

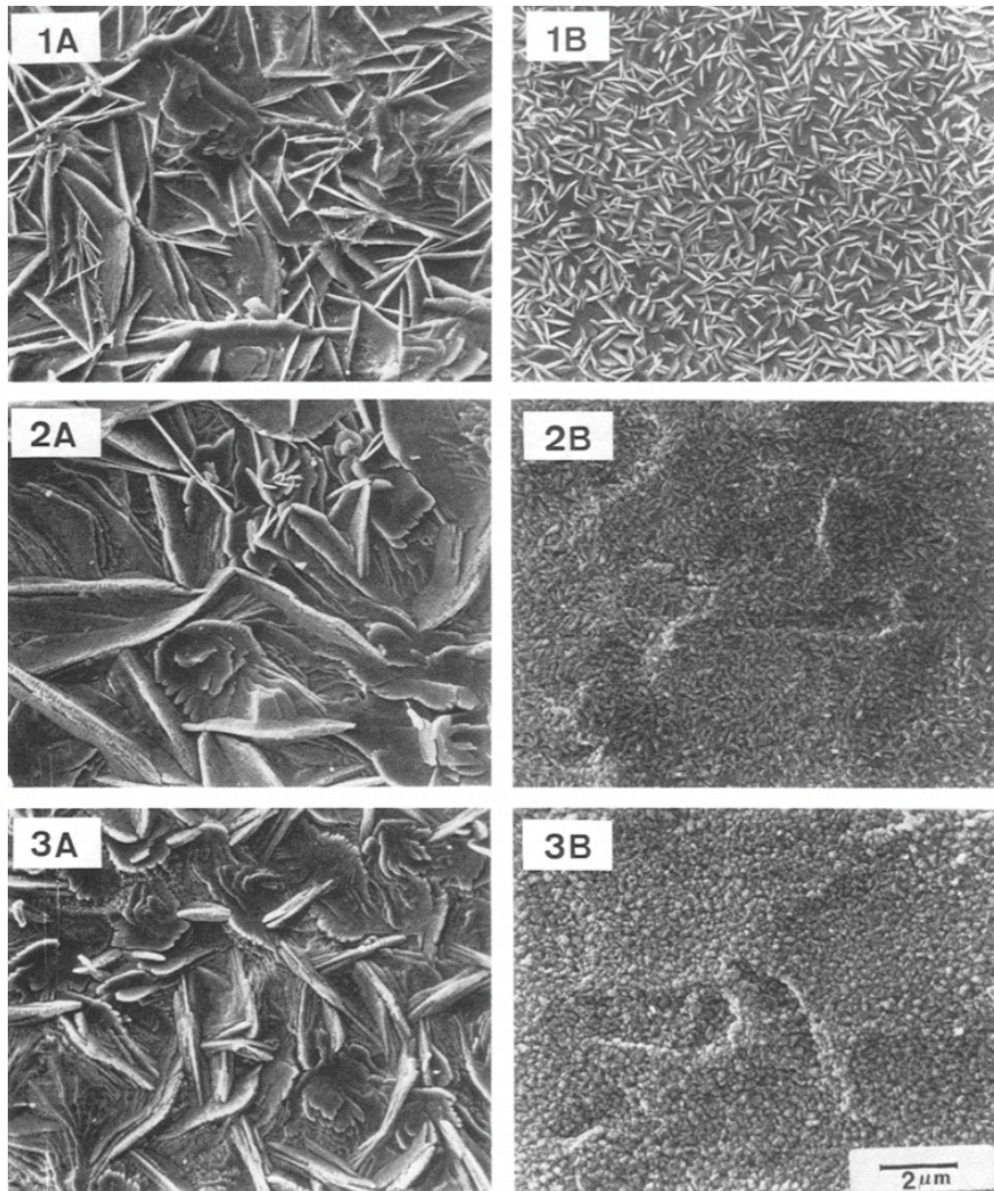


Figure 2.4 SEM Images of Hopeite (Sample 1A Spray and 1B Immersion), Phosphophyllite apart from Hopeite (Sample 2A Spray and 2B Immersion), Predominantly Phosphophyllite (Sample 3A Spray and 3B Immersion) Crystals [38]

CHAPTER 3

MATERIALS AND METHODS

3.1 Experimental Procedures Used in Electrocoating

To investigate the effect of different parameters on electrocoating process, a pilot scalesetup is created in the laboratory by using a rectifier which provides the necessary potential to two electrodes (anode and cathode) up to 400 V. A 3 liter glass vessel is used as a reactor. A 5x10 cm bare steel plate is the anode. Cathode substrate is 10x20 cm commercially obtained pre-phosphated (Chemetall Gardobond TE24) steel plate. Photos of the instruments used in the setup are given in Figure 3.1.

3.1.1 Materials Used

Paint dispersions are prepared by using commercially obtained PPG ED 7210 pigment paste and binder emulsions. The pigment paste and binder are used as is. DI water is used as a dispersant.

3.1.2 Electrocoating of the Panels

A magnetic stirrer (Hei Standard Model by Heidolph Instruments, Germany) is used for heating and mixing of the dispersion. A rectifier (Pulseline Model by Danış Electricity, Turkey) which provides the necessary potential to two electrodes (anode and cathode) up to 400 V is used. An oven (Heratherm Model by Thermo Scientific Corp, UK) with operating temperatures up to 250 °C is used to bake the coatings.



Figure 3.1 Test Setup; a) Reaction Bath; Anode and Cathode b) Rectifier 0-400V c) Oven 250 °C

The resin dispersion that includes paint micelles is added to cataphoresis vessel. The micelles consist of positively charged paint moieties containing epoxy resin, crosslinker, pigment paste and some additives and negatively charged acetic acid (acidic) moieties in ionic balance. Thus when the current is given to the anode and cathode, positively charged paint moieties move towards cathode and negatively charged acid moieties move towards anode. Schematic illustration of paint micelle movement in the dispersion is given in Figure 3.2.

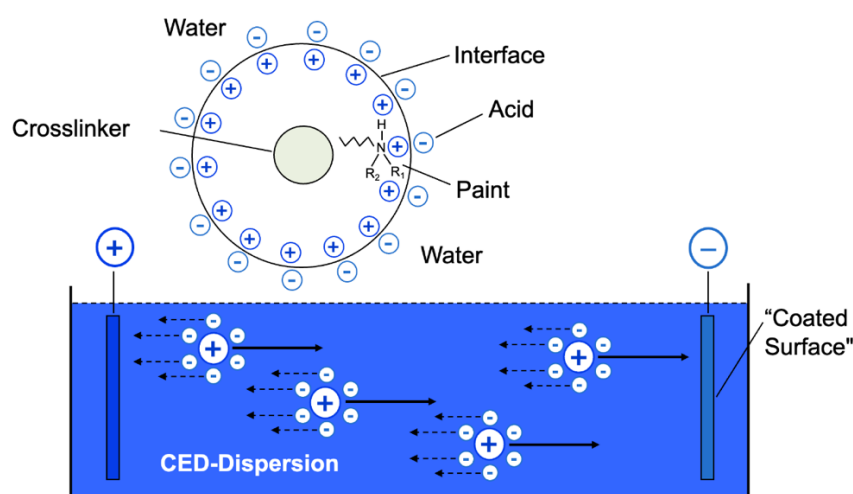


Figure 3.2 Schematic illustration of paint micelle movement in the dispersion.

In the test setup anode and cathode are immersed in a 3 L tank, cathode is the substrate that will be coated. When electric current is given to the anode and cathode, electrons move from anode to cathode, that will result with electrolysis of water. At the cathode, reduction reaction of water, and at the anode oxidation reaction of water occurs. Hydrogen gas is released in cathode, oxygen gas is released in the anode. Because of the reduction reaction in the cathode, OH^- ions are generated and pH around cathode increases too much. Positively charged paint moieties move toward the cathode and neutralize with OH^- ions and consecutively deposit on the cathode

surface. Negatively charged acidic moieties move toward anode and neutralize with H⁺ ions. Schematic illustration of electrodeposition process is given in Figure 3.3.

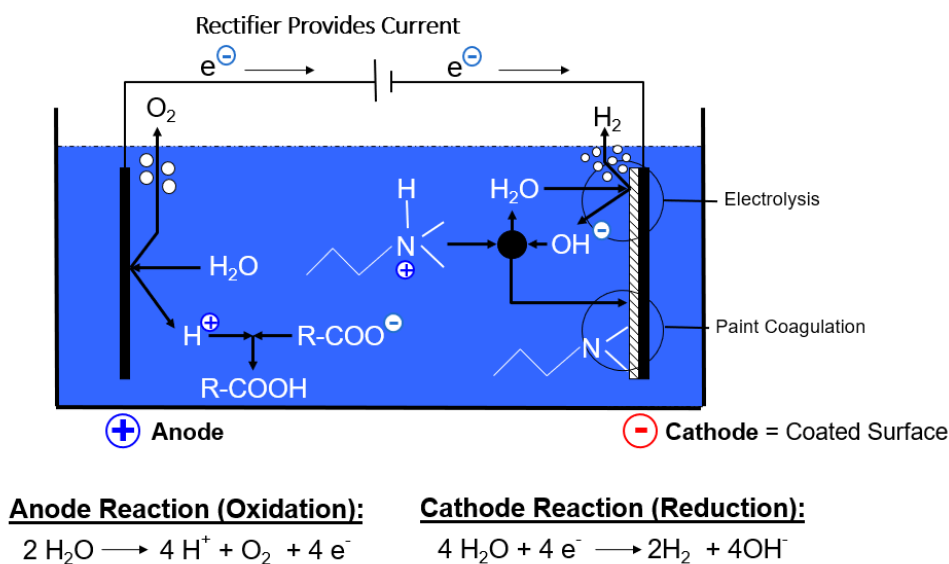


Figure 3.3 Schematic illustration of electrodeposition process.

3.1.3 Structural and Morphological Characterization

ATR- Fourier transform-infrared (FTIR) spectroscopy is used in order to confirm that commercially obtained resin and pigment materials are showing characteristic epoxy structure or not. At least 64 scans were signal-averaged in the wavenumber range of 400 to 4000 cm⁻¹ with a resolution of 4 cm⁻¹.

Tescan Vega 3 scanning electron microscope (SEM), is used to analyze surface morphology of phosphated and electrocoated panels. Prior to SEM analysis parts are coated with Au-Pd with 4 nm thickness with Leica EM ACE200.

3.1.4 Performance Analysis

For stone chip resistance test; An Erichsen Steinschlagprüfgerät VDA Model 508 equipment is used with 4-5 mm in size, rust free angular chilled iron grit “Diamant” stone material. Ford FLTM BI 157-06 internal test method is used as a test standard. This test method is used to determine the resistance of paint, on exterior body surface, to stone chipping. To perform this test, 2000 g chilled iron grit is blasted to the coating surface for 30 seconds with an air pressure of 2.0 bar. Then test panels are subjected to a water immersion test for 72 h, within one hour of removing the panels from water immersion grit blasting is repeated as defined above. Evaluation is done by using Evaluation Standards Photographs.

For water immersion test; a GFL Typ 1008 Water Bath and a 28 mm wide 3M no.898 adhesion tape is used. Ford FLTM BI 104-01 internal test method is used as a test standard. This method is used to determine the resistance to failure of painted test panels when immersed in water. Test panels are immersed in a container full of deionized water with a conductivity lower than 10 micro ohms/cm at 32 ± 1 °C for the time required by relevant engineering standard. Then an X scribe is applied by using a carbide tip scriber, onto the test surface after water immersion. Adhesion tape is applied across the surface by using firm finger pressure. Tape is removed by pulling back rapidly and adhesion loss is evaluated together with blistering.

For adhesion test; a TQC Sheen CC2000 Cross cut Adhesion tester and a 28 mm wide 3M no.898 adhesion tape is used. Ford FLTM BI 106-01 internal test method is used as a test standard. To perform this test, the panels are cut by using the cross cut tester perpendicularly. Adhesion tape is applied across the surface by using firm finger pressure. Tape is removed by pulling back rapidly and adhesion loss is evaluated by using classification patterns.

A Weisstechnik SC Test Chamber is used for Salt Spray Corrosion Resistance test. ASTM B117 test method is used as a test standard. Prior to testing an X scribe is applied by using a carbide tip scriber onto the test surface. Then test panels are subjected to salt spray fog for a certain time. After the test, adhesion tape is applied across the surface by using firm finger pressure. Tape is removed by pulling back rapidly and adhesion loss is evaluated. Loss of adhesion after the tape test from scribed lines and occurrence of blistering and adhesion loss beyond the scribed lines are evaluated.

For Hardness test; a BYK-Gardner 5855 Pendulum Hardness Tester is used. ASTM D4366 test method is used as a test standard. This method works on the basis of the damping time of a pendulum oscillating on a surface, depending on the surface hardness.

For Impact Resistance; Erichsen Model 304 Impact Tester is used. ASTM D2794 test method is used as a test standard. In this case, a defined weight with a fixed diameter, is dropped onto the sample through a guide tube. After the impact, the deformed zone of the specimen surface is examined for cracks and flaking and the height causing the cracks and flaking is reported as test result.

3.1.5 Thermal Analysis

Two different thermal analyses were carried out to determine the thermal behavior of all electrocoating samples. First of all, differential scanning calorimetry analyses (DSC) were used to determine the important transition temperatures during a heating profile from 30° to 200°C at a rate of 10°C/min under nitrogen flow with Shimadzu DSC-60. Then, thermogravimetric analyses (TGA) were conducted to determine the thermal degradation temperatures of the specimens under a heating rate of 20°C/min from 30° to 900°C under nitrogen flow with Shimadzu DTG-60H.

3.1.6 Surface Characterization

Film thickness measurements are done with ElektroPhysik Minitest 4500 coating thickness gauge. Gloss measurements are done with Sheen Model 160 Tri-microgloss 20-60-85 equipment.

Roughness measurements are conducted with Jenoptik Waveline W5 Portable Surface Roughness Tester. Roughness is a precise measurement of the surface to define surface texture properties. For the roughness measurements Ra parameter is used for the evaluations. Ra represents the arithmetic mean roughness value from the amounts of all profile values. During the tests, 4.8 mm length of the surface is measured in terms of roughness and Ra parameter response is recorded.

3.2 Statistical Methods Used in Parameter Sifting

To conduct further analysis on the investigated parameters by using DOE method [39], some of the critical parameters are required to sift. Correlation analysis is a useful method to assess critical parameters according to their statistical association. Minitab™ 17 software is used for Correlation Analysis. Details of the correlation analysis is defined below.

3.2.1 Correlation analysis

The primary purpose of linear correlation analysis is to measure the strength of linear association between two variables (X and Y). If X increases and there is no definite shift in the values of Y, there is no correlation or no association between X and Y. If X increases and there is a shift in the values of Y, there is a correlation. The correlation is positive when Y tends to increase and negative when Y tends to decrease. If the ordered pairs (X, Y) tend to follow a straight-line path, there is a

linear correlation. The preciseness of the shift in Y as X increases determines the strength of the linear correlation.

The Correlation Coefficient always is a value between -1 and $+1$. The Correlation Coefficient for the population is symbolized by ρ (the Greek letter rho) which is estimated by the sample Correlation Coefficient represented by r (also known as Pearson's Correlation Coefficient). A Correlation of -1 indicates a strong negative relationship, one factor increases the other decreases. A Correlation of $+1$ indicates a strong positive relationship, one factor increases so does the other. A schematic illustration of " r " correlation coefficient is given in Figure 3.4.

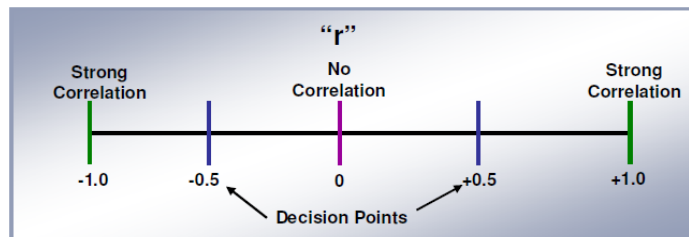


Figure 3.4 Schematic illustration of " r " correlation coefficient.

3.2.2 Regression Analysis

Correlation only tells us the strength of a linear relationship, not the numerical relationship. The last step to proper analysis of Continuous Data is to determine the regression equation. The Regression Equation can mathematically predict Y for any given X. Correlation only tells us the strength of a relationship while regression gives the mathematical relationship or the prediction model. R^2 (R-Sq) describes the amount of variation in the observed response values that is explained by the predictor(s). The Regression Analysis generates a prediction model based on the best fit line through the data represented by an equation.

3.3 Design of Experiment (DOE)

Design of Experiments (DOE) is a scientific method of planning and conducting an experiment that will yield the true cause and effect relationship between the critical X variables and the Y variables of interest. DOE is iterative in nature and may require more than one experiment at times [39].

2-level Full Factorial designs are generally noted as 2^k where k is number of input variables or factors and 2 is the number of the levels all factors used.

3.4 Experimental Procedures Used in Phosphating

3.4.1 Materials Used

To investigate the effect of different time and temperature parameters to zinc phosphating process, a pilot test setup is created in the laboratory by using a magnetic stirrer. A 3 liter glass vessel is used as a reactor. Substrate is 10x20 cm zinc coated (galvanized) steel plate. Zinc Phosphate solution is commercially obtained Chemetall Gardobond TE24 material and used as is. This material is a trication pretreatment material that consists of Zn, Mn and Ni as cations.

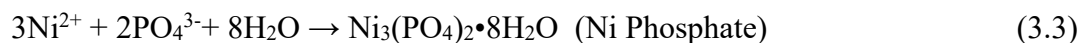
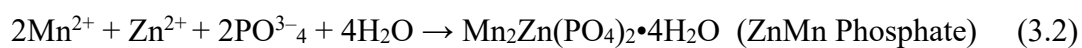
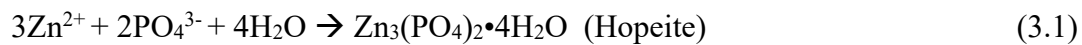
3.4.2 Phosphating of the Panels

Temperature of the solution is controlled by a thermometer during the process. Prior to zinc phosphating process, substrate panels are degreased and activated properly. Activated panels are immersed into the phosphate bath at specified time and temperatures. After phosphating each panel is rinsed properly with DI water. Test setup is given in Figure 3.5.



Figure 3.5 Phosphating Test Setup.

In this study, Low-Zinc Manganese Modified trication phosphating process is applied on zinc galvanized steel. There are Zn, Mn and Ni cations in the bath formulation. Hopeite, ZnMn Phosphate and Ni Phosphate are expected to form.



3.4.3 Structural and Morphological Analysis

Tescan Vega 3 scanning electron microscope (SEM), is used to analyze surface morphology of phosphated and electrocoated panels. Prior to SEM analysis parts are coated with Au-Pd with 4 nm thickness with Leica EM ACE200.

ImageJ software is used to analyze dimensional distribution of the phosphate crystals. For each condition 70 to 100 crystals are investigated in terms of dimensional analysis. Coating weight of zinc phosphate layer of each condition is measured by using Chemetall GardoMeter equipment.

CHAPTER 4

RESULTS AND DISCUSSION

4.1 Preliminary Assessment of Operational Parameters on Electrocoating Process

Some preliminary tests were conducted to understand which parameters are mostly affecting the surface quality and stone chip resistance of the coatings. As will be discussed in detail below, surface quality of the coatings in terms of roughness, dirt, crater and pinholes and physical properties in terms of stone chip resistance, adhesion, hardness, and thickness were investigated by revealing the influences of seven different parameters. Investigated parameters are deposition voltage, induction time, bath temperature, pigment/binder ratio, solid content ratio, organic solvent content ratio and baking conditions, respectively.

For further understanding of each parameter, in addition to surface quality evaluations and performance tests, each parameter is also investigated in terms of thermal properties. Glass transition temperature of the different conditions are determined.

While examining the effects of seven different parameters, experiments were carried out by keeping other parameters constant. Preliminary test conditions are given in Table 4.1.

Table 4.1 Preliminary test conditions of electrocoating parameters.

Investigated Parameter	Voltage (V)	Induction Time (sec)	Induction Temperature, °C	Pigment/Binder Ratio	Solid Content	Organic Solvent Ratio	Baking Conditions
Voltage, V	200	135	30	0.15	21%	2.47%	175 °C – 20’’
	300						
	400						
Induction time, sec	300	100	30	0.15	21%	2.47%	175 °C – 20’’
		135					
		170					
		200					
Bath Temperature, °C	300	135	17.5	0.15	21%	2.47%	175 °C – 20’’
			25				
			30				
			35				
			40				
Pigment/Binder Ratio	300	135	30	0.05	21%	2.47%	175 °C – 20’’
				0.15			
				0.25			
Solid Content, %	300	135	30	0.15	15%	2.47%	175 °C – 20’’
					21%		
					27%		
Organic Solvent Ratio, %	300	135	30	0.15	21%	2.47%	175 °C – 20’’
						4.85%	
						7.11%	
Baking Conditions	300	135	30	0.15	21%	2.47%	135 °C – 20’’
							175 °C – 20’’
							195 °C – 20’’

Before beginning the studies, resin and pigment materials to be used are analyzed by FTIR spectroscopy to confirm that the polymer has an epoxy – amine structure. Characteristic peaks are seen for epoxy – amine structure in FTIR spectra of the binder and pigment paste emulsions.

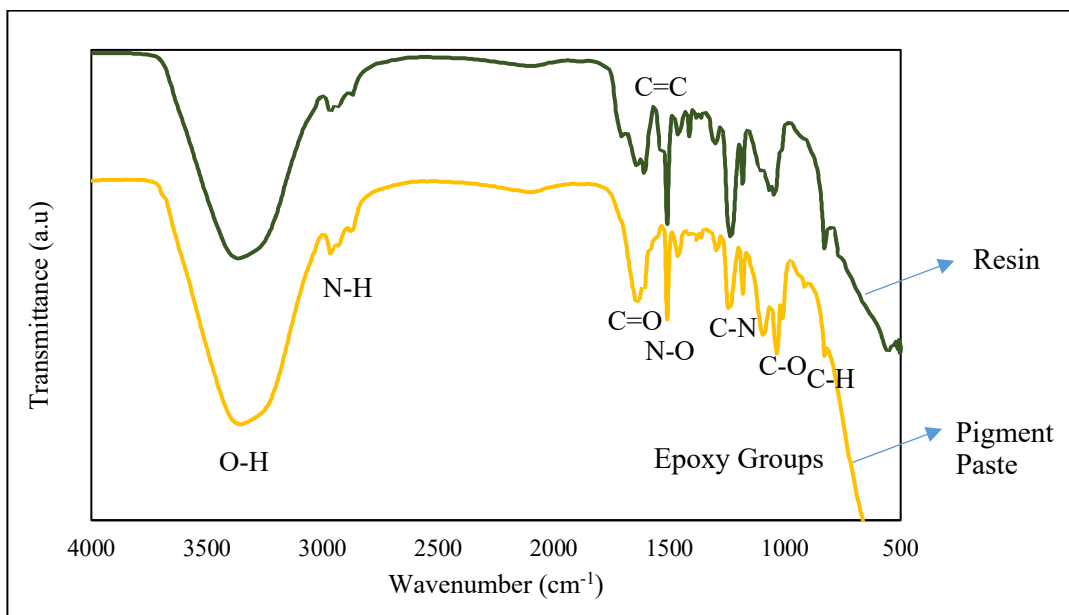


Figure 4.1 FTIR Spectra for Resin and Pigment Paste.

Panels to be coated are previously phosphated with standard commercial Chemetall Gardobond TE24 Phosphate baths in a reference mass production line. SEM images of phosphated panels taken before the electrocoating process are given in Figure 4.2. It is seen that the Hopeite crystals have the characteristic needle-like shape.

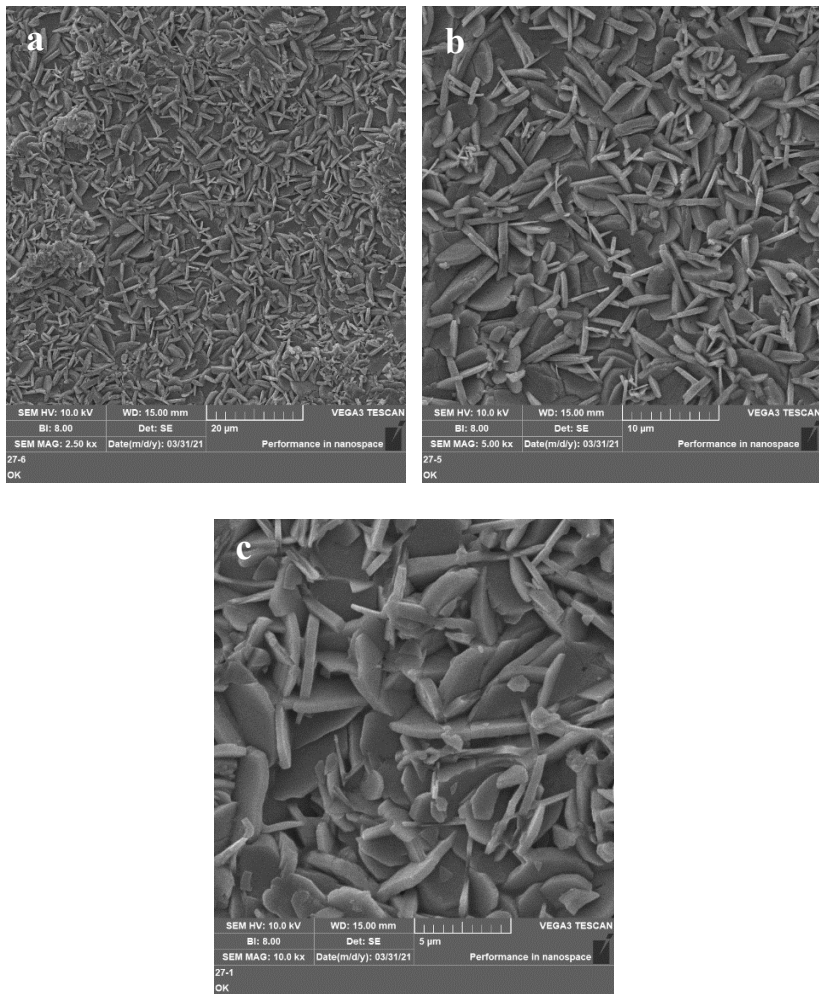


Figure 4.2 SEM images of phosphated steel panels at different magnifications.

a) 2.50 kx b) 5.00 kx c) 10.0 kx

4.1.1 Effect of Deposition Voltage

To understand the effect of different deposition voltages on electrocoating process, three different deposition voltages 200, 300 and 400 V are used respectively, and their effect on some physical properties that are mentioned above are investigated. Process parameters are given in Table 4.2.

Table 4.2 Process parameters to understand the effect of deposition voltage.

Investigated Parameter	Voltage (V)	Induction Time (sec)	Induction Temperature, °C	Pigment/Binder Ratio	Solid Content	Organic Solvent Ratio	Baking Conditions
Voltage, V	200	135	30	0.15	21%	2.47%	175 °C – 20’’
	300						
	400						

4.1.1.1 Physical Properties

It is seen that; film thickness is directly proportional to deposition voltage. Film thickness is increasing with increased voltage to very high values. Roughness of the surface also increases inevitably with increased voltage and film thickness. Gloss of the surface increases up to a certain film thickness, then sharply decreases with the increased thickness and roughness. The surface quality measurement results are given in Figure 4.3 and tabulated in Table A.1.

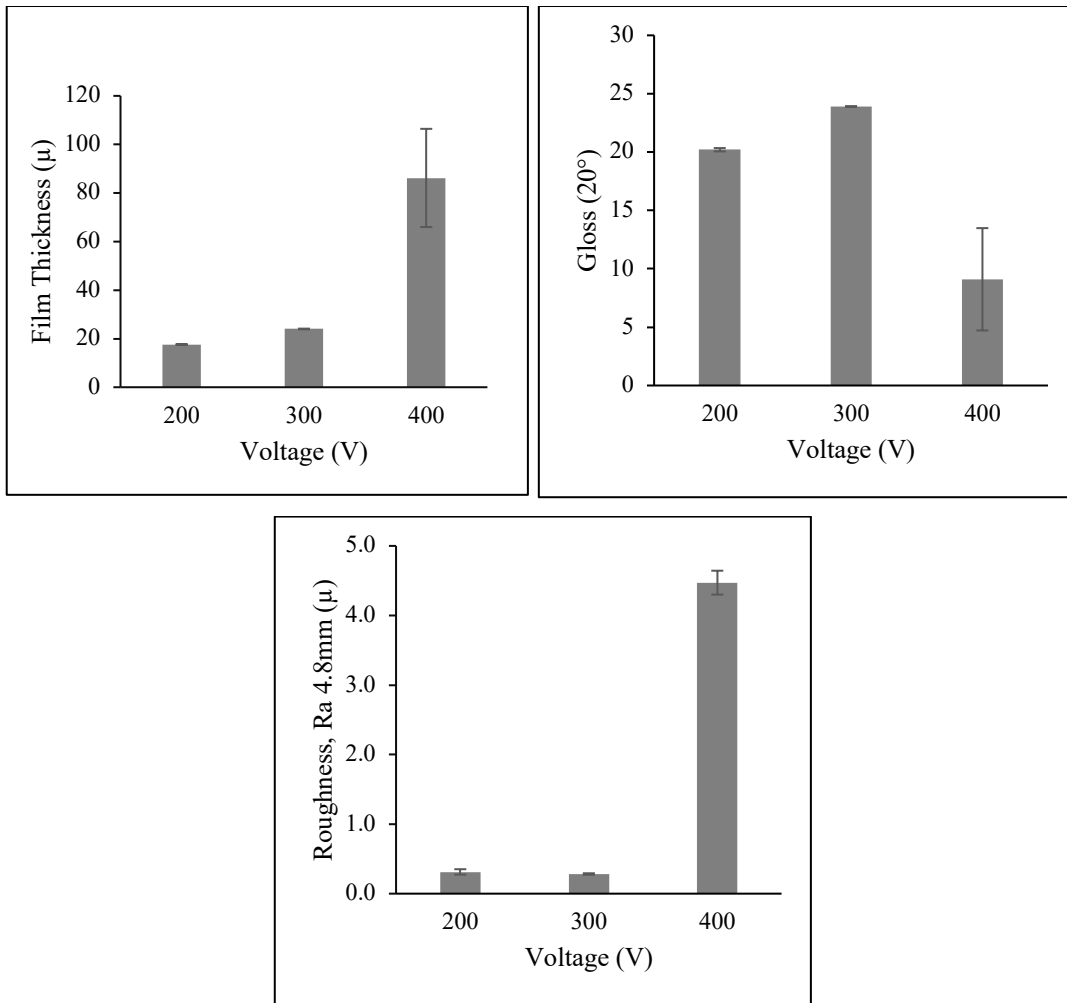


Figure 4.3 Surface measurements according to voltage levels. (a) Film Thickness (b) Gloss (c) Roughness

Effect of deposition voltage levels of the coatings on the mechanical properties were evaluated by impact resistance, hardness and stone chip resistance tests. Impact resistance and hardness seem to decrease with increased film thickness. Stone chip resistance of the surface also decreases with increased voltage and thickness. Physical properties results are given in Figure 4.4 and tabulated in Table A.1.

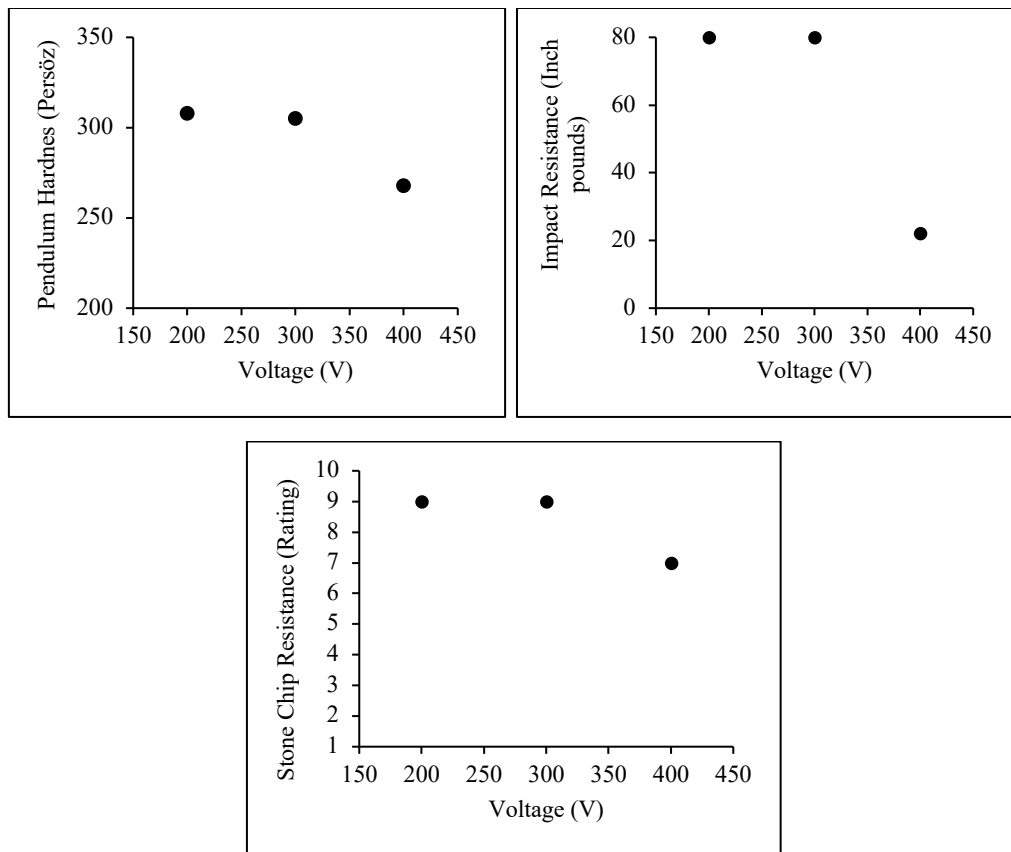


Figure 4.4 Mechanical properties according to voltage levels. (a) Hardness (b) Impact Resistance (c) Stone Chip Resistance

A cross-cut adhesion test is applied to the coatings to understand if the adhesion level is good enough for most purposes or not. At all levels of voltage application, the adhesion level is found as Grade 0 which is classified as “Pass” with the highest grade.

4.1.1.2 Morphological Analysis

Since distribution, accumulation and agglomeration level of the pigments and fillers in the matrix have significant influences on the mechanical and other properties of the electrocoatings, SEM studies were conducted on the surface of all compositions. SEM images taken at a magnification of 5.00 kx given in Figure 4.5 show that medium level of voltage (300V) resulted in rather uniform distribution with lower

degree of agglomeration and lower surface defects in epoxy matrix. Lower voltage levels resulted in large pores and pinholes with insufficient distribution and low coating thickness. Upper voltage levels resulted in high level of pinholes, high pigment and filler accumulation and unnecessarily increased film thickness with a rough surface.

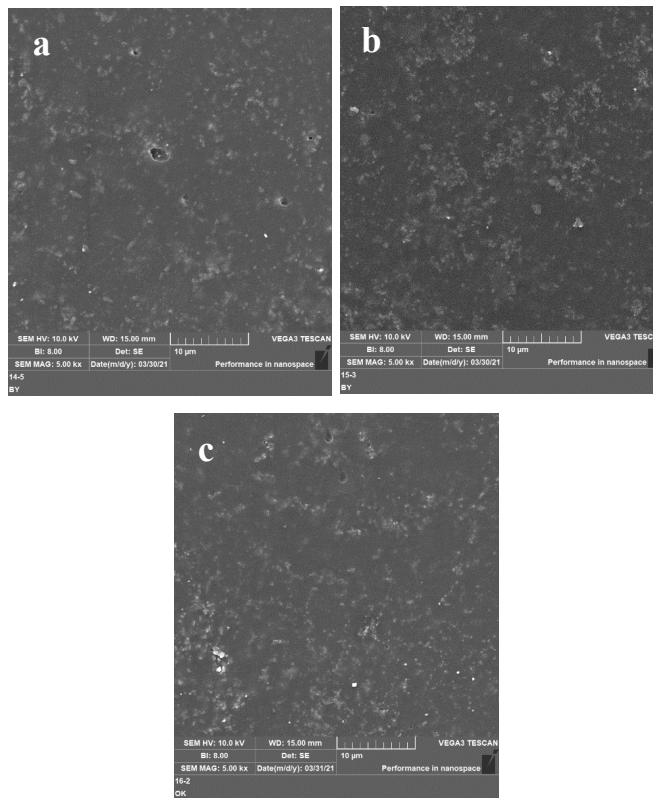


Figure 4.5 SEM images (5.00 kx) of coated panels at different deposition voltages. (a) 200V (b) 300V (c) 400V

4.1.1.3 Thermal Analysis

Effects of voltage levels on the thermal behavior of the specimens were studied by DSC and TGA analyses. Glass transition temperature (T_g) of an epoxy system increases with cross-linking density. Garcia *et al.* [20] indicated that T_g of a cataphoretic epoxy coating decrease with increasing deposition voltage since with higher deposition voltages the pigment content in the coating is also higher and a

trapping effect exerted by the pigments can reduce the mobility of the molecules of the reactive system. This reduces the chance of encounters between epoxy resin and curing agent. This non-reactive groups can result in a plasticizing effect and reduce T_g [20].

Glass transition temperatures of the specimens coated at different deposition voltages are given in Figure 4.6. It is seen that with the increased deposition voltage glass transition decreases, similar to the study of Garcia *et al.* [20] This can be explained also with the increased pigment content in the coating with the increased deposition voltages. The inorganic pigments in the composition result in a plasticizing effect and reduce cross-linking density, thus glass transition temperature also decrease. In addition to that, at very high voltage of 400V, glass transition temperature increases slightly compared to 300V. This can be explained with the decrease of surface conductivity at very high film thickness resulted in the decrease of the pigments that move to the coating surface because of decreased electrical attraction.

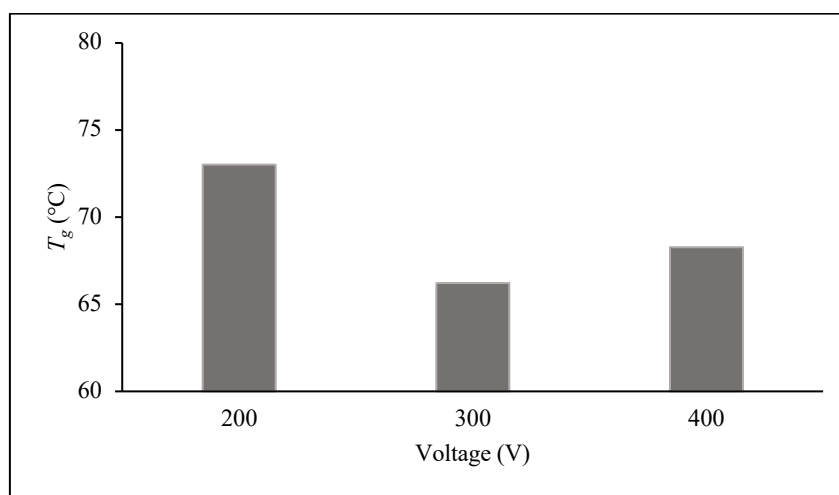


Figure 4.6 Glass Transition Temperature vs Deposition Voltage, Obtained by DSC Analysis.

Thermo-gravimetric (TGA) analyses are conducted in order to determine degradation process and pigment content of each of the coatings applied at different deposition voltages. Residue percentage of each specimen were given in Figure 4.7, while both DSC and TGA data determined were tabulated in Table A.8.

In the study of Garcia *et al.* [20] induction time of deposition is arranged to obtain the same film thickness, as 20 microns, at each deposition voltage. Their study indicated that as the cathodic voltage increases a higher residual weight is detected at the same operating film thickness of 20 microns which obtained with decreased induction times according to increased deposition voltages, meaning that the proportion of inorganic matter was higher. This is explained by the deposition process itself since as the deposition voltage increases, the resin micelles which migrate towards the cathode are able to transport more and more pigments to the metallic substrates [20].

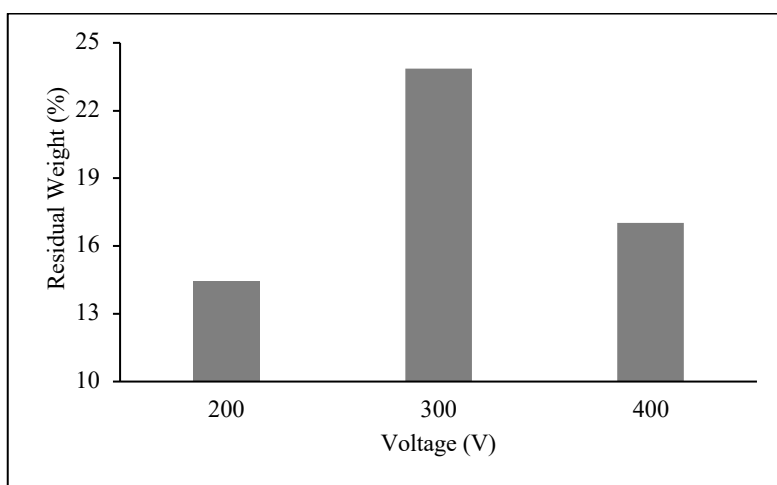


Figure 4.7 Residual weight vs deposition voltage, obtained by TGA analysis.

In this study, induction time is kept constant for each deposition voltage, so film thickness is reached up to very high levels in high deposition voltage of 400V. TGA analysis shows that, residual percentage of the specimens are very low as 14.43% at

200V, but increased up to 23.85% at 300V, then a decrease to 17.02% is seen at 400V. Between 200V and 300V, film thicknesses are close to each other, there is only 6-8 microns difference in the film thickness but at 400V application film thickness increases up to 90 microns. At low levels of voltage, pigment ratio in the coating is lower, thus T_g is higher and residual weight is lower. Pigment content is increased with increased voltage up to 300V. At very high voltages such as 400V, film thickness increases to high values around 100 microns. This resulted in the insulation of the surface. Insulation of the surface resulted in the slowing of induction. Thus pigments are not able to move forward to the cathode because of the decrease in electrical attraction. Also increased amount of bubbles and pinholes that deteriorate the homogeneity of the coating because of inevitable gassing in the reaction at high voltages may decrease the pigment ratio at high voltage levels.

4.1.2 Effect of Induction Time

To understand the effect of different induction times on electrocoating process, four different induction times as 100, 135, 170 and 200 sec are used respectively, and their effect on some physical properties that are mentioned above are investigated. Process parameters are given in Table 4.3.

Table 4.3 Process parameters to understand the effect of induction time.

Investigated Parameter	Voltage (V)	Induction Time (sec)	Induction Temperature, °C	Pigment/Binder Ratio	Solid Content	Organic Solvent Ratio	Baking Conditions
Induction time, sec	300	100	30	0.15	21%	2.47%	175 °C – 20”
		135					
		170					
		200					

4.1.2.1 Physical Properties

It is seen that; film thickness is also directly proportional to induction time such as deposition voltage, but the effect of increase in the film thickness is not as high as deposition voltage since induction time does not affect the electrical attraction between the ions. It is seen that film thickness changes between 20 to 30 microns with changing induction times while deposition voltage affects the thickness with much more variation of 20 to 90 microns. Roughness of the surfaces are close to each other since the film thicknesses are not changing sharply even though it can be interpreted that roughness tends to increase with increased film thickness while gloss tends to decrease at the same time, such as seen in deposition voltage studies. The surface quality measurement results are given in Figure 4.8 and tabulated in Table A.2.

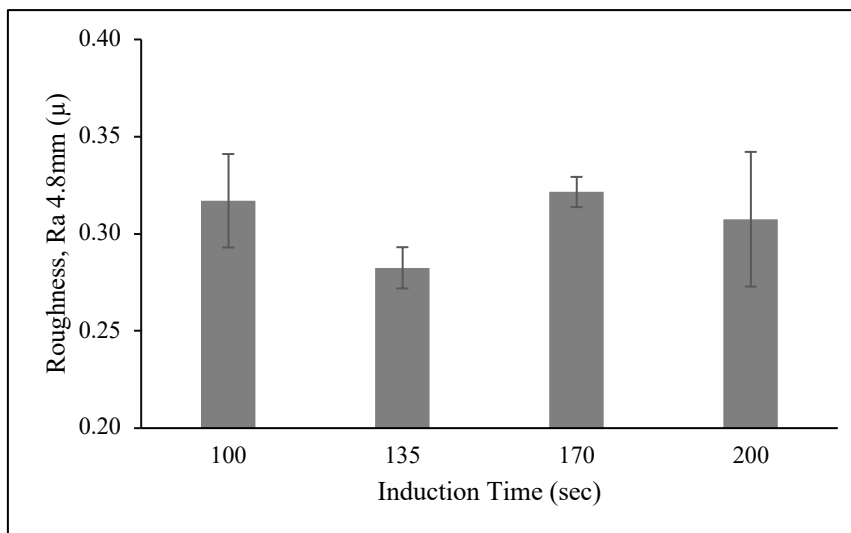
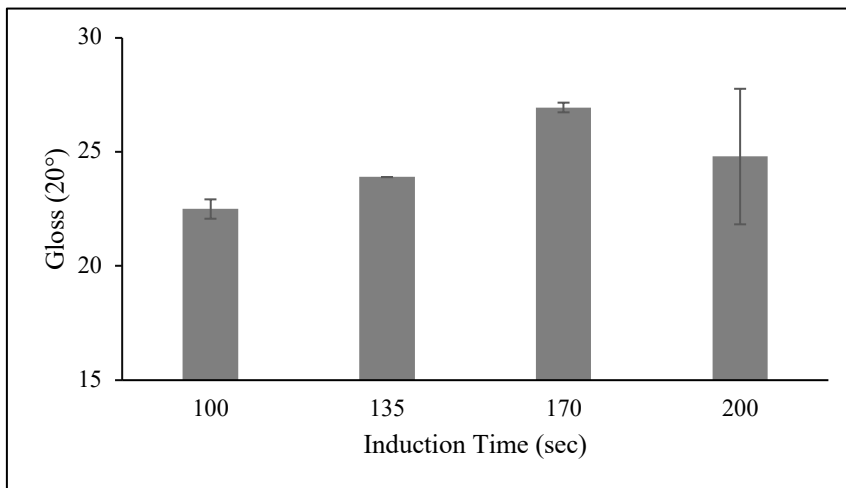
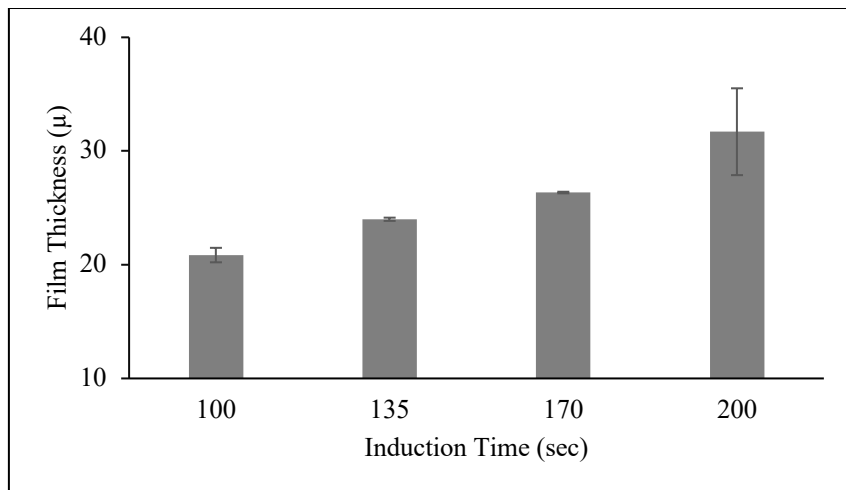


Figure 4.8 Surface Properties according to induction times. (a) Film Thickness (b) Gloss (c) Roughness

Effects of induction time of the coatings on the mechanical properties were evaluated by impact resistance, hardness and stone chip resistance tests. All investigated mechanical properties decreased with increased film thickness as in the deposition voltage studies. Mechanical properties results are given in Figure 4.9 and tabulated in Table A.2.

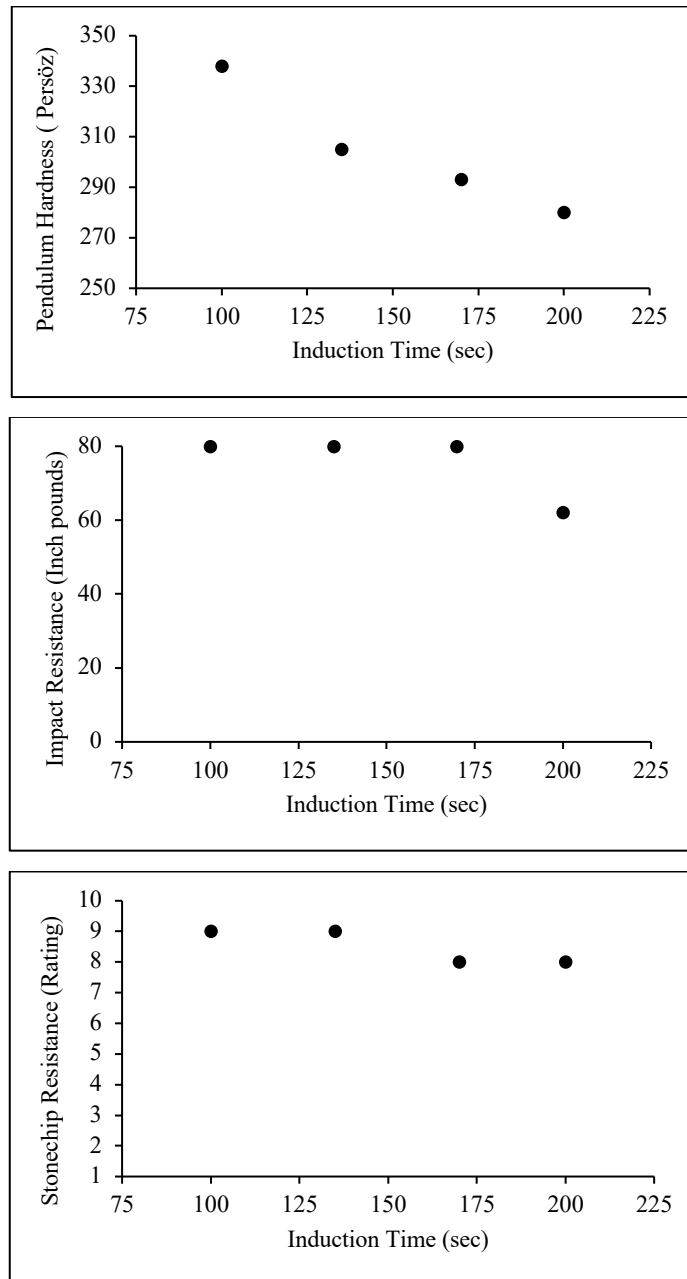


Figure 4.9 Mechanical Properties according to induction times. (a) Hardness (b) Impact Resistance (c) Stone Chip Resistance

At all levels of induction times, cross-cut adhesion test result is found as Grade 0, which is classified as pass.

4.1.2.2 Morphological Analysis

SEM studies were conducted on the surface of all compositions. SEM images taken at a magnification of 10.0 kx given in Figure 4.10 show that each induction time resulted in rather uniform distribution and negligible surface defects in epoxy matrix. A lower degree of pigment density is taking attention at the surface coated with 200 sec of induction time.

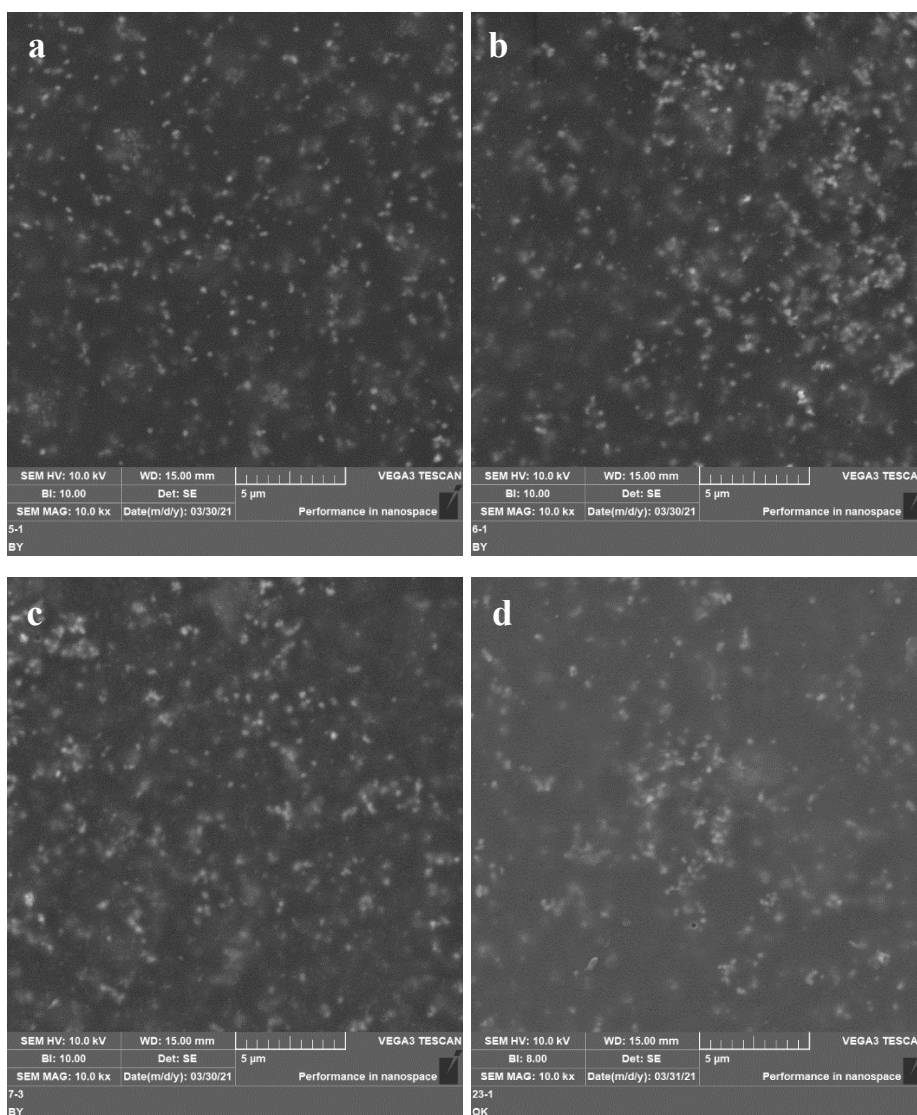


Figure 4.10 SEM images (10.0 kx) of coated panels at different induction times.
 (a) 100 sec (b) 135 sec (c) 170 sec (d) 200 sec

4.1.2.3 Thermal Analysis

Effects of induction time levels on the thermal behavior of the specimens were studied by DSC and TGA analyses. It is well known that the glass transition (T_g), of an epoxy system increases with cross-linking density as mentioned above. Glass transition temperatures of the specimens coated at different induction times are given in Figure 4.11. It is seen that there is not a significant difference between glass

transition temperatures of the specimens while the specimen coated at 200 seconds shows a slight increase in T_g that can be interpreted with the decreased amount of pigment content in the coating.

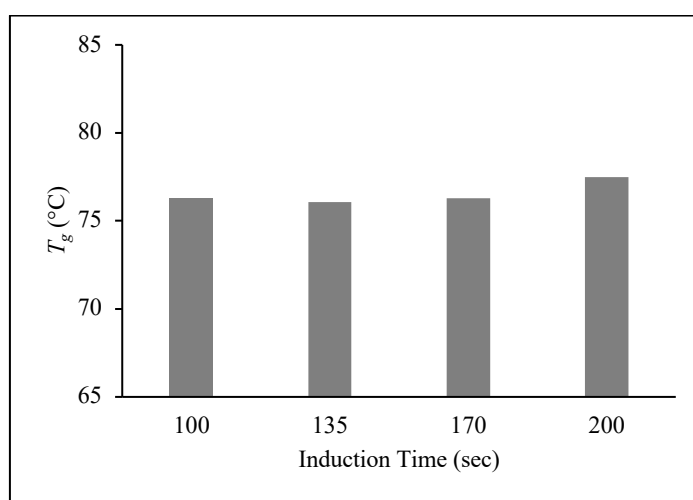


Figure 4.11 Glass transition temperature vs induction time, obtained by DSC analysis.

Residue percentage of each specimen given in Figure 4.12, while the both DSC and TGA data determined tabulated in Table A.9. TGA analysis shows that, residual percentage of the specimens are decreasing with increased induction times. This can be explained by decreased pigment ratio with increased induction times since as the film thickness increase while deposition, surface becomes insulated and induction slows. Thus pigments are not able to move forward to the cathode because of the decrease in electrical attraction.

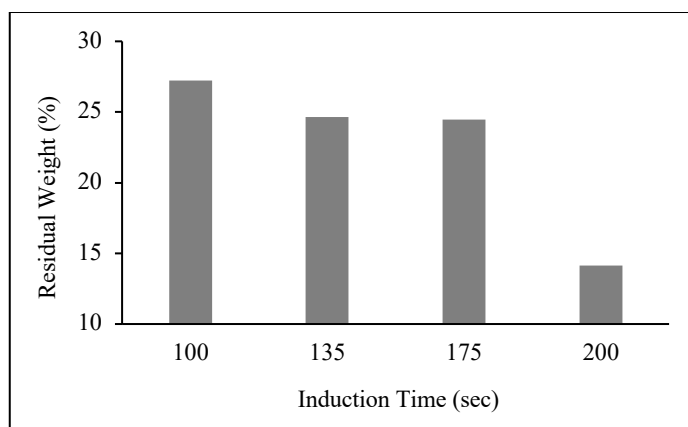


Figure 4.12 Residual weight vs induction time, obtained by TGA analysis.

4.1.3 Effect of Bath Temperature

To understand the effect of bath temperature on electrocoating reaction, five different temperatures (17.5, 25, 30, 35, 40 °C) are used, and their effect on some physical properties that are mentioned above are investigated. Process parameters are given in Table 4.4.

Table 4.4 Process parameters to understand the effect of bath temperature.

Investigated Parameter	Voltage (V)	Induction Time (sec)	Induction Temperature, °C	Pigment/Binder Ratio	Solid Content	Organic Solvent Ratio	Baking Conditions
Bath Temperature, °C	300	135	17.5	0.15	21%	2.47%	175 °C – 20”
			25				
			30				
			35				
			40				

4.1.3.1 Physical Properties

It is seen that, film thickness is also directly proportional to bath temperature as well as deposition voltage and induction time studies. The effect of the increase in the film thickness is not as high as deposition voltage but higher than induction time effect. It is seen that film thickness changes between 15 to 55 microns since this value changes between 20 to 30 microns with changing induction times from 20 to 90 microns with changing deposition voltages. In this case, film thickness increases with increased temperature most probably due to the increased mobility of resin and pigment moieties. Since the film thickness of the surface is very low at low temperatures roughness of the surface is very high due to non-homogeneous film forming. Surface becomes smoother with increased temperature up to 20-25 microns of film thickness. Then film thickness continues to increase again with increased bath temperature and roughness starts to increase again after a certain film thickness. Gloss of the surface changes inversely to the roughness of the surface. Whenever the roughness decreases gloss increases, and whenever the roughness increases, gloss starts to decrease. The surface quality measurement results are given in Figure 4.13 and tabulated in Table A.3.

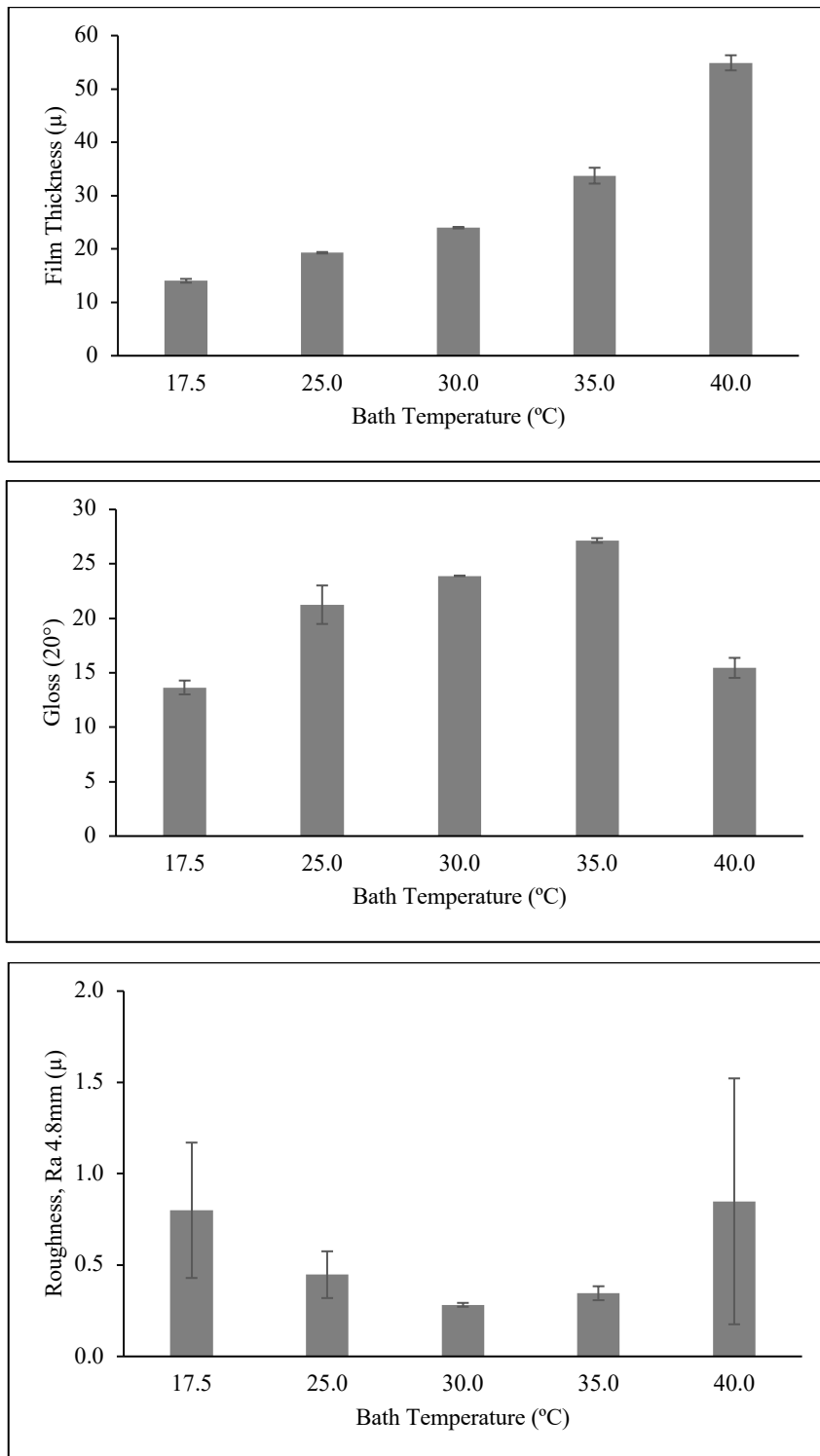


Figure 4.13 Surface Properties according to bath temperatures. (a) Film Thickness (b) Gloss (c) Roughness

Impact resistance and hardness seem to decrease with increased film thickness. Stone chip resistance of the surface decreases with increased bath temperature and thickness. Mechanical properties results are given in Figure 4.14 and tabulated in Table A.3.

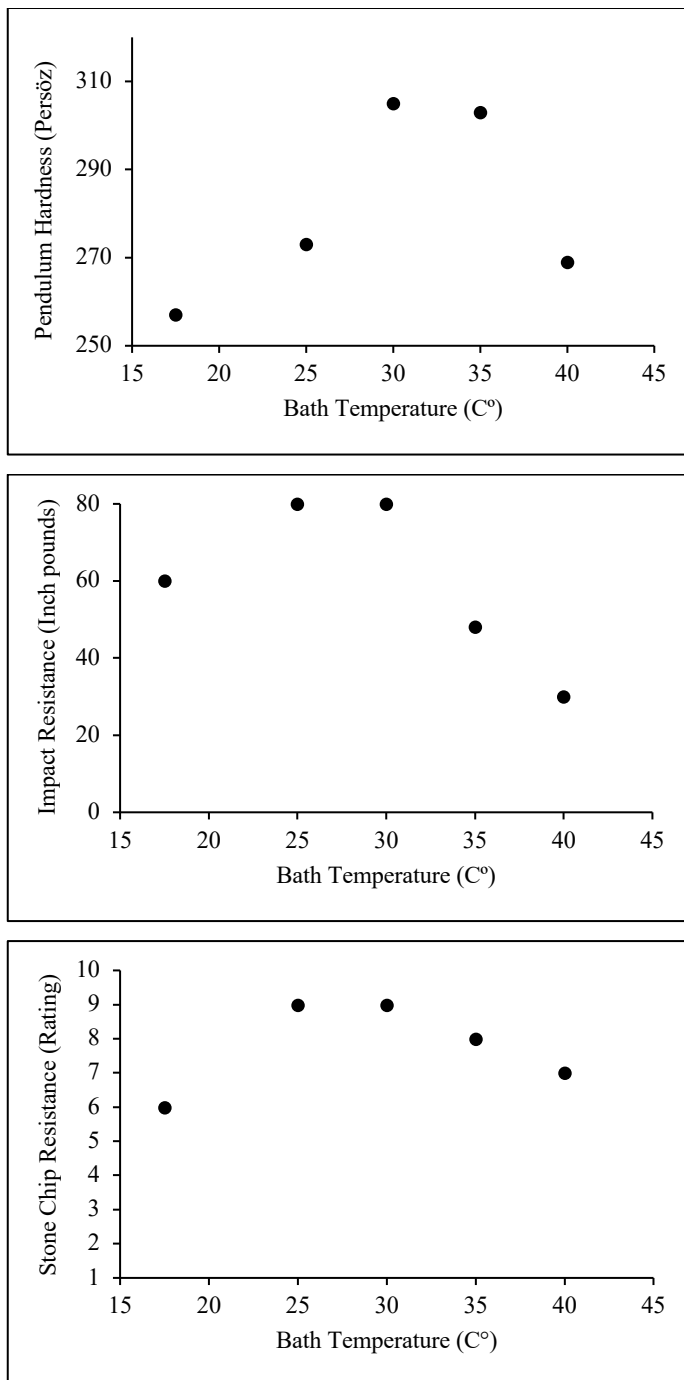


Figure 4.14 Mechanical Properties according to bath temperatures. (a) Hardness (b) Impact Resistance (c) Stone Chip Resistance

At all bath temperatures the adhesion level is found as Grade 0, which is classified as pass.

4.1.3.2 Morphological Analysis

SEM studies were conducted on the surface of all compositions. SEM images taken at a magnification of 10.0 kx given in Figure 4.15 show that coatings at low temperatures (17.5 °C and 25 °C) are seen insufficient and non-homogeneous and there are significant surface defects. Coatings at relatively higher temperatures (30 °C, 35 °C and 40 °C) are presenting more homogeneous and sufficient coatings. A higher degree of pigment agglomeration is taking attention at the surface coated at 17.5 °C. Macroscopic images of insufficient coating at low bath temperature and pinholes at high bath temperatures are given in Figure 4.16.

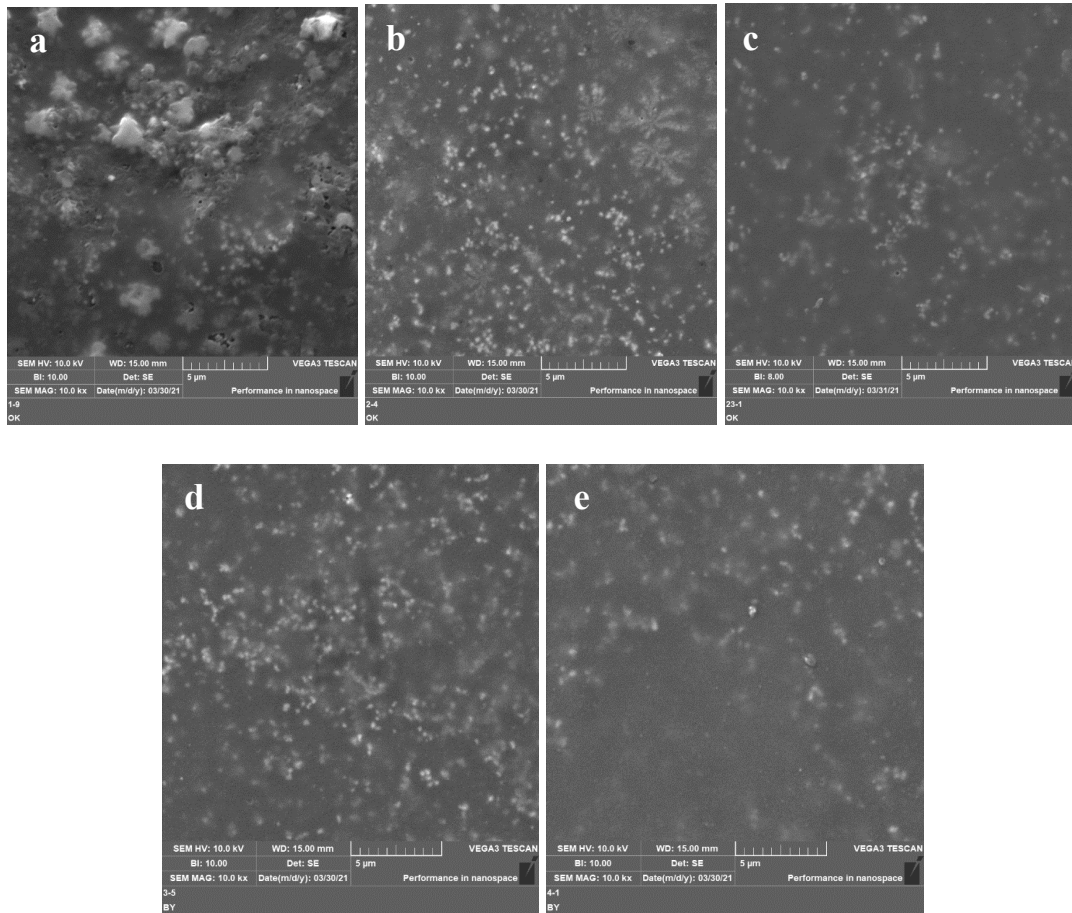


Figure 4.15 SEM images (10.0 k.x) of coated panels at different bath temperatures.
 a) 17.5 °C b) 25 °C c) 30 °C d) 35 °C e) 40 °C

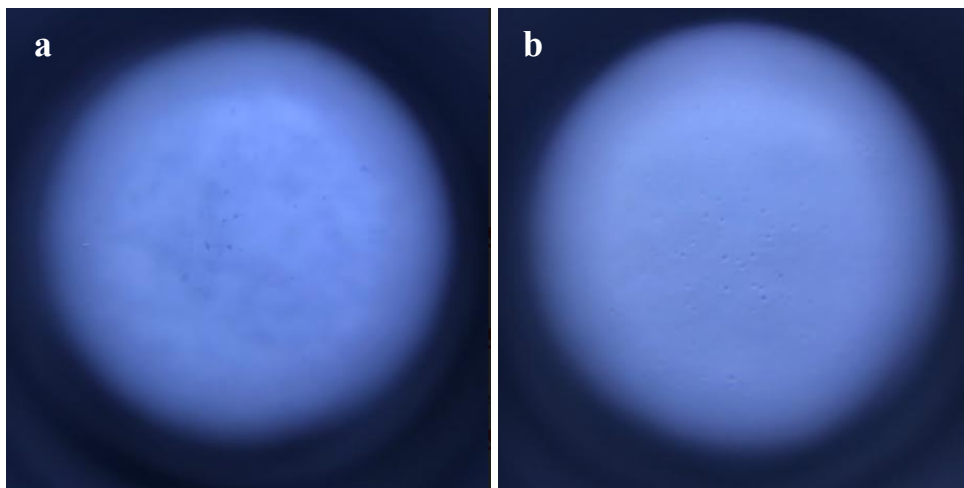


Figure 4.16 Macroscopic images of a) insufficient coating at low bath temperature 17.5 °C and b) pinholes at high bath temperature 40 °C.

4.1.3.3 Thermal Analysis

Effects of bath temperature levels on the thermal behavior of the specimens were studied by DSC and TGA analyses. Glass transition temperatures of the specimens coated at different bath temperatures are given in Figure 4.17. It is seen that at low temperatures the glass transition is the lowest, this can be interpreted with the high pigment accumulation seen in SEM analysis, which can cause a plasticizing effect between crosslinks and reduce T_g . Glass transition temperature seems to increase with increased bath temperatures that can be interpreted with the more homogeneous coating structures that provide good crosslinking reactions. At 40 °C bath temperature, again a slight decrease in glass transition is seen that can be interpreted with the increased pigment ratio due to the increased mobility of the moieties at high bath temperatures.

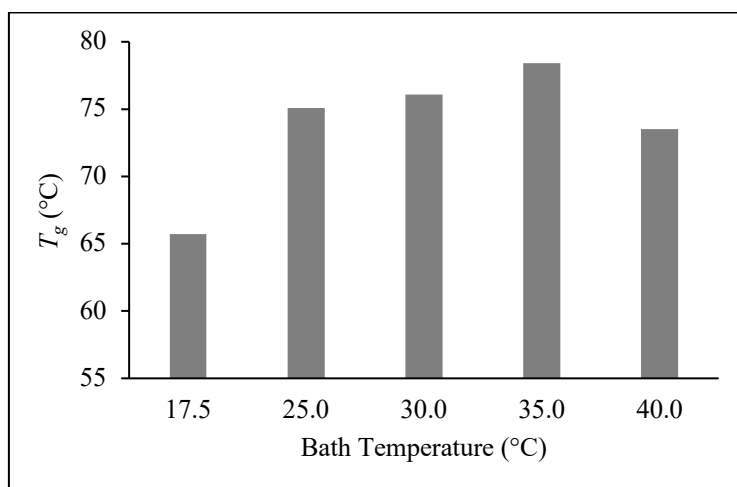


Figure 4.17 Glass transition temperature vs bath temperatures, obtained by DSC analysis.

Residue percentage of each specimen were given in Figure 4.18, while both DSC and TGA data determined were tabulated in Table A.10. TGA analysis shows that, residual percentage of the specimens are decreasing with increased bath temperatures

up to 30 °C explained with decreased pigment ratio in the coating structure. With increased temperatures higher than 30 °C, the mobility of the moieties are also increased too much and increase in the residual weight can be explained with increased pigment ratio, which is also compatible with DSC results.

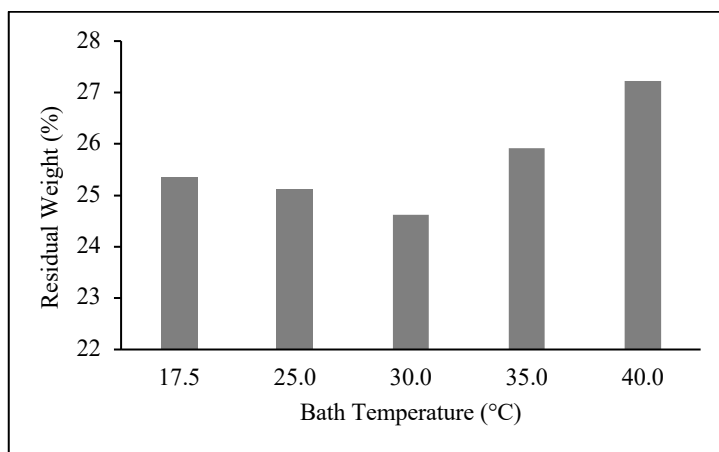


Figure 4.18 Residual weight vs bath temperature, obtained by TGA analysis.

4.1.4 Effect of Pigment over Binder Ratio

To understand the effect of pigment over binder ratio (p/b ratio) on electrocoating reaction, three different p/b ratios (0.05, 0.15, 0.25) are used, and their effect on some physical properties that are mentioned above are investigated. Process parameters are given in Table 4.5.

Table 4.5 Process parameters to understand the effect of pigment over binder ratio.

Investigated Parameter	Voltage (V)	Induction Time (sec)	Induction Temperature, °C	Pigment/Binder Ratio	Solid Content	Organic Solvent Ratio	Baking Conditions
Pigment/Binder Ratio	300	135	30	0.05	21%	2.47%	175 °C – 20”
				0.15			
				0.25			

4.1.4.1 Physical Properties

It is seen that, there is no strong correlation between film thickness and p/b ratio. There is approximately 10 microns difference between changing p/b ratios from 0.05 to 0.25. Roughness of the surface is very high, it reaches almost 0.75 at the highest binder ratio. Even though the roughness is very high, gloss is also the highest due to the increased amount of resin content in the formulation. Roughness decreases with increased pigment ratio to acceptable ranges around 0.25. Gloss also decreases with increased pigment ratio as expected. The surface quality measurement results are given in Figure 4.19 and tabulated in Table A.4.

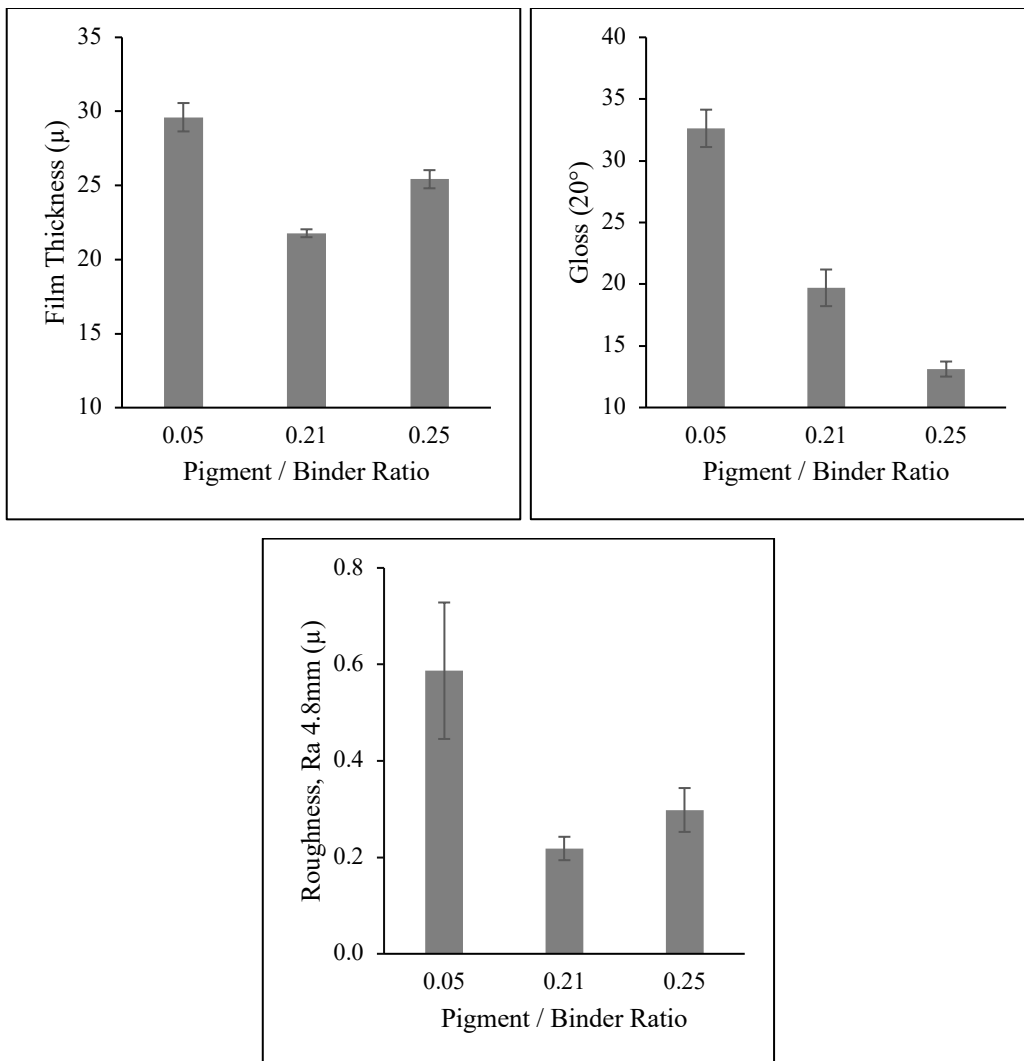


Figure 4.19 Surface Properties according to Pigment/Binder Ratio. (a) Film Thickness (b) Gloss (c) Roughness

Impact resistance is high enough for all test specimens, it seems that the sensitivity of the testing equipment is not enough to distinguish the effect of pigment over binder ratio on the test specimens. Hardness increases with increased pigment ratio. At low levels of pigment ratio hardness is the lowest. Besides stone chip resistance is also the lowest at low pigment ratio. Stone chip resistance of the surface is not proportional to p/b but compatible with film thickness.

It increases with low film thickness and decreases with high film thickness. Also it can be said that; with increased pigment ratio, hardness of the surface is increasing but stone chip resistance of the surface is decreasing after a certain value since the decrease of resin ratio also decrease the crosslinking density in the formulation. Resin ratio is critical for the mechanical properties of the formulation. Mechanical properties results are given in Figure 4.20 and tabulated in Table A.4.

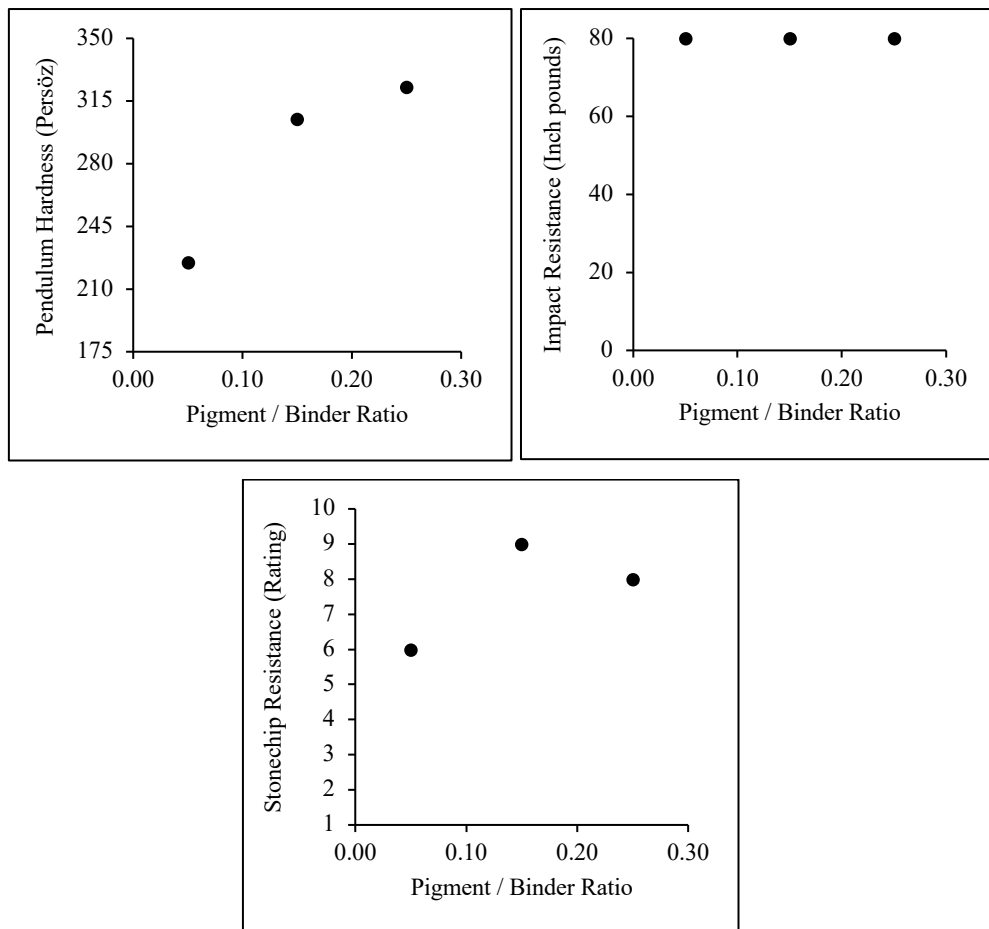


Figure 4.20 Mechanical properties according to pigment/binder ratio. (a) Hardness (b) Impact Resistance (c) Stone Chip Resistance

At all pigment/binder ratios the adhesion level is found as Grade 0 (Pass).

4.1.4.2 Morphological Analysis

Craters and pinholes are occurred mostly on the surface at very low pigment ratio. ED accumulations and larger pinholes are seen on high pigment ratios. According to the SEM analysis given in Figure 4.21, coatings at different pigment/binder ratios are significantly different. At low pigment levels pinholes are appeared mostly on the surface and coating density is relatively lower, at high pigment levels pigment agglomerations, surface defects and larger pores are seen in SEM analysis. Macroscopic image of craters and pinholes at 0.05 p/b ratio are given in Figure 4.22.

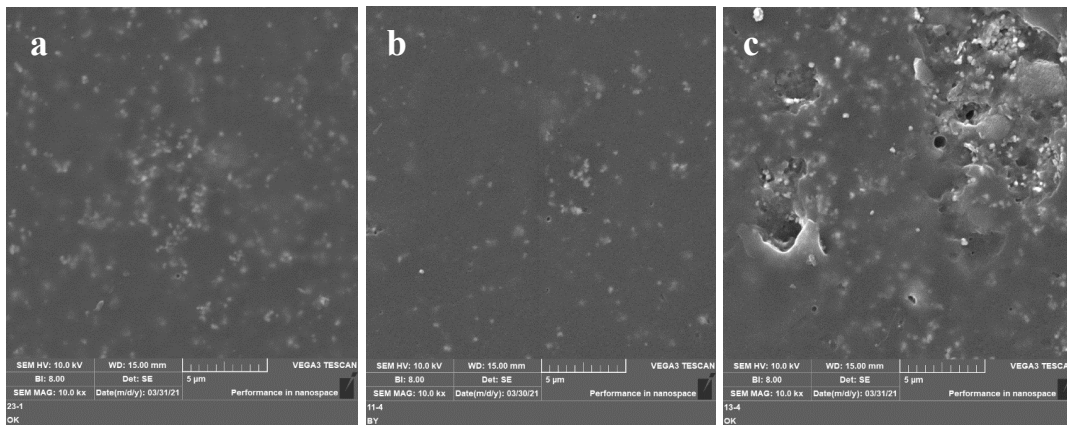


Figure 4.21 SEM images (10.0 kx) of coated panels at different pigment over binder ratios. a) 0.05 b) 0.15 c) 0.25

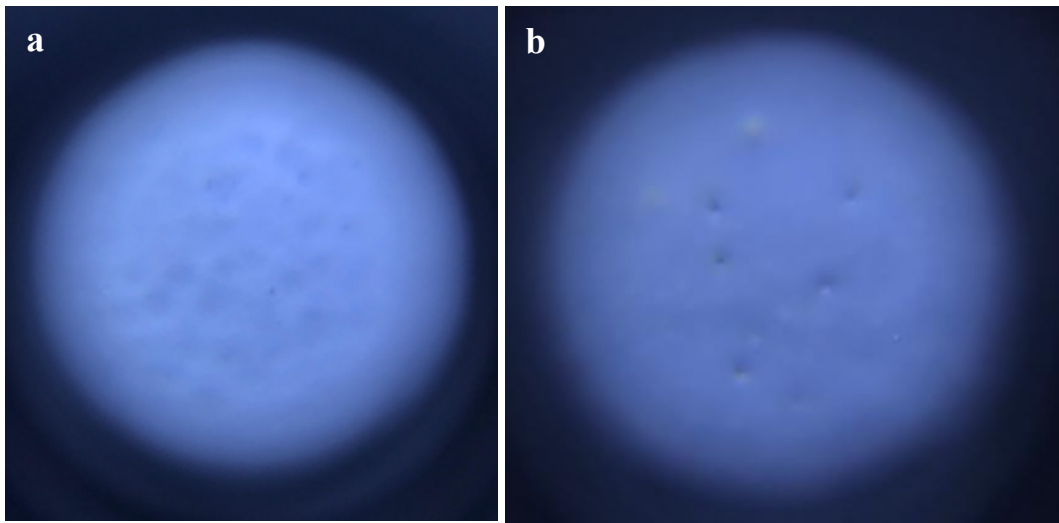


Figure 4.22 Macroscopic image of craters and pinholes that are seen at low p/b ratio (0.05). a) Craters b) Pinholes

4.1.4.3 Thermal Analysis

DSC and TGA analyses are conducted to see the effects of p/b ratio on the thermal behavior of the specimens. Glass transition temperatures of the specimens coated at different p/b ratios are given in Figure 4.23. It is seen that at low pigment ratios the glass transition is the highest, this can be interpreted with the higher crosslinking density of the resin unaffected by trapping effect of the pigment. At high levels of pigment ratio, pigment accumulation, which is also seen in SEM analysis, causes a plasticizing effect between crosslinks and reduce T_g .

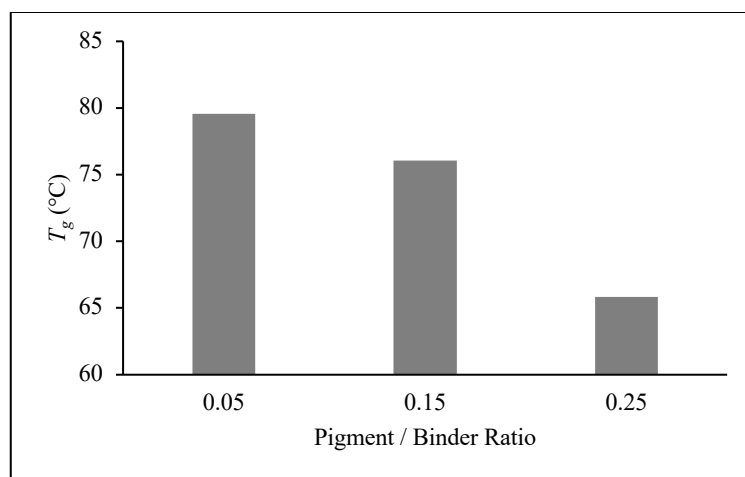


Figure 4.23 Glass transition temperature vs pigment/binder ratios, obtained by DSC analysis.

Residue percentage of each specimen were given in Figure 4.24, while the both DSC and TGA data determined were tabulated in Table A.11. TGA analysis shows that, residual percentage of the specimens are increasing with increased pigment ratio as expected, explained with increase in inorganic content in the coating structure which is also compatible with DSC results.

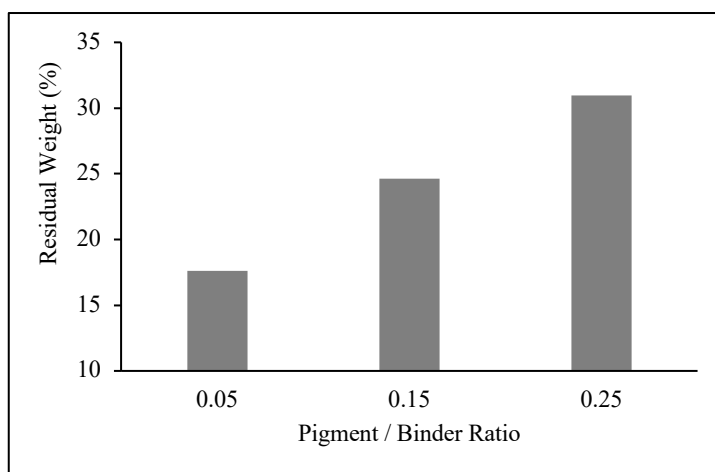


Figure 4.24 Residual weight vs pigment/binder ratios, obtained by TGA analysis.

4.1.5 Effect of Solid Content Ratio

To understand the effect of solid ratio in the dispersion on electrocoating reaction, 3 different solid ratios (15, 21, 27 %) are examined, and their effect on some physical properties that are mentioned above are investigated. Process parameters are given in Table 4.6.

Table 4.6 Process parameters to understand the effect of solid content ratio.

Investigated Parameter	Voltage (V)	Induction Time (sec)	Induction Temperature, °C	Pigment/Binder Ratio	Solid Content	Organic Solvent Ratio	Baking Conditions
Solid Content, %	300	135	30	0.15	15%	2.47%	175 °C – 20’’
					21%		
					27%		

4.1.5.1 Physical Properties

It is seen that, there is not a significant proportionality between film thickness and solid content ratio. There is approximately 4-5 microns difference between changing solid content ratios from 15% to 27%. Roughness of the surfaces are very close to each other and all of them are changing from 0.20 to 0.25 that is acceptable for most purposes. Gloss of the surfaces are also close to each other and changing around 20 at 20° measurement angle. The surface quality measurement results are given in Figure 4.25 and tabulated in Table A.5.

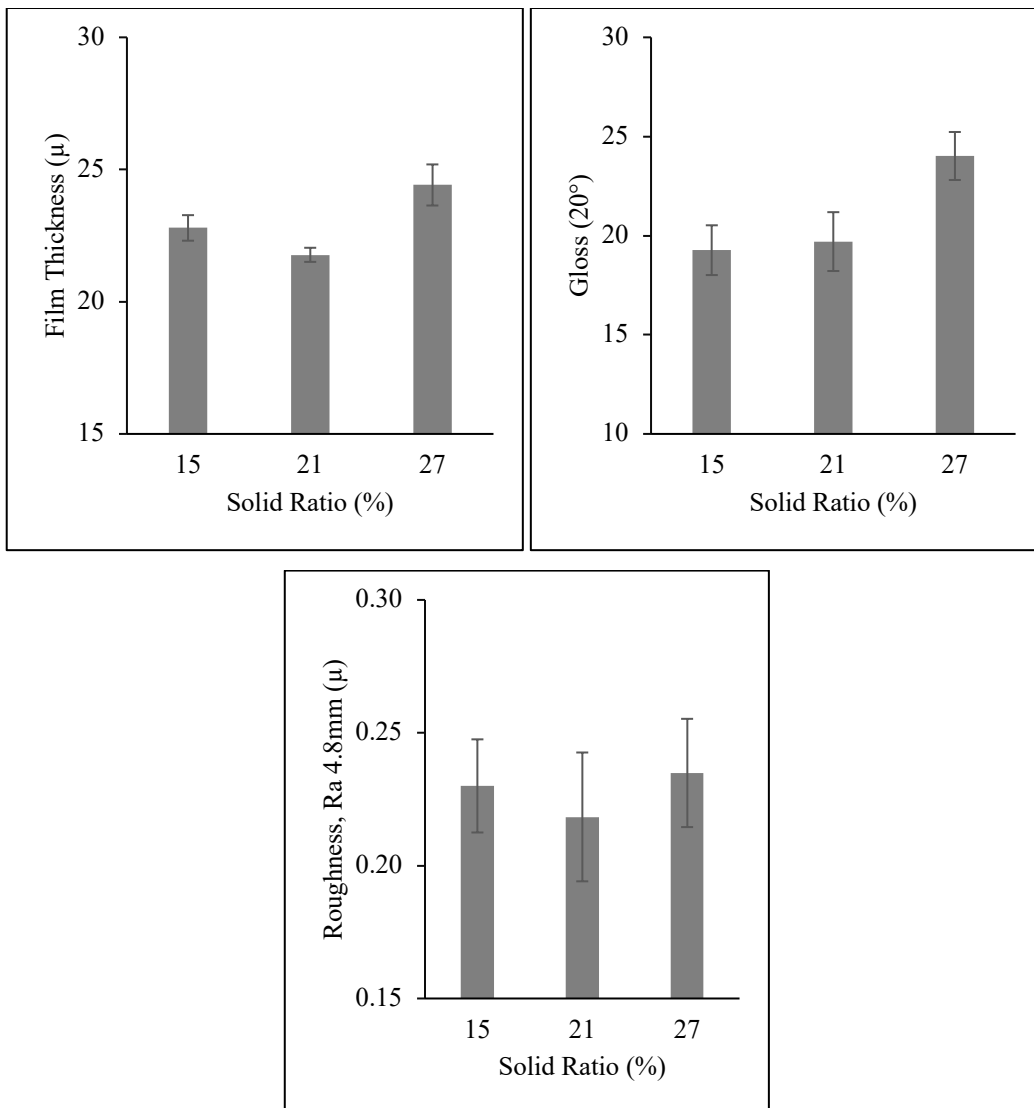


Figure 4.25 Surface Properties according to solid content ratio. (a) Film Thickness (b) Gloss (c) Roughness

Impact resistance is high enough for all test specimens, it seems that the sensitivity of the testing equipment is not enough to distinguish the difference. Hardness increases with increased solid content ratio. As seen on pigment/binder ratio study, at low levels of solid content ratio hardness is the lowest. Besides stone chip resistance is also the lowest at low solid content ratio. Stone chip resistance of the surface is not proportional to solid content but compatible with film thickness such as seen in pigment/binder ratio studies.

It increases with low film thickness and decreases with high film thickness. Also it can be said that; with increased solid content ratio, hardness of the surface is increasing but stone chip resistance of the surface is decreasing after a certain value since the decrease of the mobility of the moieties decrease the crosslinking density in the formulation. Mechanical properties results are given in Figure 4.26 and tabulated in Table A.5.

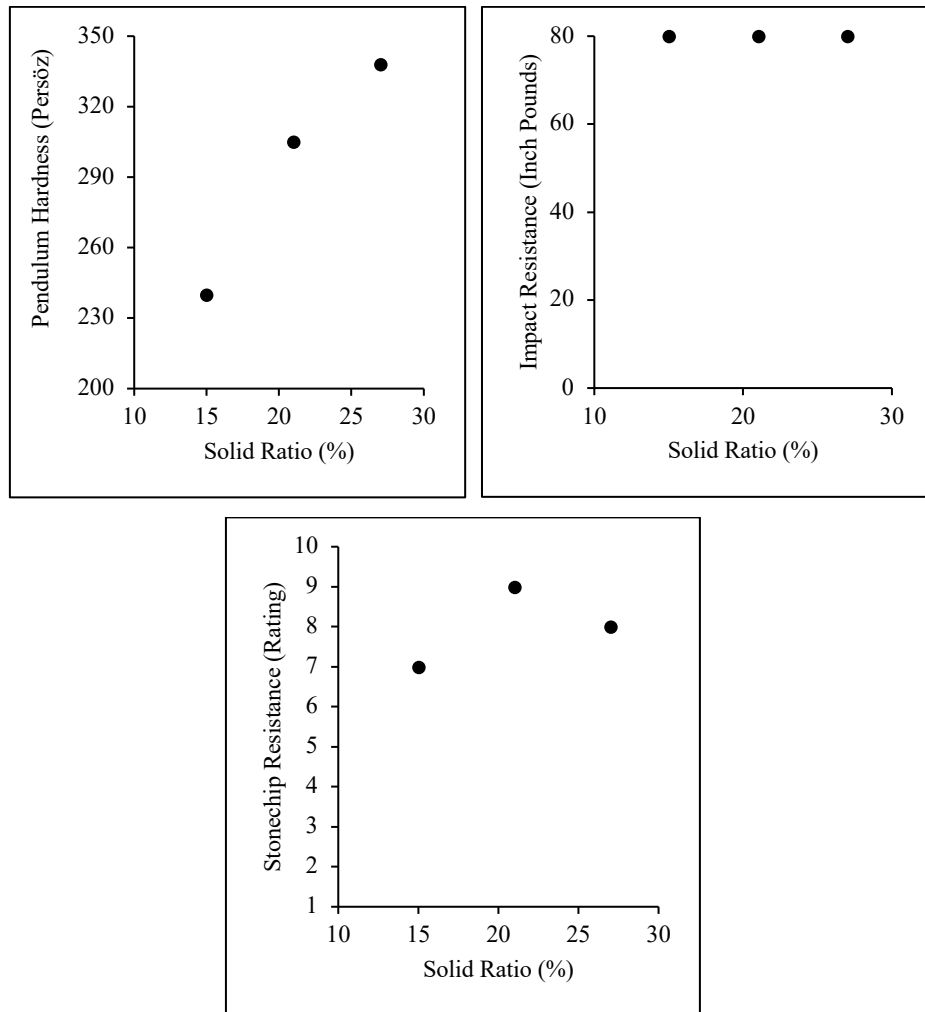


Figure 4.26 Mechanical properties according to solid content ratio. (a) Hardness (b) Impact Resistance (c) Stone Chip Resistance

A cross-cut adhesion test is applied to the coatings to understand if the adhesion level is good enough for most purposes or not. At all solid content ratios the adhesion level is found good enough especially for automotive coatings.

4.1.5.2 Morphological Analysis

SEM images taken at a magnification of 2.5 kx given in Figure 4.27 show that no specific surface defects or significant differences are seen on the coatings at different solid content ratios.

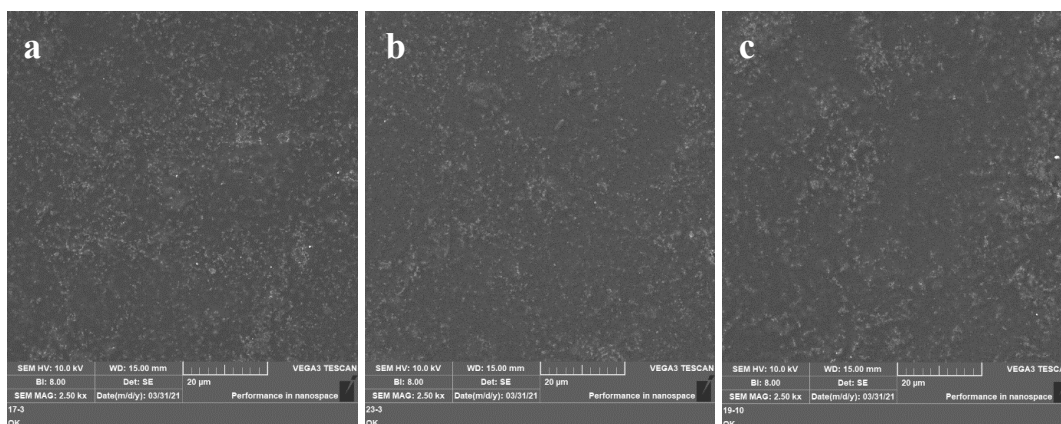


Figure 4.27 SEM images (2.5 kx) of coated panels at different solid content ratios.
a) 15% b) 21% c) 27%

4.1.5.3 Thermal Analysis

Effects of solid content ratio on the thermal behavior of the specimens were studied by DSC and TGA analyses. Glass transition temperatures of the specimens coated at different solid content ratios are given in Figure 4.28. The results are very similar to pigment over binder ratio studies. Higher resin amount in the coating results in increased crosslinking density. It is seen that at low solid content ratios the glass transition is the highest, this can be interpreted with the uniform coating structure that has a higher crosslinking density. Amount of the transported resin with the

increased mobility of the moieties due to low viscosity of the solution increases at low viscosity mediums. At high levels of solid content ratio, viscosity of the solution increase and mobility of the moieties decrease, so a blocking effect can be occurred by pigment moieties that cause a slight decrease in glass transition temperature.

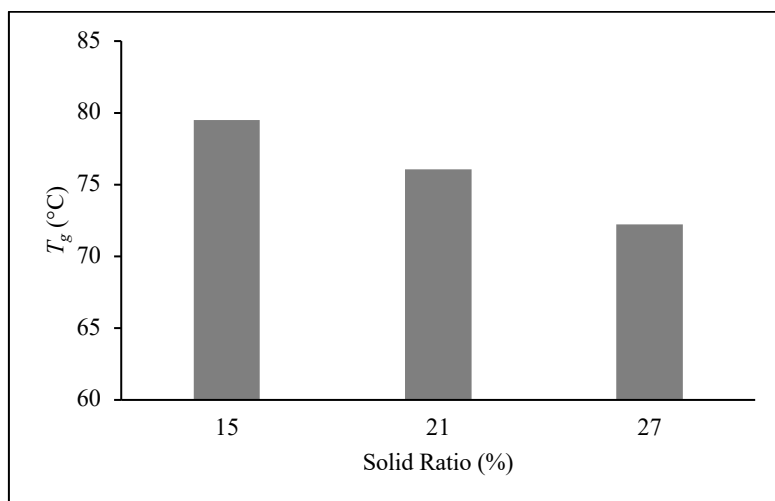


Figure 4.28 Glass transition temperature vs solid content ratios, obtained by DSC analysis.

Residue percentage of each specimen were given in Figure 4.29, while both DSC and TGA data determined were tabulated in Table A.12. TGA analysis shows that, residual percentage of the specimens are increasing with increased solid content ratio as expected, explained with increase in inorganic content in the coating structure which is also compatible with DSC results due to decreased mobility of the moieties.

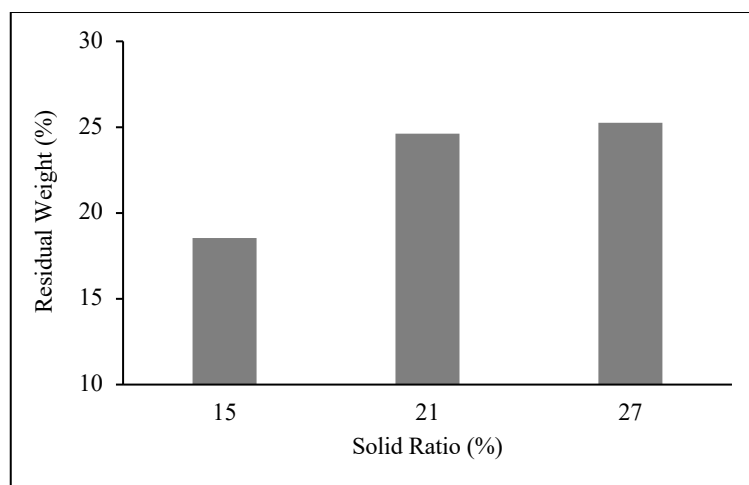


Figure 4.29 Residual weight vs solid content ratios, obtained by TGA analysis.

4.1.6 Effect of Organic Solvent Content Ratio

To understand the effect of organic solvent ratio in the dispersion on electrocoating reaction, three different organic solvent ratios (2.47, 4.85, 7.11%) are used, and their effect on some physical properties that are mentioned above are investigated. Process parameters are given in Table 4.7.

Table 4.7 Process parameters to understand the effect of organic solvent content ratio.

Investigated Parameter	Voltage (V)	Induction Time (sec)	Induction Temperature, °C	Pigment/Binder Ratio	Solid Content	Organic Solvent Ratio	Baking Conditions
Organic Solvent Ratio, %	300	135	30	0.15	21%	2.47%	175 °C – 20”
						4.85%	
						7.11%	

4.1.6.1 Physical Properties

It is seen that film thickness is proportional to organic solvent ratio. Increased solvent ratio increases mobility of the moieties that resulted in increase in the film thickness of the coating. Roughness of the surface is increasing with increased solvent ratio as expected because of increased film thickness. The results are compatible to previous parameter investigations. Gloss of the surface is optimum at low levels of solvent ratio. With increased film thickness gloss is decreasing, surface is getting deteriorated. The surface quality measurement results are given in Figure 4.30 and tabulated in Table A.6.

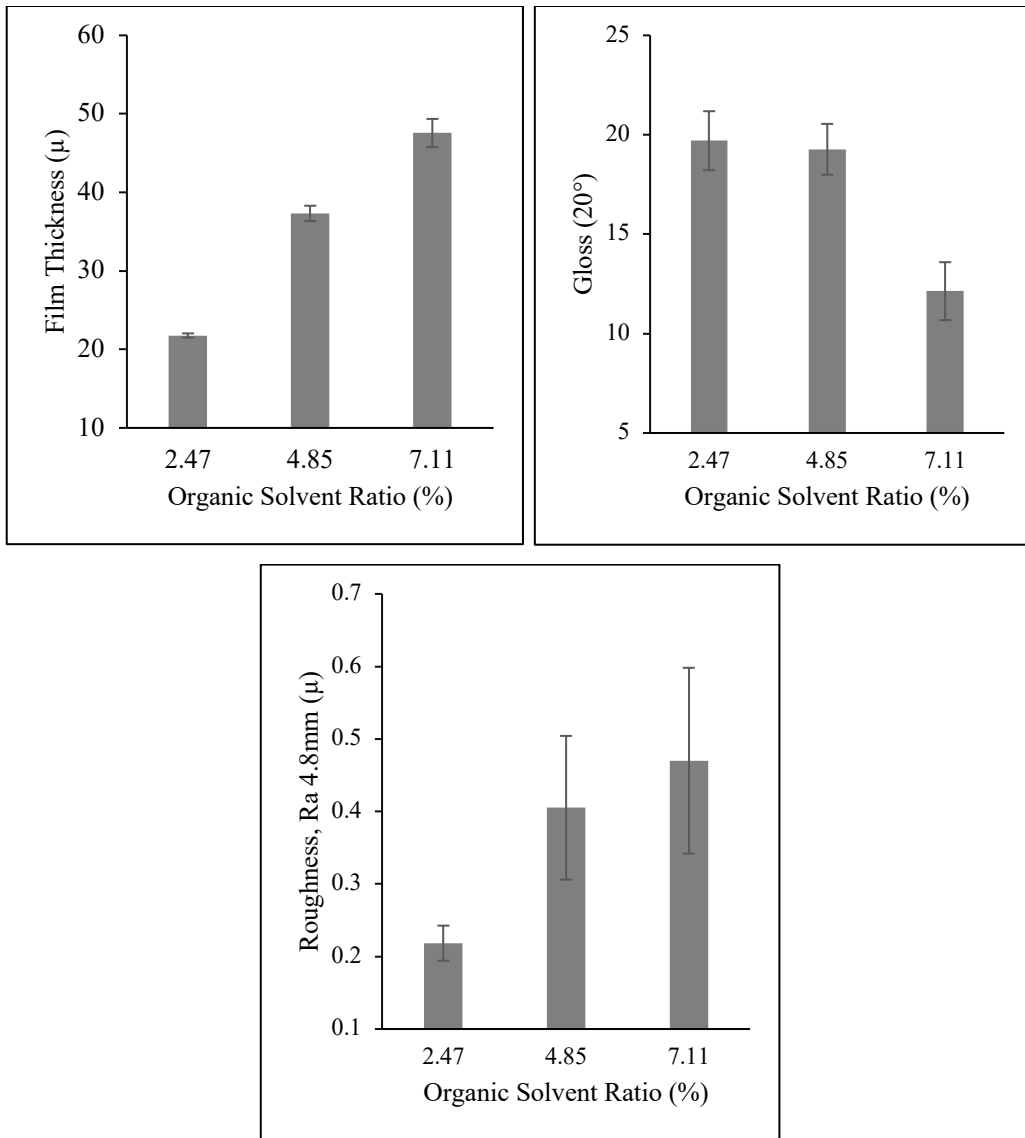


Figure 4.30 Surface Properties according to Organic Solvent Ratio. (a) Film Thickness (b) Gloss (c) Roughness

According to the mechanical analysis, impact resistance and stone chip resistance of the coatings are decreasing with increased organic solvent ratio. The decrease in impact resistance and stone chip ratio can be explained with the high film thicknesses which are around 40-50 microns at higher organic solvent ratios. Hardness seems not proportional to organic solvent ratio. Mechanical properties results are given in Figure 4.31 and tabulated in Table A.6.

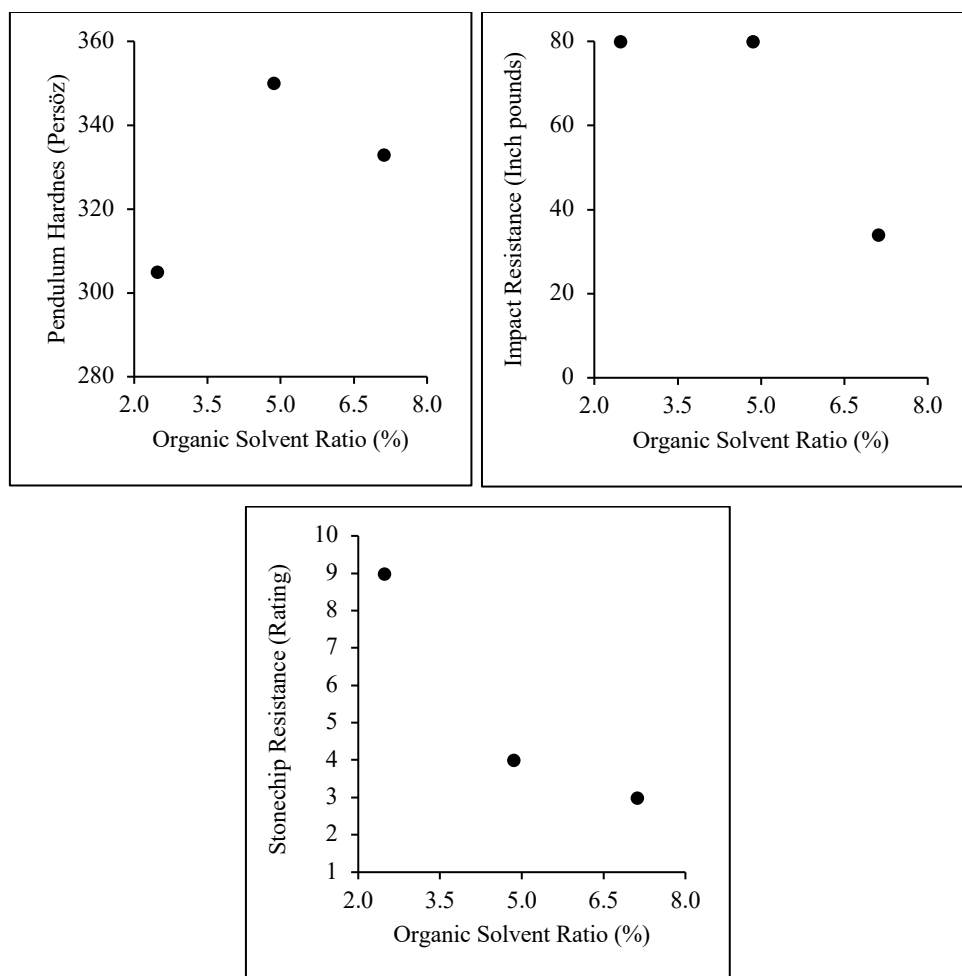


Figure 4.31 Mechanical properties according to organic solvent ratio. (a) Hardness (b) Impact Resistance (c) Stone Chip Resistance

At all organic solvent ratios, the adhesion level is Grade 0 (Pass).

4.1.6.2 Morphological Analysis

At high organic solvent levels surface defects and larger pores are seen in SEM analysis which can be explained with excessively increased film thickness due to the increased mobility of the moieties because of the decrease in solution viscosity. Viscosity decrease in the paint dispersion provides a facilitator effect on movements

of the electrically conductive media including pigment and resin micelles, which result in higher film thickness. SEM images are given in Figure 4.32.

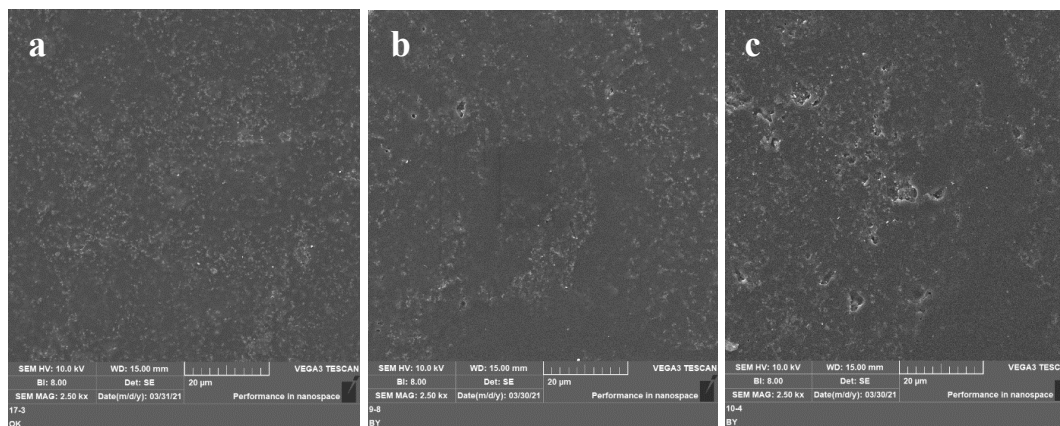


Figure 4.32 SEM images (2.5 kx) of coated panels at different organic solvent ratios. a) 2.47% b) 4.85% c) 7.11%

4.1.6.3 Thermal Analysis

Effect of organic solvent ratio on the thermal behavior of the specimens were studied by DSC and TGA analyses. Glass transition temperatures of the specimens coated at different organic solvent ratios are given in Figure 4.33. The results are very similar and there is not a significant difference between different organic solvent ratios.

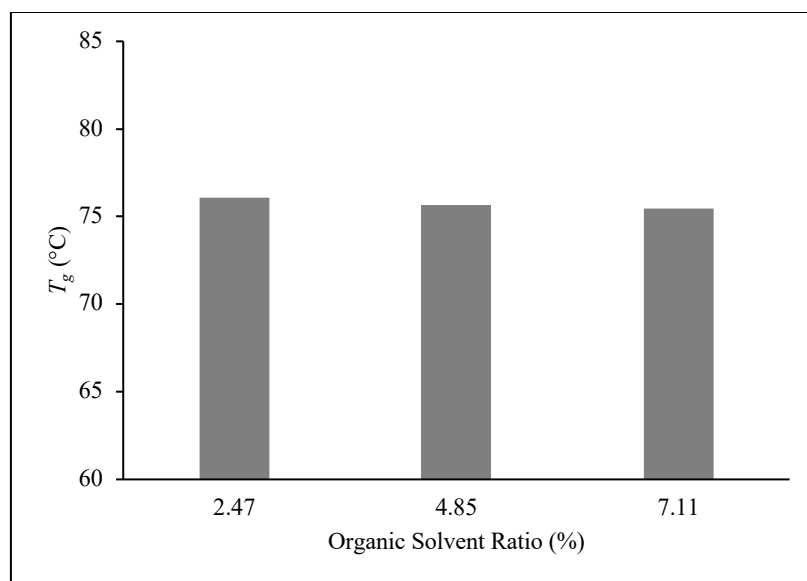


Figure 4.33 Glass transition temperature vs organic solvent ratios, obtained by DSC analysis.

Residue percentage of each specimen were given in Figure 4.34, while both DSC and TGA data determined were tabulated in Table A.13. TGA analysis shows that, residual percentage of the specimens are close to each other except for the 4.85% specimen. This can be explained with non-homogeneity of the coating surface.

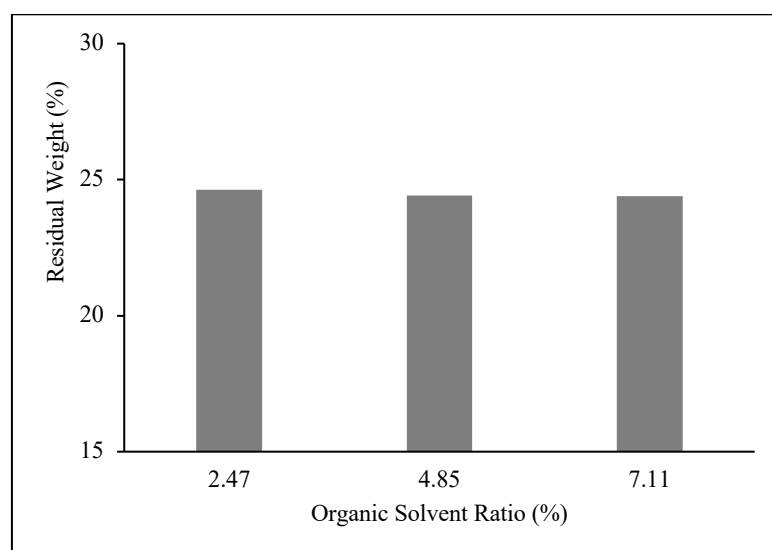


Figure 4.34 Residual weight vs organic solvent ratios, obtained by TGA analysis.

4.1.7 Effect of Baking Temperature

In this part of the study, to understand the effect of baking temperature on electrocoating reaction, three different baking temperatures (at 135, 175, 195 °C - 20'') are used, and their effect on some physical properties that are mentioned above are investigated. Process parameters are given in Table 4.8.

Table 4.8 Process parameters to understand the effect of baking temperature.

Investigated Parameter	Voltage (V)	Induction Time (sec)	Induction Temperature, °C	Pigment/Binder Ratio	Solid Content	Organic Solvent Ratio	Baking Conditions
Baking Conditions	300	135	30	0.15	21%	2.47%	135 °C – 20''
							175 °C – 20''
							195 °C – 20''

4.1.7.1 Physical Properties

Film thickness has no relation with baking temperature since the coating reaction is not affected from the baking conditions. At 135 °C the coating seemed underbaked, the surface was very glossy and smooth like a mirror, but very soft as well that nails made some scratches easily on the surface. It is seen that roughness of the surface is very low at underbake conditions but is increasing with increased crosslinks and stays almost constant with fully crosslinking. There is not a significant difference between 175 and 195 °C coated panels in terms of roughness and gloss. Gloss of the surface is very high at underbake conditions but decreasing with increased crosslinks and stays almost constant with fully crosslinking. The surface quality measurement results are given in Figure 4.35 and tabulated in Table A.7.

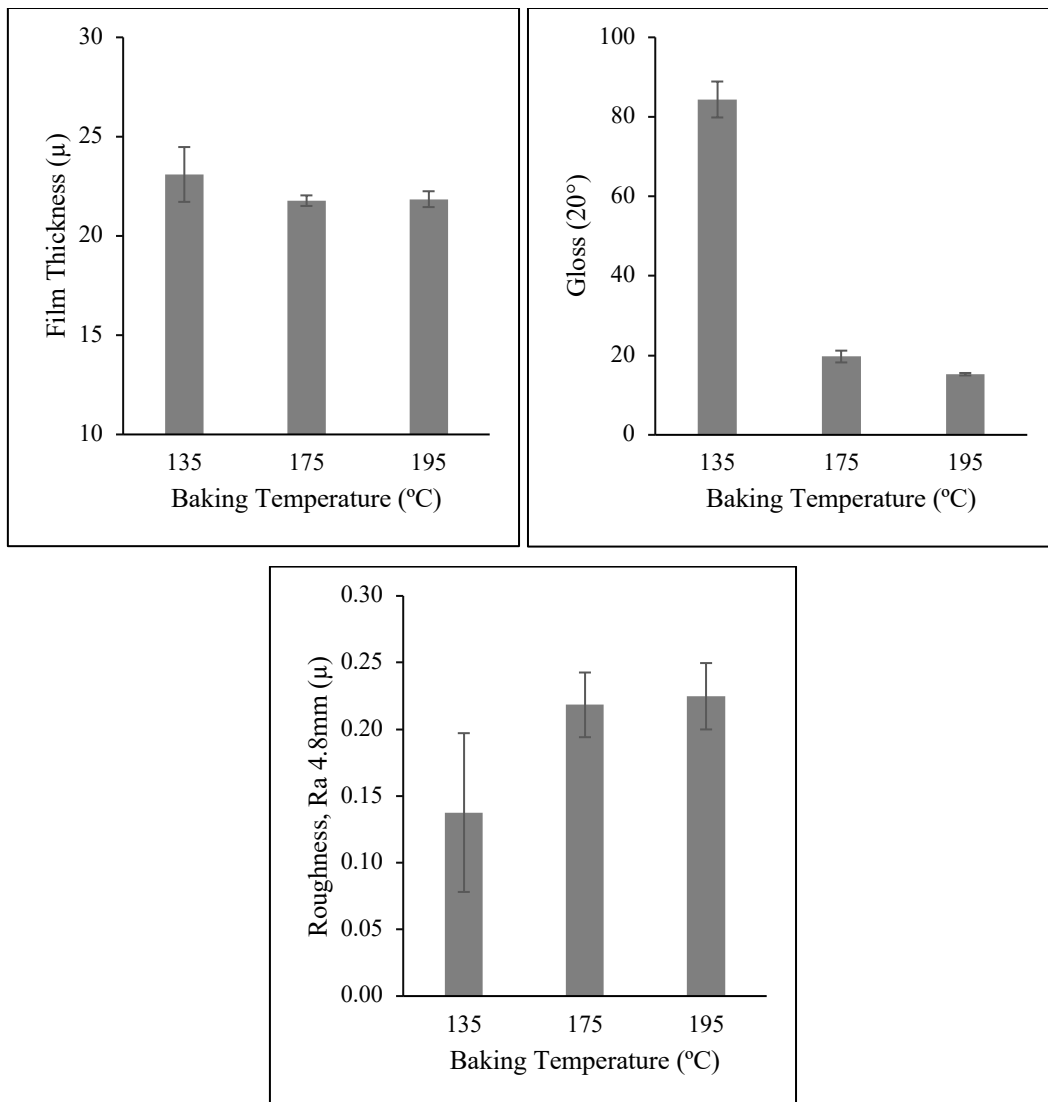


Figure 4.35 Surface Properties according to baking temperatures. (a) Film Thickness (b) Gloss (c) Roughness

According to the mechanical analysis, hardness seems very low at underbake condition but increases with improved baking conditions at higher temperatures. Impact resistance is high enough for most purposes, that the sensitivity of the equipment is not good enough to distinguish the difference, and stone chip resistance of the coatings are increasing with increased baking temperatures. Mechanical properties results are given in Figure 4.36 and tabulated in Table A.7.

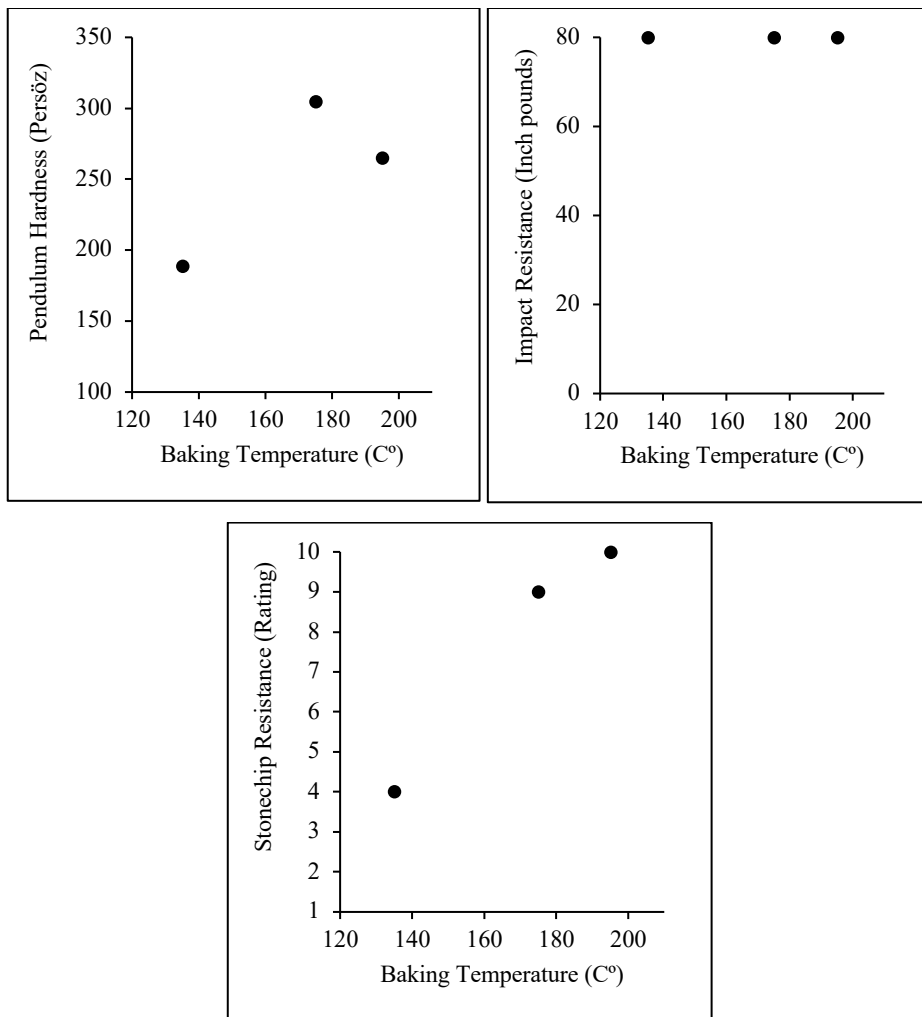


Figure 4.36 Mechanical properties according to baking temperatures. (a) Hardness (b) Impact Resistance (c) Stone Chip Resistance

Cross-cut adhesion test result for each specimen is classified as pass.

4.1.7.2 Morphological Analysis

According to the SEM analysis, underbake condition is drawing attention, the panels that baked at 175 and 195 °C have a uniform coating structure where the specimen coated at 135 °C has lots of deformations and nonconformity. SEM images of the coatings are given in Figure 4.37 and Figure 4.38.

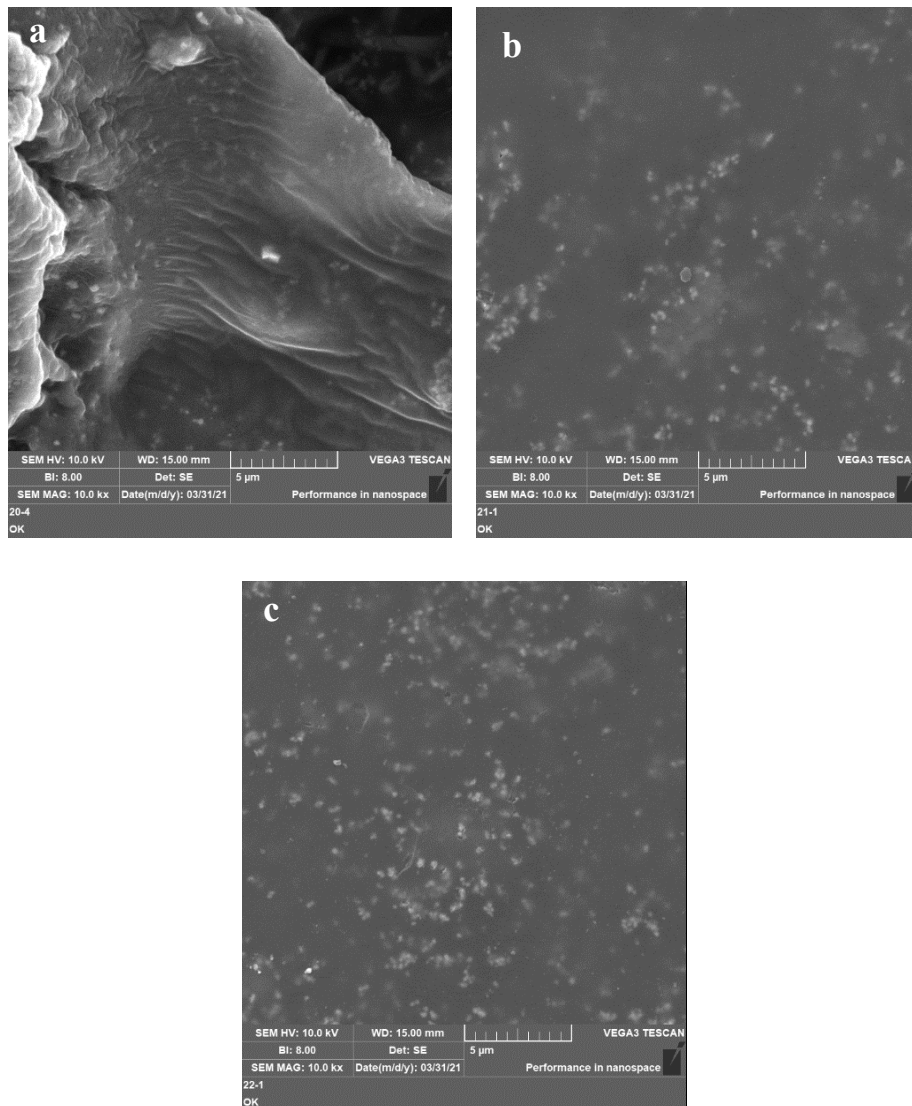


Figure 4.37 SEM images (10.0 kx) of coated panels at different baking temperatures. a) 135 °C b) 175 °C c) 195 °C

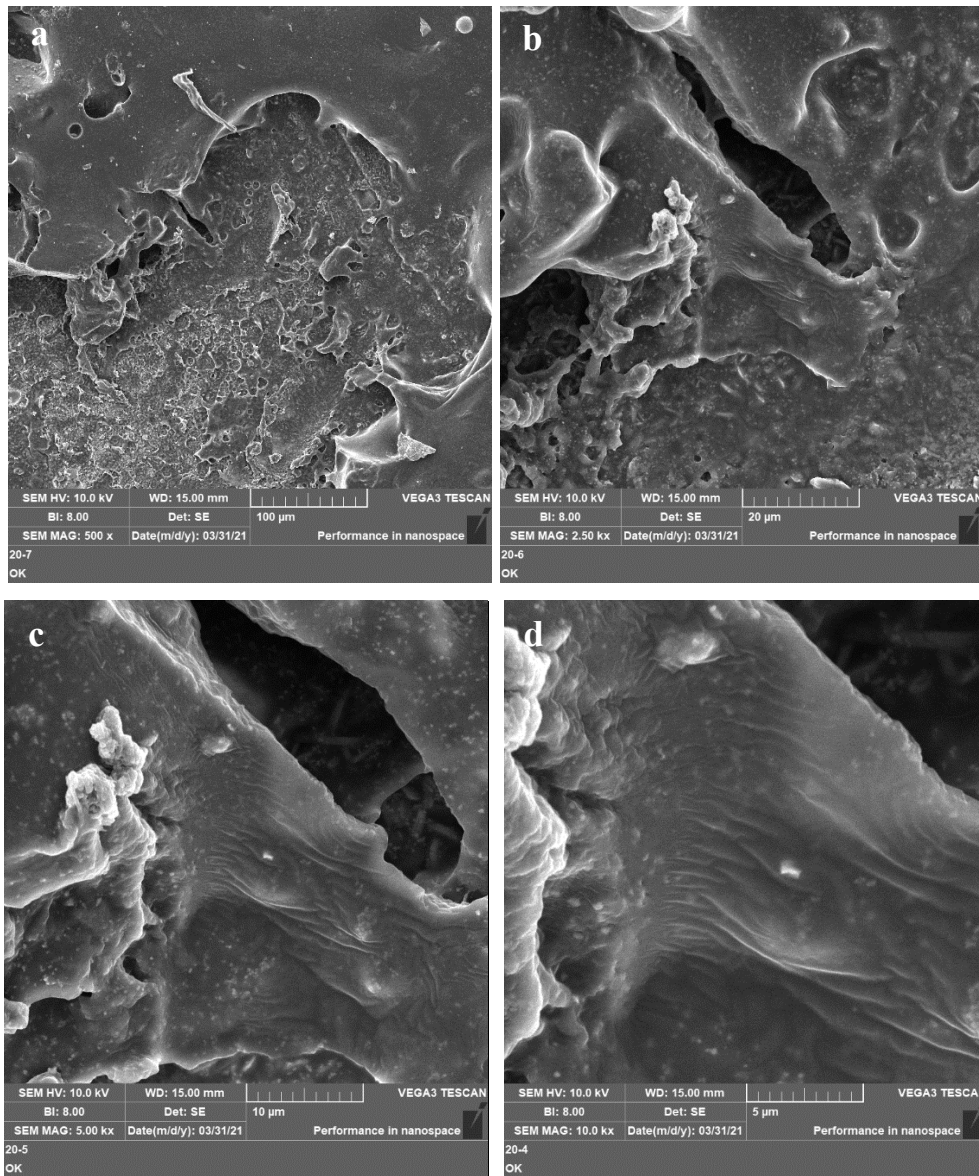


Figure 4.38 SEM images of 135 °C baking condition at different magnifications.
a) 500x b) 2.50 kx c) 5.00 kx d) 10.00 kx

4.1.7.3 Thermal Analysis

Effects of baking conditions on the thermal behavior of the specimens were studied by DSC and TGA analyses. Glass transition temperatures of the specimens coated at different baking conditions are given in Figure 4.39. It is seen that at low baking conditions the glass transition is the lowest, this can be interpreted with the insufficient crosslinking density of the resin which is underbaked. At high levels of curing temperature, crosslinking density is increased as well as T_g .

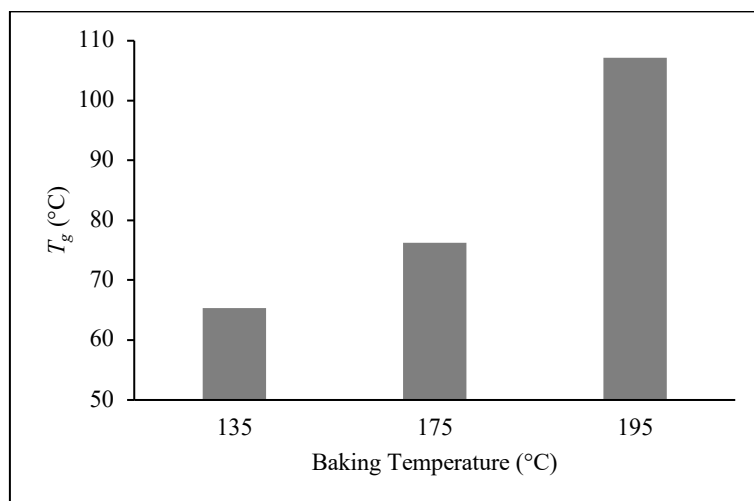


Figure 4.39 Glass transition temperature vs baking temperatures, obtained by DSC analysis.

Residue percentage of each specimen were given in Figure 4.40, while both DSC and TGA data determined were tabulated in Table A.14. TGA analysis shows that, residual percentage of the specimens are close to each other for 135 and 175 °C but increased at overbake condition which is 195 °C. This can be explained with the increased trapping effect to inorganic contents by increased crosslinking density at overbaking condition.

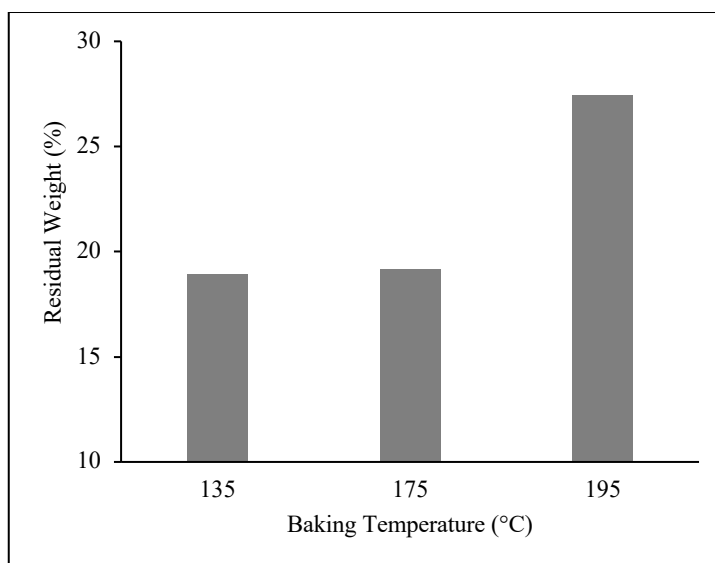


Figure 4.40 Residual weight vs baking temperatures, obtained by TGA analysis.

4.1.8 Overall Evaluation of Preliminary Assessment

4.1.8.1 Surface Quality and Performance Analysis

Surface quality in terms of roughness, dirt, crater and pinholes and physical properties in terms of stone chip resistance, adhesion, hardness and thickness were investigated by revealing the influences of seven different parameters.

Investigated parameters are deposition voltage, induction time, bath temperature, pigment/binder ratio, solid content ratio, organic solvent content ratio and finally baking conditions, respectively. Roughness is required to be in its lowest value in order to obtain a smooth and durable coating prior to primer and topcoat applications. Increase in roughness is not desired and porosity of the surface affects the overall coating quality adversely. Film thickness also should be low enough to eliminate unnecessary material cost. The surface should be free from any deteriorations such

as dirt, pinholes or craters. Stone chip resistance and other mechanical properties of the surface should be in its maximum value while the roughness is in its lowest.

According to the preliminary assessments, deposition voltage, bath temperature, coating time and organic solvent ratio parameters were found to be directly related to the film thickness of the coating. While the increase in the film thickness is acceptable up to a certain level, it affects the surface properties positively. Increase in the thickness above a certain level causes quality problems such as surface roughness and gloss reduction, and also negatively affects physical properties such as hardness and stone chip resistance. SEM studies revealed that at low bath temperatures coating is insufficient and pigment agglomerations occurred on the surface.

While the pigment/binder ratio does not directly affect the film thickness, it has been determined that low pigment ratios cause crater and pinhole problems on the surface, while high pigment ratio causes dullness on the surface and a decrease in stone chip resistance. Craters and pinholes are occurred mostly on the surface at very low pigment ratio. Electrocoat accumulations and larger pinholes are seen on high pigment ratios. According to the SEM analysis, coatings at different pigment/binder ratios are significantly different. At low pigment levels pinholes are appeared mostly on the surface and coating density is relatively lower, at high pigment levels pigment accumulations, surface defects and larger pores are seen in SEM analysis.

The solid matter ratio is not directly related to the film thickness, but as the solid ratio increases, the surface hardness and stone chip resistance increase, but after a certain level is exceeded, it has a negative effect on the stone chip resistance. While the curing temperature did not affect the parameters such as film thickness and surface quality, it was observed that curing at high temperatures caused yellowing on the surface, but positively affected the stone chip resistance, according to the measurement result found as Rating 10.

4.1.8.2 Thermal Properties

According to the literature, it is known that increasing the crosslinking density in coatings increases the glass transition temperature. According to the tests, it was observed that increasing the application voltage increased the amount of pigment molecules carried, as mentioned in the literature, and showed a plasticizer effect between the cross-links and decreased the glass transition temperature. This situation was supported by TGA analysis, and it was observed that the residual amount increased with increasing voltage.

As the induction time increases, as long as other parameters are not changed, the glass transition temperature increases slightly, while the residual amount decreases. This is explained by the decrease in the conductivity of the surface as the film thickness increases during the coating and the decrease in the rate of pigment carried by electrical interaction over time.

Increasing the bath temperature causes excessive increase in the film thickness. According to the thermal analysis, at high temperatures, the glass transition temperature (T_g) decreases and the residual ratio increases. This is explained by the increase in the kinetic energy with the increase in temperature, resulting with increase in the mobility of the molecules and increasing the amount of transported pigment molecules.

As the pigment ratio and solids ratio increase, the T_g decreases and the residual ratio increases. Both cases are explained by the fact that the transported pigments create a plasticizer effect between the cross-links, and the stone impact strength decreases due to the decrease in T_g at high pigment and solid ratios.

The increase in the organic solvent ratio increases the film thickness very much, which is explained by the increased molecular mobility due to the decreased

viscosity. While no significant difference is observed in the glass transition temperature and the residual ratios, the stone chip resistance decreases with increasing film thickness.

The curing temperature directly affects the glass transition temperature and the T_g value increases considerably at increasing temperatures, which is explained by the increase in the crosslinking density with temperature. Contrary to what is expected, there is an increase in the residual amount at high temperatures, which is explained by the increased crosslinking density and the exposure of the inorganic content to the trapping effect. As expected, it was observed that the stone chip resistance increased with the increase of T_g . Increase in crosslinking density is positively affecting the mechanical properties of the surface but it is not desired to have a full crosslink in the coating system since it will decrease the adhesion strength of the surface with the above paint layers.

4.2 Determination of Optimum Electrocoating Parameters by Using DOE

In the first part of the study, while examining the effects of seven different parameters, experiments were carried out by keeping other parameters constant. It was decided to conduct a DOE to understand how the results were affected when more than one parameter was changed at the same time. Since doing DOE with seven parameters would require too many tests, it was decided that some parameters should be removed from the DOE model. In order to eliminate some of the parameters statistical correlation analysis between the roughness and stone chip resistance results of the seven parameters are investigated.

Roughness is required to be in its lowest value in order to obtain a smooth and durable coating prior to primer and topcoat applications. Increase in roughness is not desired and porosity of the surface affects the overall coating quality adversely. Film thickness also should be low enough to eliminate unnecessary material cost. The

surface should be free from any deteriorations such as dirt, pinholes or craters. Stone chip resistance and other mechanical properties of the surface should be in its maximum value while the roughness is in its lowest.

For preliminary sifting of the critical parameters, R-sq values for both roughness and stone chip resistance values are taken into account and if the R-sq value is high enough, this parameter is decided to keep in model for DOE analysis. To provide the upper and lower limits of DOE analysis, the possible lowest values of each parameter are chosen to give the minimum roughness and maximum stone chip resistance values.

Minitab™ 17 software is used to find if there is a correlation between those parameters and investigated features statistically. The results of the preliminary statistical analysis are planned to use in a DOE (Design of Experiment) study to sift some of the parameters that are not affecting the results too much.

Correlation ratios (R-sq) were calculated using Minitab™ 17 software in order to understand whether a statistical relationship could be established between the surface roughness and stone chip resistance of all investigated parameters. Accordingly, it has been observed that the surface roughness value has a statistically significant relationship with voltage, pigment ratio and solvent ratio, and there is a relatively low correlation between the application time and temperature and the solid ratio. It was observed that the stone chip resistance was highly correlated with the application temperature, curing temperature, solvent ratio and application time, and had a relatively low correlation with the voltage, pigment ratio and solid ratio. Correlation and Regression analysis results are given in Table 4.9.

Accordingly, in order to reach the desired minimum surface roughness and maximum stone chip resistance values; it is understood that it would be appropriate to keep the curing temperature, solvent ratio and solid ratio constant and to make the

DOE in a way that would give optimum values of voltage, application time, temperature and pigment ratio.

Table 4.9 Statistical analysis results of ED parameters vs roughness and stone chip resistance.

	<i>Roughness</i>				<i>Stone Chip Resistance</i>			
	<i>Pierson Coef., r</i>	<i>R-sq</i>	<i>Min Value</i>	<i>Max Value</i>	<i>Pierson Coef., r</i>	<i>R-sq</i>	<i>Min Value</i>	<i>Max Value</i>
P/B Ratio	-0.680	77.00%	0.221	0.586	0.655	42.90%	6	9
Voltage	0.862	99.90%	0.283	4.472	-0.870	75.00%	7	9
Bath Temp	-0.050	43.80%	0.283	0.849	-0.850	97.80%	7	9
Induction time	0.028	44.70%	0.283	0.322	-0.900	81.10%	8	9
Baking Temp	0.694	51.20%	0.137	0.225	0.984	93.80%	4	10
Solid Ratio	0.079	12.20%	0.221	0.234	0.500	25.00%	7	9
Org Solvent Ratio	0.705	53.70%	0.218	0.470	-0.940	88.10%	3	9

Since stone chip resistance is not a numerical measurement result but a grade classification, it is not possible to use this value in the statistical evaluations. In order to convert this data into a meaningful numerical data, it is examined whether there is a statistical relationship between the film thickness and the stone chip resistance. Preliminary measurements showed that, stone chip resistance and film thickness of the coatings are correlated up to 93.3%.

Around 20 micron film thickness which is also the specification limit for most purposes, stone chip resistance gives the best performance as seen in Figure 4.41.

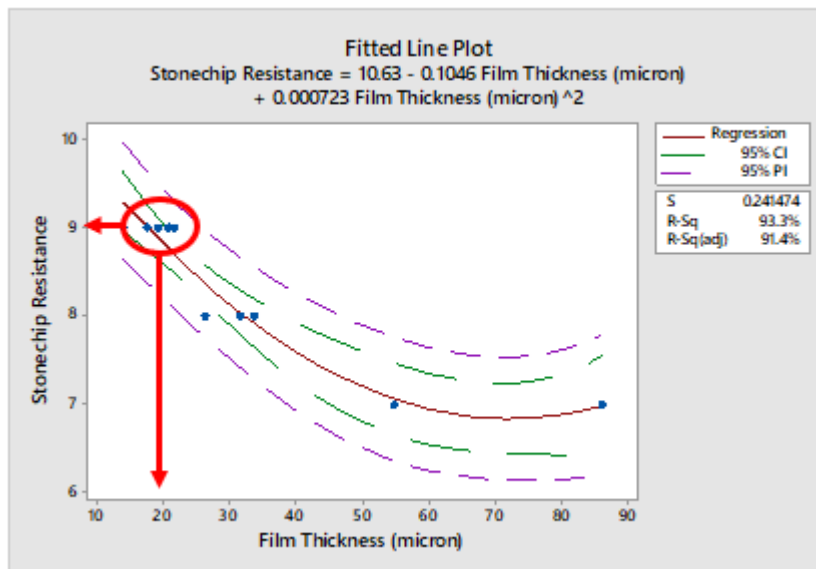


Figure 4.41 Correlation Analysis of Stone Chip Resistance vs Film Thickness.

A total of 48 experiments ($2^4 \times 3$) are conducted for the 2 level full factorial DOE with 4 factors and 3 repeating to determine optimum parameters. The objective is to obtain the minimum roughness value at 20 micron film thickness target where stone chip resistance, hardness and gloss are maximum at the same time. So in the Minitab™ 17 response optimizer tool to have maximum stone chip resistance, film thickness target is set to be as 20 microns, roughness is set to be minimum, hardness and gloss is set to be maximum.

Three of seven parameters are kept constant for each study. Minitab™ 17 software is used for creating and analyzing the DOE studies. Parameter limits for the DOE study is tabulated in Table 4.10. Measurements of DOE studies are tabulated in Table 4.11.

Table 4.10 Parameter limits for DOE study.

Parameter	<i>Lower Limit</i>	<i>Upper Limit</i>
Pigment / Binder Ratio, %	13	15
Voltages, V (3 step)	315	345
Bath Temperature, °C	29	32
Induction Time, min (3 step)	3	6
Baking Temperature	175 °C at 20 min	
Solid Ratio, %	21	
Organic Solvent Ratio, %	2.47	

Table 4.11 The 2 level full factorial experiment design with 4 factors and 3 repeating.

StdOrder	<i>P/B Ratio</i>	<i>Voltage, V</i>	<i>Induction Time, min</i>	<i>Bath Temp, °C</i>
1	0.13	315	3	29
2	0.15	315	3	29
3	0.13	345	3	29
4	0.15	345	3	29
5	0.13	315	6	29
6	0.15	315	6	29
7	0.13	345	6	29
8	0.15	345	6	29
9	0.13	315	3	32
10	0.15	315	3	32
11	0.13	345	3	32
12	0.15	345	3	32
13	0.13	315	6	32
14	0.15	315	6	32
15	0.13	345	6	32
16	0.15	345	6	32
17	0.13	315	3	29
18	0.15	315	3	29
19	0.13	345	3	29
20	0.15	345	3	29
21	0.13	315	6	29
22	0.15	315	6	29
23	0.13	345	6	29
24	0.15	345	6	29
25	0.13	315	3	32
26	0.15	315	3	32
27	0.13	345	3	32
28	0.15	345	3	32
29	0.13	315	6	32
30	0.15	315	6	32
31	0.13	345	6	32
32	0.15	345	6	32
33	0.13	315	3	29
34	0.15	315	3	29
35	0.13	345	3	29
36	0.15	345	3	29
37	0.13	315	6	29
38	0.15	315	6	29
39	0.13	345	6	29
40	0.15	345	6	29
41	0.13	315	3	32
42	0.15	315	3	32
43	0.13	345	3	32
44	0.15	345	3	32
45	0.13	315	6	32
46	0.15	315	6	32
47	0.13	345	6	32
48	0.15	345	6	32

48 experiments are completed for DOE studies. Coated panels are examined in terms of roughness, film thickness, hardness and gloss, the values of the measurements are taken as response variables. By using the “Response Optimizer” tool of Minitab™ 17 program, optimum test conditions are determined to provide minimum 20 microns film thickness together with minimum roughness, maximum hardness and maximum gloss values, respectively. Response variables of the DOE study is given in Table 4.12.

Table 4.12 Response variables of the DOE study.

StdOrder	<i>Roughness, μ</i> <i>Ra 4.8mm</i>	<i>Film Thickness, μ</i>	<i>Hardness,</i> <i>persöz</i>	<i>Gloss 20°</i>
1	0.38	11.43	368	17.0
2	0.20	15.70	361	22.8
3	0.38	10.37	351	22.0
4	0.18	16.57	340	27.6
5	0.29	8.17	363	20.1
6	0.21	24.70	361	26.6
7	0.30	11.80	363	28.8
8	0.21	25.47	360	26.3
9	0.37	11.57	350	19.3
10	0.23	21.33	352	29.2
11	0.32	12.13	372	22.9
12	0.15	19.97	360	30.9
13	0.29	23.27	363	19.1
14	0.18	29.80	379	35.4
15	0.24	22.57	337	26.9
16	0.19	35.17	255	35.2
17	0.37	7.97	376	18.0
18	0.21	14.70	346	25.0
19	0.40	10.73	358	22.6
20	0.30	15.30	330	17.6
21	0.33	10.50	364	19.0
22	0.20	24.40	361	26.6
23	0.33	11.17	343	27.4
24	0.20	24.47	353	28.8
25	0.40	11.87	355	18.3
26	0.22	20.03	370	28.6
27	0.29	11.80	362	21.9
28	0.20	19.93	285	33.2
29	0.26	23.57	363	20.9
30	0.17	30.07	385	35.7
31	0.28	18.90	344	22.6
32	0.17	31.93	349	42.0
33	0.34	9.60	358	16.7
34	0.25	13.87	363	26.2
35	0.32	10.23	360	21.8
36	0.23	15.93	355	23.4
37	0.36	12.03	353	18.3
38	0.21	23.73	355	25.5
39	0.33	12.93	358	28.2
40	0.19	25.70	351	30.4
41	0.35	11.43	354	19.4
42	0.21	20.97	347	28.6
43	0.30	13.67	371	21.9
44	0.16	21.80	337	31.2
45	0.29	21.97	359	20.2
46	0.19	29.03	381	33.7
47	0.20	23.47	355	24.9
48	0.16	33.27	346	38.5

After completing all of the 48 experiments, response values are uploaded to the Minitab™ 17 software. By using the response optimizer tool of the program, net film thickness is targeted to be 20 microns since this thickness gives the best stone chip performance, roughness is chosen to be as minimum as possible, gloss and hardness values are chosen as maximum as possible. Response optimizer interface is given in Figure A.1.

A model is created by using Response Optimizer tool. According to the model optimum p/b ratio, voltage, time and temperature values to obtain minimum roughness, maximum hardness and gloss values with 20 micron film thickness with 95% confidence interval is determined. Model summary is given in Figure A.2.

R-sq value of the model, that show the amount of the correlation of the parameters is found as 90.25% which is adequately high. VIF number that indicates Variance Inflation Factor detects correlation among predictors. If $VIF = 1$ it indicates no relation among predictors. If $VIF > 1$ indicates predictors are correlated to some degree. If VIF changes between 5 and 10 indicates regression coefficients are poorly estimated and are unacceptable. The VIF number of the predictors in the model is found as 1, means that predictors are independent from each other, and the model is acceptable.

According to the DOE Response Optimizer tool, the minimum roughness value to be reached is found as 0.1701 at the film thickness of 20.5 microns. This roughness value is a highly competitive one when compared to mass production roughness levels which is around 0.30 and above. Response Optimizer output is given in Figure A.3.

The optimum parameters to obtain this roughness and film thickness value both together is given below in Table 4.13.

Table 4.13 Optimum parameters according to the DOE response optimizer.

Parameter	<i>Optimum Parameters</i>
Pigment / Binder Ratio, %	15
Voltages, V (3 step)	345
Bath Temperature, °C	32
Induction Time, min (3 step)	3
Baking Temperature	175 °C at 20 min
Solid Ratio, %	21
Organic Solvent Ratio, %	2.47

This optimum case represented one of the 48 test conditions that we had already tested. Average measurement results for the optimum condition is given in Table 4.14.

Table 4.14 Measurement results at optimum parameters.

Parameter	<i>Measurement Results</i>
Roughness, Ra (4.8 mm)	0.17
Film Thickness, μ	20.5
Gloss 20°	32
Hardness	327

According to the measurement results, a regression equation to achieve roughness value with independent variables is given in Figure 4.42.

```

Regression Equation in Uncoded Units
Roughness AVR = 0,9 - 95 p/b ratio - 0,008 voltage - 3,5 time + 0,09 temp
+ 0,34 p/b ratio*voltage + 38 p/b ratio*time + 2,5 p/b ratio*temp
+ 0,0134 voltage*time + 0,00006 voltage*temp + 0,106 time*temp
- 0,135 p/b ratio*voltage*time - 0,0099 p/b ratio*voltage*temp
- 1,20 p/b ratio*time*temp - 0,00043 voltage*time*temp
+ 0,0043 p/b ratio*voltage*time*temp
    
```

Figure 4.42 Regression equation for roughness.

This equation helps to make a prediction of roughness value by using pigment/binder ratio, voltage, bath temperature and induction time variables. According to the statistical outputs, equation works with a 90.25% accuracy. A graph was drawn with the measurements versus software predictions. The graph given in Figure 4.43, confirms the accuracy of the prediction.

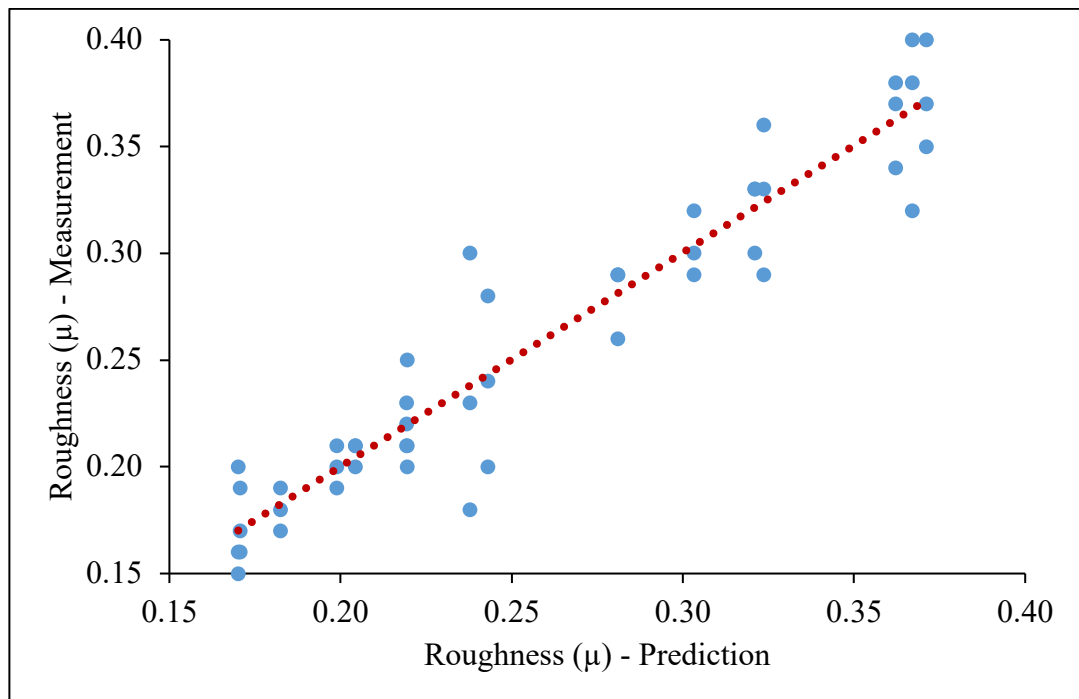


Figure 4.43 Minitab predictions versus measurements for roughness value.

4.3 Determination of Optimum Phosphating Parameters by Using DOE

Phosphating is the most critical step of pretreatment which is applied prior to electrocoating process. It is mandatory to increase the adhesion of the electrocoating to the steel surface to provide best corrosion protection. Phosphating affects the adhesion of the surface by increasing the surface area. Popic *et al.* [40] reported that the rough surface of zinc phosphating brings higher density of secondary bonding

(Van der Waals and hydrogen bonding) at the interface, as well as creating an effective mechanical interlocking occurred by coating liquid to flow into the porous surface of the substrate. The quality of phosphating process is also important for the physical and mechanical properties of the final product.

In this chapter of the study, the aim is to determine the optimum operation parameters of the phosphating bath in terms of temperature and time to achieve better corrosion resistance of the coating by arranging coating weight and crystal size. Another DOE design is created to determine optimum conditions for pretreatment bath. The only operational variables in the phosphating process are time and temperature in the mass production. Therefore, a three level two factorial design is used to create DOE parameters.

Minitab™ 17 software is used for creating and analyzing the DOE studies. A three level full factorial DOE method is used with two factors, with four repeating to determine optimum parameters to obtain the minimum coating weight where number of phosphate crystals are at maximum per unit surface area. Increased number of phosphate crystals per unit area provides a good adhesion between phosphate layer and electrocoat material, that results in a good corrosion resistance [7]. DOE limits are given in Table 4.15.

The objective of the DOE is to decrease coating weight per unit surface area, to increase number of phosphate crystals per unit surface area.

Table 4.15 DOE limits for phosphating parameter optimization.

Factors	<i>Lower Level</i>	<i>Middle Level</i>	<i>Upper Level</i>
Temperature, °C	45	55	65
Time, sec	60	120	180

According to the DOE of 2 factors, 3 level with 4 repeating, a total of 36 ($3^2 \times 4$) tests are conducted. Coating weight per unit surface area is measured for each coating. The results of DOE are given in Table 4.16.

Table 4.16 Measurement results for phosphating DOE study.

StdOrder	Temperature (°C)	Time (sec)	Coating Weight (g/m²)
1	45	60	3.20
2	45	120	3.10
3	45	180	3.00
4	55	60	3.10
5	55	120	3.00
6	55	180	3.00
7	65	60	3.00
8	65	120	3.40
9	65	180	3.80
10	45	60	3.10
11	45	120	3.10
12	45	180	3.00
13	55	60	3.00
14	55	120	3.20
15	55	180	3.10
16	65	60	3.10
17	65	120	3.20
18	65	180	4.00
19	45	60	3.20
20	45	120	3.10
21	45	180	2.80
22	55	60	3.00
23	55	120	3.10
24	55	180	3.10
25	65	60	3.20
26	65	120	3.40
27	65	180	4.00
28	45	60	3.20
29	45	120	3.10
30	45	180	2.90
31	55	60	3.00
32	55	120	3.10
33	55	180	3.10
34	65	60	3.40
35	65	120	3.40
36	65	180	4.00

By using Minitab™ 17, the results of DOE are analyzed. It is seen that coating weight is correlated with temperature and time up to 93.05%, since R-Sq is found as 93.05%. The model summary and the regression equation is given in Figure A.4. To demonstrate the regression, measurement versus prediction for coating weight is given in Figure A.5.

Nine test conditions are determined and analyzed in the DOE study. Coating weight per unit surface area has been measured as a response variable. By using response optimizer tool of Minitab™ 17 software, optimum condition for minimum coating weight for unit surface area is found as 45 °C – 180 sec with an average coating weight of 2.93 g/m² (Condition “C”). Average measurement results for each condition are given in Table 4.17. Response optimizer output is given in Figure A.6.

Table 4.17 Coating weights at all conditions.

Condition	Temperature (°C)	Time (sec)	Coating Weight Avr. (g/m²)
A	45	60	3.175
B	45	120	3.100
C	45	180	2.925
D	55	60	3.025
E	55	120	3.100
F	55	180	3.075
G	65	60	3.175
H	65	120	3.350
I	65	180	3.950

4.4 Physical Performance Tests for Phosphating

A series of performance tests are applied on each condition to confirm if the condition C is really performing better than other conditions as seen in statistical results.

Since the results of this study is an important reference for automotive cathaphoresis process, Ford Motor Company internal material specifications and laboratory test methods are used for performance tests. According to the Ford Motor Company material specifications, salt spray resistance, stone chip resistance, water immersion and adhesion properties are crucial and specification limits are defined for cathodic electrocoat materials. Electrocoat material is defined as Coating System I in the specification and specification limits are given in Figure A.6.

With reference to the standard document, adhesion should be maximum Grade 0 according to the FLTM BI 106-01 internal method, stone chip resistance should be max Grade 9 according to FLTM BI 157-06 internal method. Water Immersion test duration should be 240 h according to FLTM BI 104-1 internal method and salt spray test duration should be 960 h according to FLTM BI 103-01 method.

From this technical point of view, by using the optimum electrocoating conditions defined in Section 4.2, samples have been electrocoated under 9 conditions.

All electrocoated panels have been tested according to above FORD FLTM methods. Results are given in Table 4.18.

Table 4.18 Measurement results for performance tests at all conditions.

Cond.	Temp.	Time	Adhesion	Stone Chip	Water Immersion	Salt Spray	Overall
A	45 °C	60 sec	Grade 1	8-Fail	Pass	Fail	Fail
B	45 °C	120 sec	Grade 1	8-Fail	Pass	Fail	Fail
C	45 °C	180 sec	Grade 0	10-Pass	Pass	Pass	Pass
D	55 °C	60 sec	Grade 0	9-Pass	Pass	Pass	Pass
E	55 °C	120 sec	Grade 1	8-Fail	Pass	Fail	Fail
F	55 °C	180 sec	Grade 2	7-Fail	Pass	Fail	Fail
G	65 °C	60 sec	Grade 2	6-Fail	Fail	Fail	Fail
H	65 °C	120 sec	Grade 3	6-Fail	Fail	Fail	Fail
I	65 °C	180 sec	Grade 4	6-Fail	Fail	Fail	Fail

According to the performance test results, the condition of 45 °C 180 sec (defined as C), that has found as optimum according to the statistical studies also shows the best result, together with the condition of 55 °C 60 sec (defined as D) condition. Salt spray corrosion test results of the whole conditions are given in Figure 4.44.

When compared the results, its seen that the condition C shows a better performance than the condition D even though both results are classified as Pass. Stone chip resistance results are given in Figure 4.45.

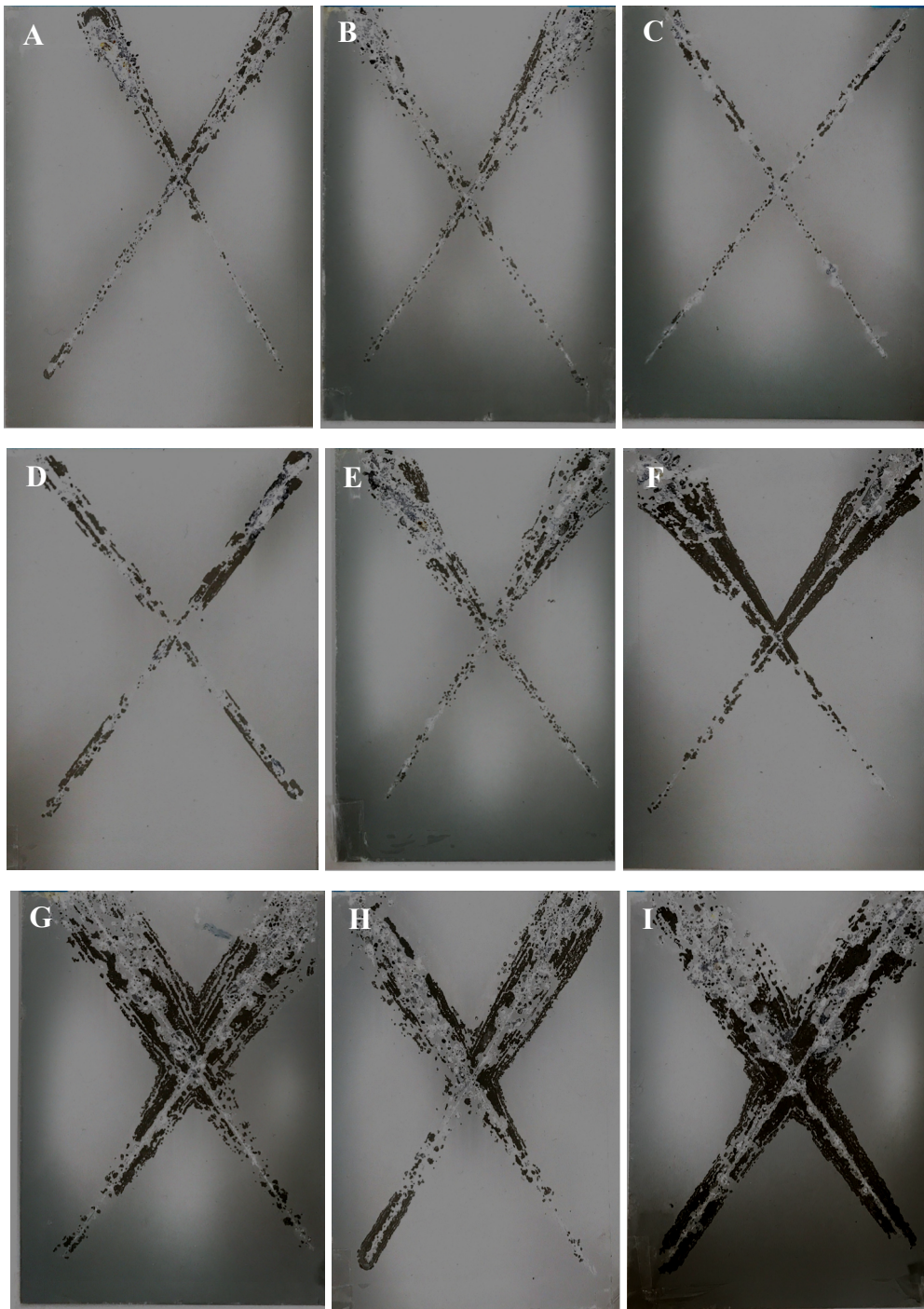


Figure 4.44 Salt spray test results at all conditions.

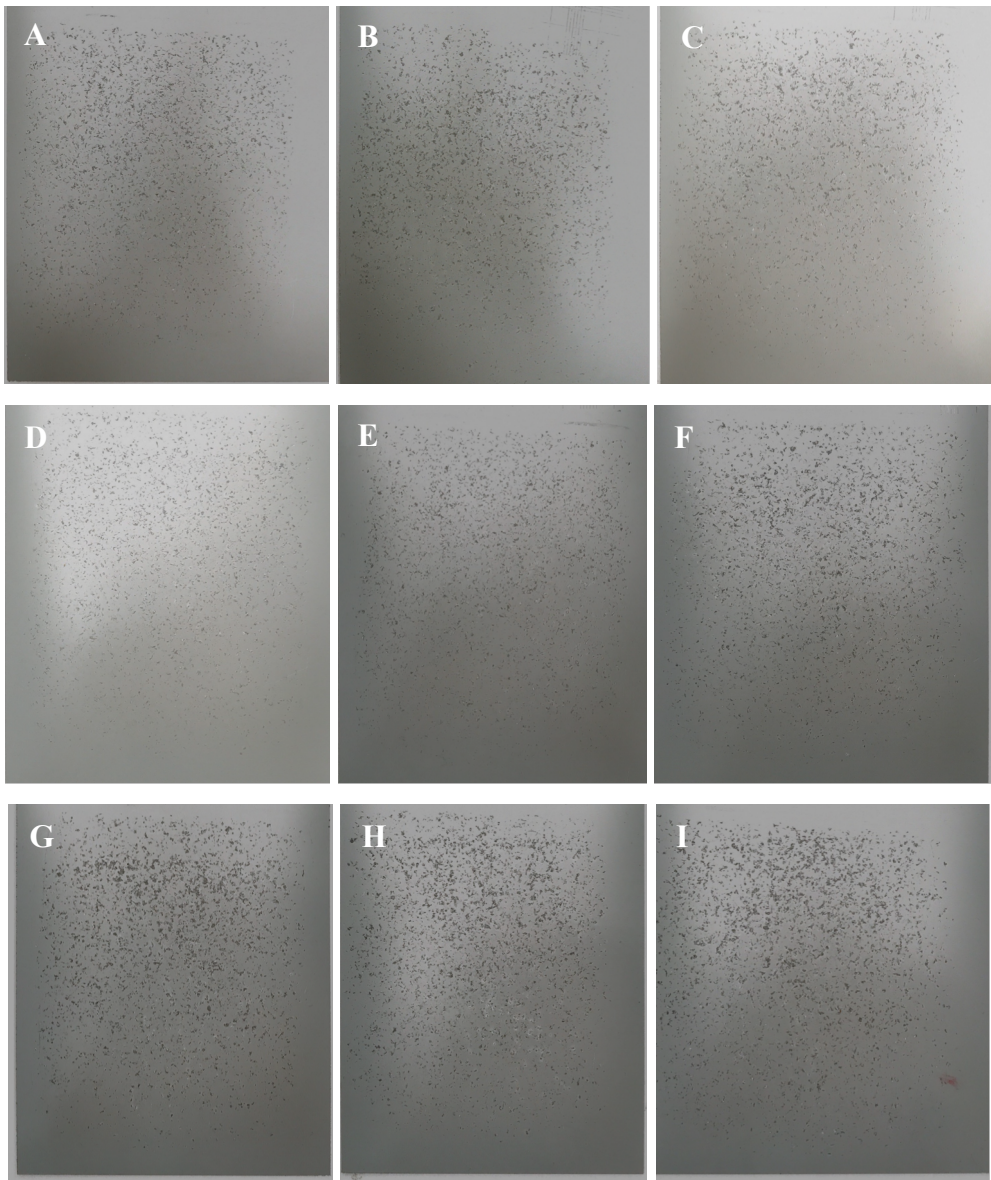


Figure 4.45 Stone chip test results at all conditions.

4.4.1 Morphological Analysis

Since the distribution of the phosphate crystals and crystal size per unit surface area have significant influences on the mechanical properties of the electrocoatings, SEM studies were conducted on the surface of all nine pretreatment conditions. To be able to make a comparison between a reference mass production line condition and the studies, a reference sample is also characterized from a reference mass production line which is mentioned in the Table 4.19 as Reference.

Table 4.19 Phosphating process parameters of all conditions including “Reference”.

Condition	Temperature (°C)	Time (sec)
A	45	60
B	45	120
C	45	180
D	55	60
E	55	120
F	55	180
G	65	60
H	65	120
I	65	180
Reference	52±1	180

SEM images taken at 10.0 kx magnification for the conditions of A to I are given in Figure 4.46.

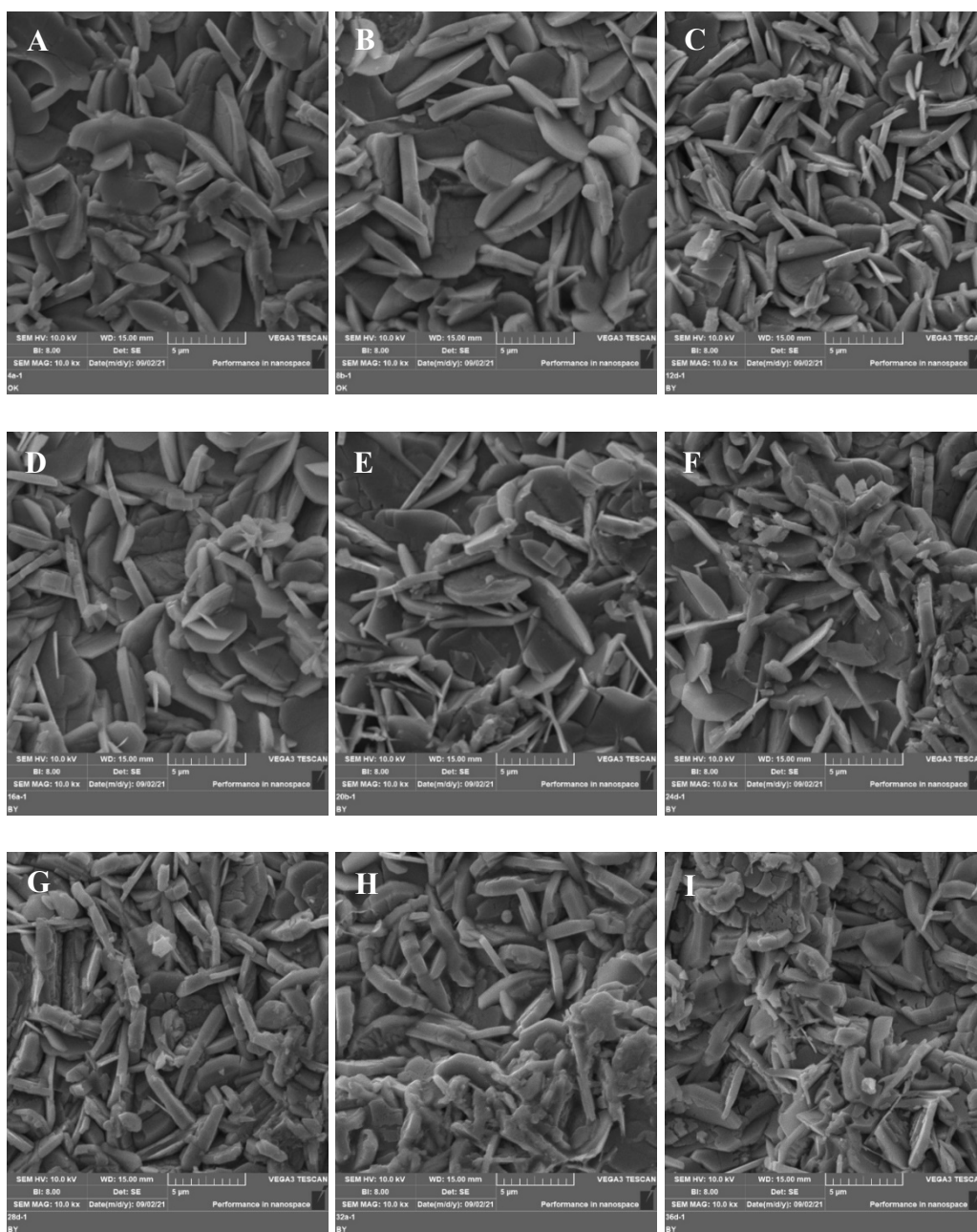


Figure 4.46 10.0 kx SEM images of all conditions of pretreatments.

SEM images of the conditions from A to I revealed that, each condition has the characteristic needle-like or plate-like shape of phosphate crystals [9, 10, 36, 37, 41]. Type of the crystals are demonstrating that the crystal structure is characteristic Hopeite structure as expected, since the substrate is galvanized steel [37, 38, 42, 43].

It was mentioned in the previous chapters that if the steel is galvanized only Hopeite crystals occur on the surface. In addition to the Hopeite crystals, due to the trication formulation of the bath, MnZn Phosphate and Ni Phosphate structures are also expected to occur on the surface with very less amounts compared to Hopeite.

Rani *et al.* [37] stated that fine-grained phosphate crystals gave less porosity and better adhesion to the steel substrate, and coating weight is less if the crystal structure is smaller and fine-grained, that resulted in good corrosion resistance. At the condition of C the crystals show a good uniformity and crystal size is lower when compared to the other conditions. It is seen that number of phosphate crystals per unit surface area at C condition is higher. According to the coating weight analysis, it is seen that the C condition has the minimum coating weight and D is following after. Average coating weight of all the conditions are given in Figure 4.47. The best physical performance results of C condition can be explained with the uniform and fine-grained crystal structure with lower coating weight.

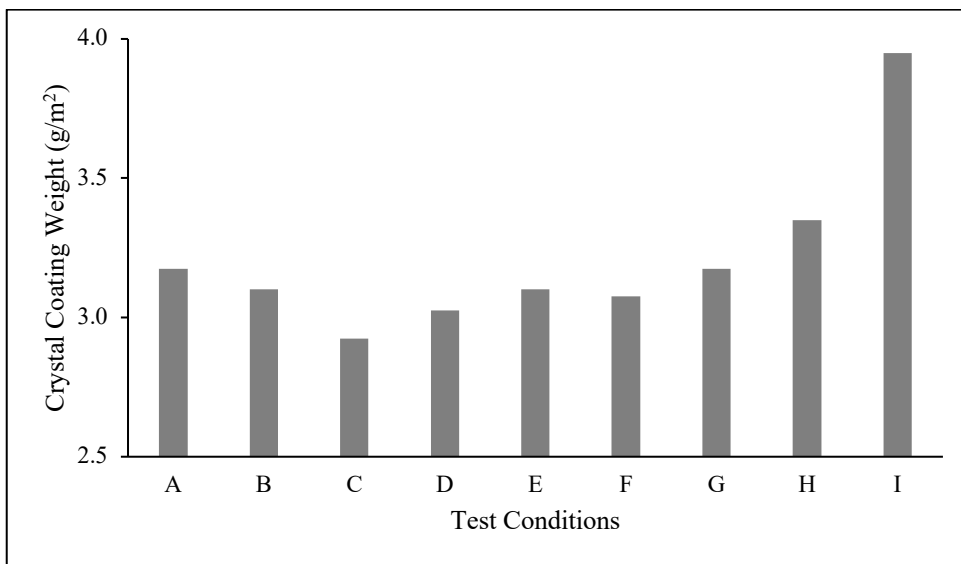


Figure 4.47 Average coating weight per unit surface area for all test conditions.

On the one hand, all the conditions between E to I resulted in insufficient adhesion, stone chip and corrosion performance, that can be explained with the irregular crystal size distribution and the agglomerations which can be recognized easily from the SEM images. It is understood that increased time and temperature adversely affects the uniform structure of phosphate crystals (conditions E, F, G, H and I), agglomerations and deformations are occurred which result in a worse adhesion performance and bad salt spray resistance consequently, which are also seen on performance test results. Hajisafari *et al.* [42] stated that a very high driving force leads to a high growth rate of phosphate crystals, and in this situation the porosity between crystals also grows, coating weight increases and coating with a high porosity is obtained. This porosity can affect the corrosion resistance of coating [42]. Zhang *et al.* [43] explained that the formation process of phosphate conversion coating is an endothermic reaction, so the increased temperature benefits the crystallization of the coating formation. As already mentioned in the various studies, it is known that Hopeite crystal grow is an endothermic reaction and increase of the heat is a driving force for the crystallization. Thus, the worse corrosion, adhesion and stone chip resistance conditions at high temperatures (conditions E, F, G, H and I) can be explained with the increased porosity of the crystal structure as well the agglomerations and non-uniform structure. Increased coating weights that is given in Figure 4.47 are also supporting this suggestion and is a result of increased crystallization.

In addition to the above, lower temperature and time conditions (conditions A and B) also result in inadequate number of phosphate crystals that result in a bad adhesion, stone chip and corrosion resistance. Oh *et al.* [41] stated that at the very early reaction stage, the phosphate structures developed horizontally in regards to the Zn layer. As the reaction time increased it was confirmed that the structures then developed vertically. At the conditions of A and B, since the temperature and time is low, it can be commented that the crystals are mostly in horizontal shape and less, and the surface area is relatively low.

The poor adhesion, stone chip and corrosion resistance observed in A and B conditions can be explained by the low surface area of the mostly horizontal and inadequate number of crystals. The comparison between A, B, C and Reference conditions at different magnifications can be seen in Figure 4.48.

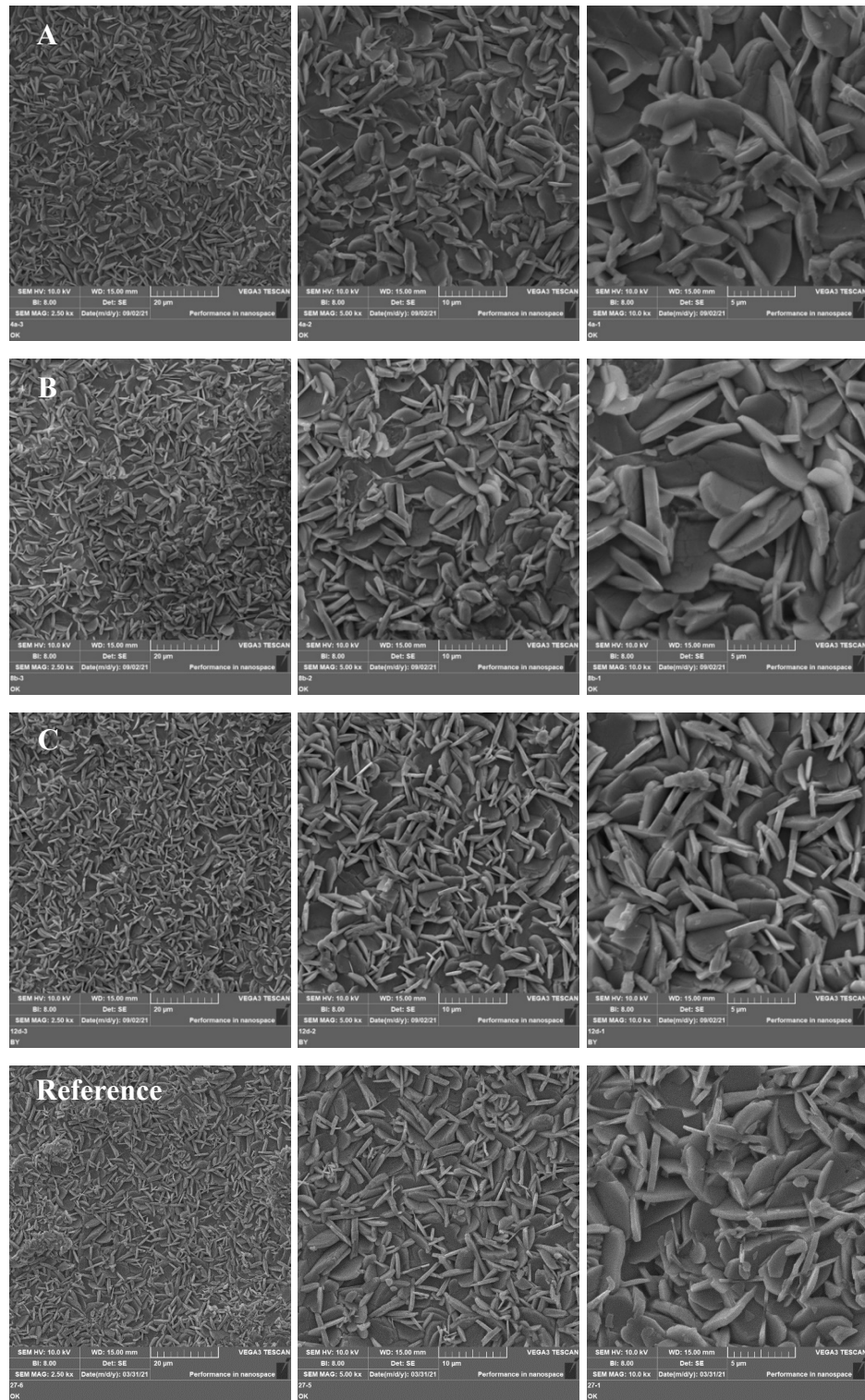


Figure 4.48 SEM images of phosphated steel panels at A, B, C and Reference conditions with different magnifications. a) 2.50 kx b) 5.00 kx c) 10.0 kx

The morphology of Reference seems similar to the test conditions of C and D when roughly investigated. Dimensional analysis should be conducted to comment on the difference of the samples. The comparison between C, D and Reference conditions at different magnifications can be seen on Figure 4.49. In all three conditions, C condition seems to have the best uniformity and homogeneous size distribution. SEM images for the conditions between E and I are given in Figure 4.50.

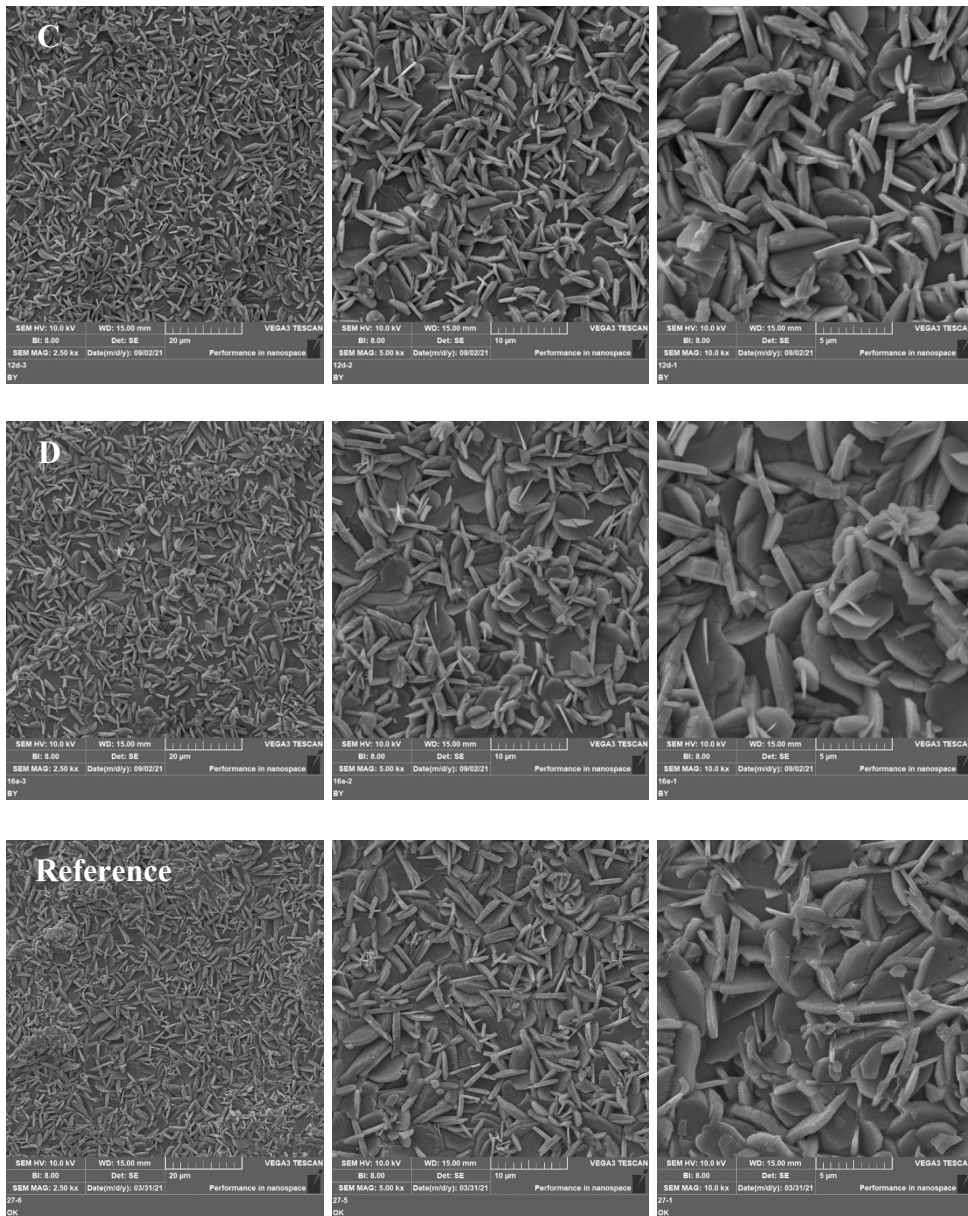


Figure 4.49 SEM images of phosphated steel panels at C, D and Reference conditions with different magnifications. a) 2.50 kx b) 5.00 kx c) 10.0 kx

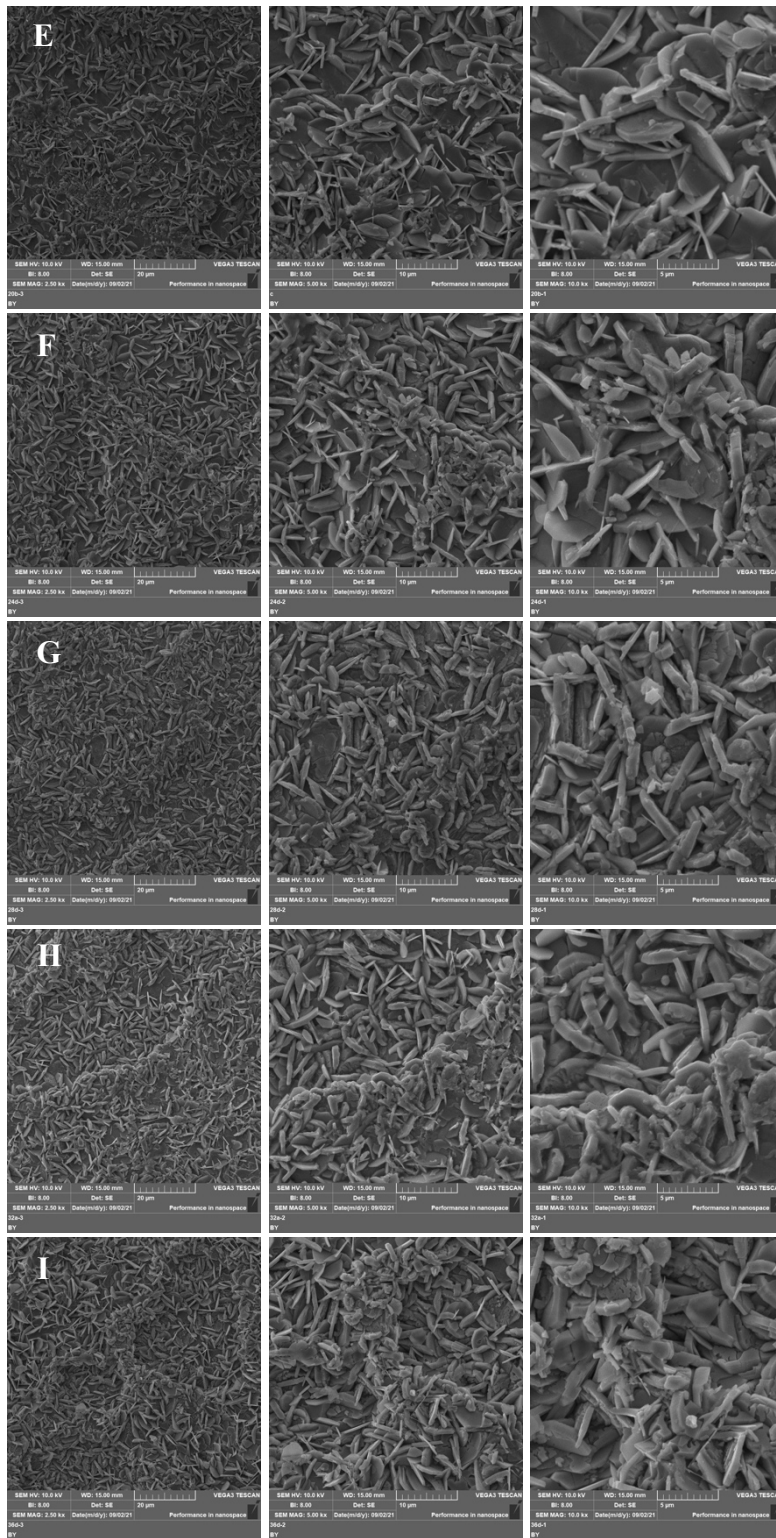


Figure 4.50 SEM images of phosphated steel panels at E, F, G, H and I Conditions with different magnifications. a) 2.50 kx b) 5.00 kx c)10.0 kx

4.4.2 Dimensional Analysis of Zinc Phosphate Crystals

By using ImageJ software, dimensional analysis of zinc phosphate crystals are performed. 70 to 100 crystals are examined for each condition. For length and thickness measurements box and whisker plot diagrams for all conditions and also reference condition are given in Figure 4.51 and Figure 4.52. Reference condition is shown in the graphs as Ref.

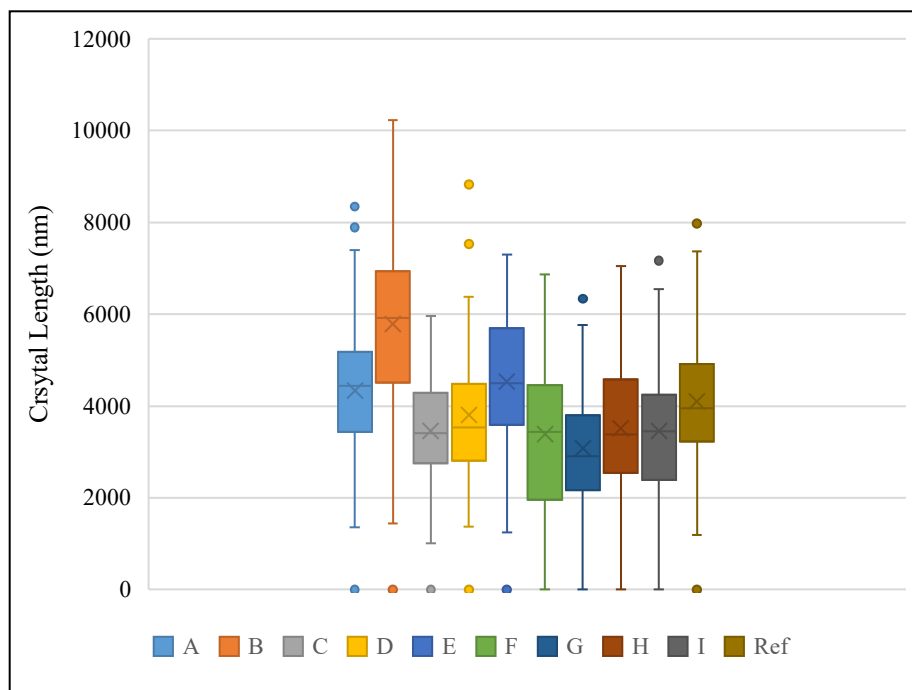


Figure 4.51 Crystal length Box and Whisker plot diagrams of all test conditions.

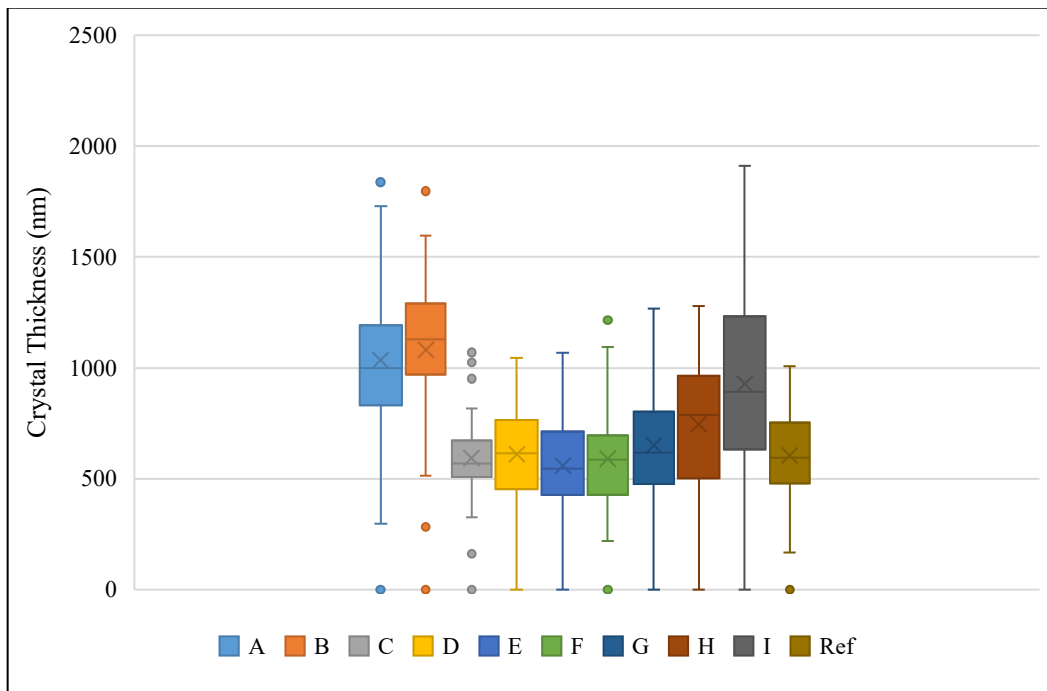


Figure 4.52 Crystal thickness Box and Whisker plot diagrams of all test conditions.

According to the analysis obtained by ImageJ software, its seen that for A and B conditions, crystal sizes are larger in terms of both length and thickness, and there are outliers in the dimensional distribution. The mean and median of the crystal length and thickness are higher than the other conditions. Reference condition states somewhere between D and E conditions as expected in both plots.

For the condition C and D which are passed from each measurement, mean and median of the distribution for both length and thickness are close to each other, but C shows a narrow and uniform distribution compared to D. Reference is also similar to the condition D.

As the temperature increases, a wider distribution is seen on both length and thickness of the disk shape crystals. For the conditions at 65 °C, duration is also affecting the thickness a lot, it seems that at higher temperatures when duration is

increased, crystal lengths remain almost constant but thickness is increased with a large distribution that resulted in poor mechanical performance at the end. Crystal size dimensional analysis results are given in Table 4.20.

Table 4.20 Crystal size dimensional distribution results for all conditions.

		<i>Mean</i>	<i>Median</i>	<i>Std Dev</i>	<i>Min</i>	<i>Max</i>
A at 45°C/60 sec	Length, nm	4761	4482	1361	2688	8342
	Thickness, nm	1070	999	297	665	1838
	<i>L/T</i>	<i>4.45</i>	<i>4.49</i>	<i>4.58</i>	<i>4.04</i>	<i>4.54</i>
B at 45°C/120 sec	Length, nm	6029	5959	1439	3808	10223
	Thickness, nm	1162	1135	283	513	1797
	<i>L/T</i>	<i>5.19</i>	<i>5.25</i>	<i>5.09</i>	<i>7.42</i>	<i>5.69</i>
C at 45°C/180 sec	Length, nm	3556	3427	1013	1845	5955
	Thickness, nm	614	572	162	327	1069
	<i>L/T</i>	<i>5.80</i>	<i>6.00</i>	<i>6.27</i>	<i>5.64</i>	<i>5.57</i>
D at 55°C/60 sec	Length, nm	3866	3541	1369	1927	8823
	Thickness, nm	637	627	190	325	1044
	<i>L/T</i>	<i>6.07</i>	<i>5.65</i>	<i>7.21</i>	<i>5.93</i>	<i>8.45</i>
E at 55°C/120 sec	Length, nm	4696	4509	1248	2913	7305
	Thickness, nm	582	547	172	268	1069
	<i>L/T</i>	<i>8.07</i>	<i>8.24</i>	<i>7.24</i>	<i>10.87</i>	<i>6.83</i>
F at 55°C/180 sec	Length, nm	3470	3449	1449	1141	6870
	Thickness, nm	605	586	221	269	1215
	<i>L/T</i>	<i>5.74</i>	<i>5.88</i>	<i>6.57</i>	<i>4.24</i>	<i>5.65</i>
G at 65°C/60 sec	Length, nm	3147	2909	1200	1091	6338
	Thickness, nm	670	628	240	267	1267
	<i>L/T</i>	<i>4.70</i>	<i>4.63</i>	<i>5.00</i>	<i>4.09</i>	<i>5.00</i>
H at 65°C/120 sec	Length, nm	3592	3396	1219	1665	7055
	Thickness, nm	773	804	273	305	1279
	<i>L/T</i>	<i>4.65</i>	<i>4.22</i>	<i>4.46</i>	<i>5.46</i>	<i>5.52</i>
I at 65°C/180 sec	Length, nm	3528	3511	1278	1897	7170
	Thickness, nm	954	891	416	308	1911
	<i>L/T</i>	<i>3.70</i>	<i>3.94</i>	<i>3.07</i>	<i>6.16</i>	<i>3.75</i>
Ref at 52°C±1 /180 sec	Length, nm	4199	3961	1195	2036	7979
	Thickness, nm	622	601	169	322	1006
	<i>L/T</i>	<i>6.75</i>	<i>6.60</i>	<i>7.08</i>	<i>6.32</i>	<i>7.93</i>

Crystal length/thickness (L/T) parameter for all conditions together with Ref condition are showed in the graph given in Figure 4.53. It can be commented that the ratio of length/thickness mean increases with increased time and temperature up to a certain level (Condition E) and then starts to decrease. The Ref condition obviously seems to be in between the conditions D and E as expected.

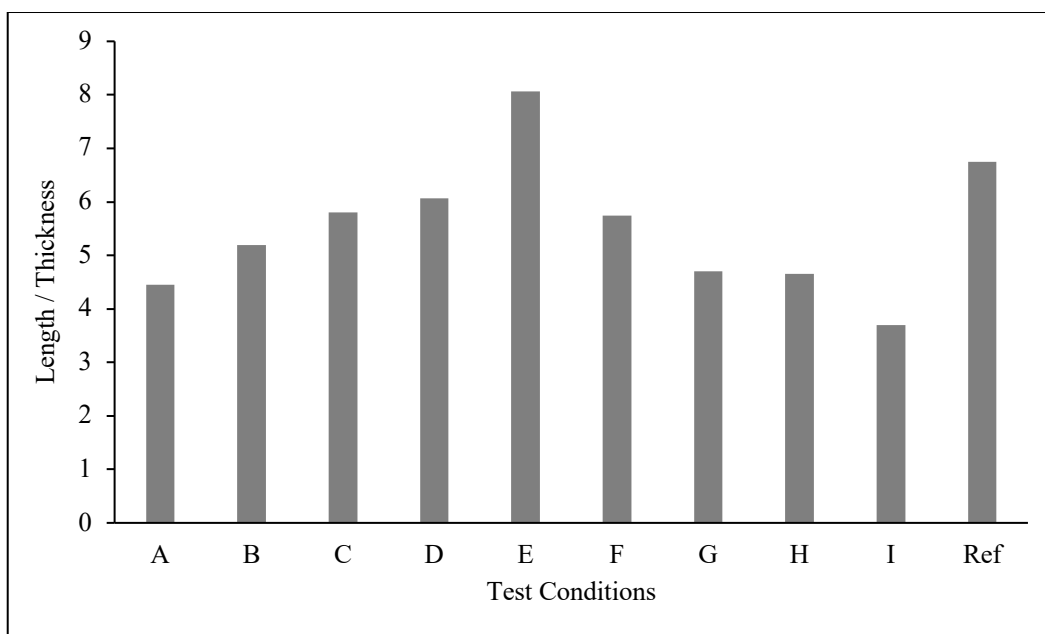


Figure 4.53 Crystal length/thickness for all test conditions.

It can be commented that with increased time and temperature, the ratio of length/thickness increases proportionally up to a level, then length stays constant, but thickness continues to grow. This can be explained with the increased density of the phosphate crystals. Hopeite crystal is known for its orthorhombic crystal structure. It is known that increased temperature and time increases coating weight and coating thickness of Hopeite [42, 43]. Increase in the thickness results in thicker crystals due to the orthorhombic growth structure of Hopeite. This results in the intense crystals which are overlapped.

4.5 Cross Comparison of Optimized Phosphating and Electrocoating Conditions with Reference Conditions

In the previous chapters of this study, the optimum process conditions for the pretreatment and electrodeposition baths for the pilot test setup are determined by using several methods.

To make a cross comparison test, reference condition is simulated in the pilot test setup. Process parameters for optimum and reference conditions for both steps are summarized in Table 4.21.

Table 4.21 Optimum and reference parameters for phosphating and electrocoating steps for the pilot test setup.

	<i>Parameter</i>	<i>Optimum Result</i>	<i>Reference</i>
Phosphating Bath Parameters	Temperature, °C	45	52 ± 1
	Duration, sec	180	180
Electrocoating Bath Parameters	Pigment/Binder Ratio, %	15	13
	Voltages, V (3 step)	345	390
	Bath Temperature, °C	32	30
	Induction Time, min (3 step)	3	3
	Baking Temperature	175 °C at 20 min	175 °C at 20 min
	Solid Ratio, %	21	18
	Organic Solvent Ratio, %	2.47	2.47

To be able to make a cross comparison between the optimum conditions and reference condition, some cross tests are performed. The results show that, the samples that obtained at optimum conditions which is determined in this study show better physical properties such as roughness and salt spray corrosion resistance. Mentioned cross comparison results are summarized in Table 4.22. Optimum phosphate condition is shown as P-OPT, optimum electrodeposition is shown as E-OPT, while the reference conditions are shown as P-S and E-S, respectively.

According to the comparison results, it can be said that electrocoating parameters are highly affecting surface quality measurements, such as film thickness, roughness and gloss. Roughness is decreased almost 40% in optimum condition, whereas gloss increased almost 10%.

Table 4.22 Cross comparison of performance results.

Performance Result	<i>P-S E-OPT</i>	<i>P-S E-S</i>	<i>P-OPT E-S</i>	<i>P-OPT E-OPT</i>
Roughness, μ (Ra 4.8)	0.17	0.32	0.31	0.21
Film Thickness, μ	21	27	28	22
Gloss 20°	32	28	28	30
Hardness, Persöz	327	355	356	311
Impact Resistance, Inch-Pounds	80 Pass	80 Pass	80 Pass	80 Pass
Stonechip Resistance	Grade 9 Pass	Grade 9 Pass	Grade 9 Pass	Grade 9 Pass
Salt Spray Resistance	Pass	Pass	Pass	Pass
Adhesion	Grade 0 Pass	Grade 1 Pass	Grade 0 Pass	Grade 1 Pass
Water Immersion Resistance	Pass	Pass	Pass	Pass

When the reference situation is examined in detail, the electrocoat film thickness is around 27-28 microns. In this situation there is an unnecessary thickness of 7-8 microns compared to the minimum spectral value of 20 microns. According to the results obtained in Chapter 1, the increase in the thickness of the electrocoat film had a negative effect on the stone chip resistance.

As in the optimum condition, reducing the film thickness to 20 microns both positively affects the physical performance and prevents unnecessary material consumption. In this way, almost 30% reduction in the annual consumption of electrocoat material can be achieved.

In the reference condition, it is seen that the application voltage is high and the bath temperature is low compared to the optimum condition. During the electrocoating process, the temperature of the bath rises spontaneously due to the supplied voltage. For this reason, the bath must be cooled in order to keep the temperature constant at a certain value. In addition, the high voltage used directly affects the electricity consumption together with material consumption. At this point, the fact that the process causes both more material consumption and more heating of the bath by applying high voltage, followed by more energy consumption to cool the bath, has shown that there is a serious inefficiency in the process. By decreasing application voltage, both material and energy consumption is decreased, also the heating rate of the bath decreases. By increasing application bath temperature to 32 °C instead of 30 °C reduces the energy consumed for cooling the bath.

With this study, on the one hand, the opportunity to gain efficiency in operating costs has emerged, on the other hand, the quality problems seen in mass production have been minimized. While a high roughness value at the reference condition may cause an orange peel appearance in the topcoat paint application, it may lead to customer complaints. However, the low pigment level at the reference condition may cause crater problem, resulting in extra repair costs.

Phosphating parameters are mostly affecting salt spray resistance and adhesion level of the coatings. Optimum phosphating condition gives the best salt spray resistance and adhesion results even though all the conditions are classified as pass. Salt spray resistance test results are given in Figure 4.54. While the phosphating temperature

was around 52-53 degrees in the reference condition, this value was reduced to 45 degrees in optimum condition. In this way, while the long-term corrosion resistance is positively affected, on the other hand, the amount of energy required to heat the bath can be reduced, resulting in significant cost and energy efficiency.

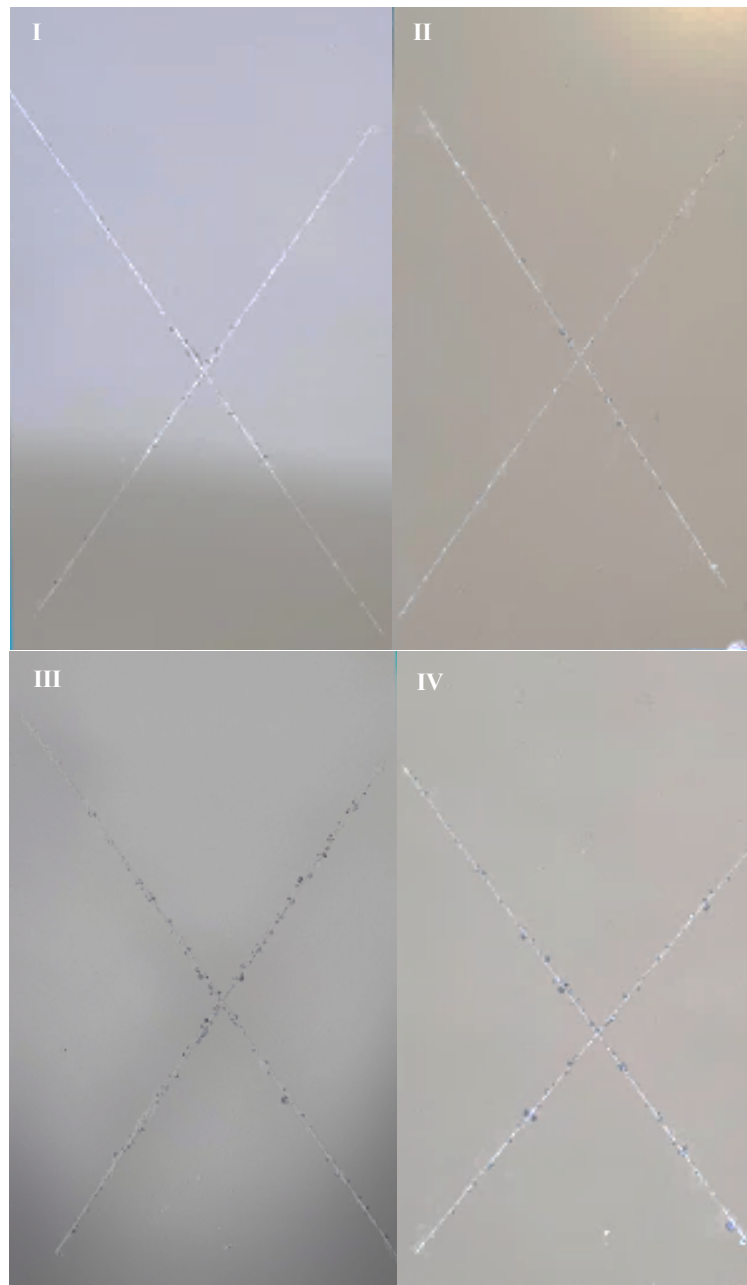


Figure 4.54 Salt spray test results. I) P-OPT and E-OPT II) P-OPT and E-S III) P-S and E-OPT IV) P-S and E-S

CHAPTER 5

CONCLUSIONS

The main conclusions drawn from all different parts of this thesis can be summarized as follows.

The increase in parameters such as voltage, application time, application temperature and solvent ratio, which directly affect the film thickness, adversely affect the surface quality and mechanical properties. Pigment and resin ratios directly affect the crater problem and gloss on the surface. Crater formation is seen on the surface at low pigment ratios, while a dullness occurs on the surface at high pigment ratios. It has been observed that parameters that directly affect the viscosity and mobility of the coating solution, such as solid matter, pigment ratio, solvent ratio and bath temperature, directly affect the thickness and mechanical strength of the coating.

In terms of thermal behavior, according to the tests, it was observed that increasing the density of the transported pigments in the electrocoat bath decreases T_g which is explained by the fact that the transported pigments create a plasticizer effect between the crosslinks, thus increase in voltage, bath temperature and pigment/binder ratio decreases T_g by increasing the amount of the transported pigments. The conditions that increase crosslinking density such as curing temperature and increased resin ratio are increased T_g as expected.

Optimum electrocoating bath conditions are obtained with 15% pigment over binder ratio, 21% solid ratio and 32 °C induction temperature, with an average film thickness of 20 microns provided by 3 min induction time with 345 V potential, that is applied in three steps, respectively.

According to the performance test results, it is observed that operating parameters of zinc phosphate conversion coatings have a significant effect on physical properties of electrocoatings such as adhesion and salt spray resistance.

Duration and temperature of conversion reaction has a meaningful statistical relationship with zinc phosphate coating weight. The increase in parameters such as application time and application temperature directly affect the coating weight. It also affects crystal morphology and dimensional distribution of zinc phosphate crystals, which result in poor mechanical properties at high temperature and time. Uniform and fine-grained crystal structure with lower coating weight gives the best physical performance after electrocoating. In this study, 180 sec at 45 °C is found as optimum condition in terms of crystal morphology, coating weight and mechanical results such as corrosion, adhesion, stone chip and water immersion resistance.

With this study, the opportunity to gain efficiency in operating costs has emerged by decreasing unnecessary material consumption by 30% and energy saving by decreasing process temperature 10 °C. Operational costs have been minimized as well as quality problems, while increasing overall performance of the product.

REFERENCES

1. Padash F, Dorff B, Liu W *et al.* Characterization of initial film formation during cathodic electrodeposition of coatings. *Prog Org Coat* 2019; 133: 395–405.
2. Merlo LE. Electrocoating. *Metal Finishing* 2010; 108: 171–175.
3. Ramamurthy AC, Buresh GA, Nagy M, Howell M. Novel instrumentation for evaluating stone impact wear of automotive paint systems. 1999.
4. Bakhtiary-Noodeh M, Moradian S, Ranjbar Z. Edge protection improvement of automotive electrocoatings in the presence of silica nanoparticles. *Surf Coat Technol* 2017; 317: 134–147.
5. Bakhtiary-Noodeh M, Moradian S, Ranjbar Z. Improvement of the edge protection of an automotive electrocoating in presence of a prepared epoxy-amine microgel. *Prog Org Coat* 2017; 103: 111–125.
6. Song G-L. A dipping E-coating for Mg alloys. *Prog Org Coat* 2011; 70: 252–258.
7. Streitberger H-J, Dössel K-F. *Automotive Paints and Coatings*. Wiley, 2008.
8. Kohli R. Methods for Monitoring and Measuring Cleanliness of Surfaces. In: *Developments in Surface Contamination and Cleaning: Detection, Characterization, and Analysis of Contaminants*. Elsevier Inc., 2012: 107–178.
9. Wolpers M, Angeli J. Activation of galvanized steel surfaces before zinc phosphating. *Ð XPS and GDOES investigations*. .
10. Donofrio J. Zinc phosphating. *Metal Finishing* 2010; 108: 40–56.

11. Acamovic NM, Drazic DM, Miskovic-stankovic VB. Influence of substrate on the formation and growth kinetics of cathodic electrocoat paint. 1995.
12. Vatistas N, Marcetic N. Coagulation-mixing and mixing-migration mechanisms of the electrocoating process. 2000.
13. Ranjbar Z, Moradian S. Characteristics and deposition behavior of epoxy-amine adducts in cathodic electrodeposition as a function of the degree of neutralization. *Colloids Surf A Physicochem Eng Asp* 2003; 219: 147–159.
14. Vatistas N. A new electrocoating technique to avoid cratering and increase voltage rupture. 1998.
15. Ranjbar Z, Moradian S. Influence of substrate on the cathodic electrodeposition behavior of waterborne epoxy resins. *Prog Org Coat* 2005; 54: 292–295.
16. Seraj S, Ranjbar Z, Jannesari A. Synthesis and characterization of an anticratering agent based on APTES for cathodic electrocoatings. *Prog Org Coat* 2014; 77: 1735–1740.
17. Reddy CM, Gaston RS, Weikart CM, Yasuda HK. Influence of surface pretreatment and electrocoating parameters on the adhesion of cathodic electrocoat to the Al alloy surfaces. 1998.
18. Reknens U, Kalnins M. Evaluation of the protective properties of organic coatings by using tape and blistering tests. 2000.
19. Ranjbar Z, Moradian S, Attar MRMZ. EIS investigation of cataphoretically electrodeposited epoxy coatings having different EEWs. *Prog Org Coat* 2004; 51: 87–90.
20. García SJ, Suay J. Optimization of deposition voltage of cataphoretic automotive primers assessed by EIS and AC/DC/AC. *Prog Org Coat* 2009; 66: 306–313.

21. Fedel M, Druart ME, Olivier M, Poelman M, Deflorian F, Rossi S. Compatibility between cathoretic electro-coating and silane surface layer for the corrosion protection of galvanized steel. *Progress in Organic Coatings*, 2010, 118–125.
22. Bučko M, Mišković-Stanković V, Rogan J, Bajat JB. The protective properties of epoxy coating electrodeposited on Zn-Mn alloy substrate. *Prog Org Coat* 2015; 79: 8–16.
23. Esfahani SL, Ranjbar Z, Rastegar S. An electrochemical and mechanical approach to the corrosion resistance of cathodic electrocoatings under combined cyclic and DC polarization conditions. *Prog Org Coat* 2014; 77: 1264–1270.
24. Esfahani SL, Ranjbar Z, Rastegar S. Comparison of corrosion protection of normal and galvanized steel coated by cathodic electrocoatings using EIS and salt spray tests. *Corrosion Engineering, Science and Technology* 2016; 51: 82–89.
25. Poelman M, Olivier MG, Gayarre N, Petitjean JP. Electrochemical study of different ageing tests for the evaluation of a cathoretic epoxy primer on aluminium. *Prog Org Coat* 2005; 54: 55–62.
26. Romano AP, Olivier MG, Vandermiers C, Poelman M. Influence of the curing temperature of a cathoretic coating on the development of filiform corrosion of aluminium. *Prog Org Coat* 2006; 57: 400–407.
27. Romano AP, Olivier MG, Nazarov A, Thierry D. Influence of crosslinking density of a cathoretic coating on initiation and propagation of filiform corrosion of AA6016. *Prog Org Coat* 2009; 66: 173–182.
28. Nazarov A, Romano AP, Fedel M, Deflorian F, Thierry D, Olivier MG. Filiform corrosion of electrocoated aluminium alloy: Role of surface pretreatment. *Corros Sci* 2012; 65: 187–198.

29. Olivier MG, Poelman M, Demuynck M, Petitjean JP. EIS evaluation of the filiform corrosion of aluminium coated by a cataphoretic paint. *Progress in Organic Coatings*, 2005, 263–270.
30. Romano AP, Olivier MG. Investigation by electrochemical impedance spectroscopy of filiform corrosion of electrocoated steel substrates. *Progress in Organic Coatings*, Elsevier B.V. 2015, 1–7.
31. Poelman M, Recloux I, Cornil N *et al.* Electrochemical study of the corrosion behaviour at the edges of electrocoated steel. *Prog Org Coat* 2012; 74: 453–460.
32. Lee YH, Kim HJ. Effect of cycloaliphatic structure of polyester on the formability and stone-chip resistance for automotive pre-coated metals. *Prog Org Coat* 2016; 99: 117–124.
33. Lonyuk M, Bosma M, Riemslog AC, Zuidema J, Bakker A, Janssen M. Stone-impact damage of automotive coatings: A laboratory single-impact tester. *Prog Org Coat* 2007; 58: 241–247.
34. Lonyuk M, Bosma M, Vijverberg CAM, Bakker A, Janssen M. Relation between chip resistance and mechanical properties of automotive coatings. *Prog Org Coat* 2008; 61: 308–315.
35. Fouladi M, Amadeh A. Effect of phosphating time and temperature on microstructure and corrosion behavior of magnesium phosphate coating. *Electrochim Acta* 2013; 106: 1–12.
36. Jiang C, Gao Z, Pan H, Cheng X. The initiation and formation of a double-layer phosphate conversion coating on steel. *Electrochem commun* 2020; 114.
37. Rani N, Singh AK, Alam S, Bandyopadhyay N, Denys MB. Optimization of phosphate coating properties on steel sheet for superior paint performance. *J Coat Technol Res* 2012; 9: 629–636.

38. Bubert H, Pulm H, Puderbach H. Investigations on Hopeite-and Phosphophyllite-Containing Phosphate Coatings on Steel. 1987.
39. Antony J. Design of Experiments and its Role Within Six Sigma. In: Design of Experiments for Engineers and Scientists. Elsevier, 2014: 201–208.
40. Jegdić B v., Bajat JB, Popić JP, Mišković-Stanković VB. Corrosion stability of polyester coatings on steel pretreated with different iron-phosphate coatings. *Prog Org Coat* 2011; 70: 127–133.
41. Oh JE, Kim YH. The corrosion resistance characteristics of Ni, Mn, and Zn phosphates in automotive body panel coatings. *Journal of Industrial and Engineering Chemistry* 2012; 18: 1082–1087.
42. Hajisafari M, Chakerizade A, Fallah M, Barati Darband G. Characterization of Zn–Mn Phosphate Coating Deposited by Cathodic Electrochemical Method. *Transactions of the Indian Institute of Metals* 2019; 72: 307–317.
43. Zhang X, Xiao G yong, Jiang C cong *et al.* Influence of process parameters on microstructure and corrosion properties of hopeite coating on stainless steel. *Corros Sci* 2015; 94: 428–437.

APPENDICES

A. Summary of Physical and Mechanical Properties of Preliminary Assessments

Table A.1 Physical and mechanical properties at different deposition voltages.

Voltage (V)	Thickness (μ)	Gloss (20°)	Roughness (μ) (Ra 4.8mm)	Pendulum Hardness (Persöz)	Impact Res. (Inch-Pounds)	Stone Chip Res. (Rating)
200	18±0.1	20±0.1	0.29±0.04	308	80	9
300	24±0.1	24±0.0	0.29±0.01	305	80	9
400	100±20	6±4.4	4.35±0.17	268	22	7

Table A.2 Physical and mechanical properties at different induction times.

Induction Time (sec)	Film Thickness (μ)	Gloss (20°)	Roughness (μ) (Ra 4.8 mm)	Pendulum Hardness (Persöz)	Impact Res. (Inch-Pounds)	Stone Chip Res. (Rating)
100	21±0.6	22±0.4	0.33±0.02	338	80	9
135	24±0.1	24±0.0	0.29±0.01	305	80	9
170	26±0.1	27±0.2	0.33±0.01	293	80	8
200	29±3.8	27±2.9	0.33±0.03	280	62	8

Table A.3 Physical and mechanical properties at different bath temperatures.

Bath Temp. (°C)	Film Thickness (μ)	Gloss (20°)	Roughness (μ) (Ra 4.8 mm)	Pendulum Hardness (Persöz)	Impact Res. (Inch-Pounds)	Stone Chip Res. (Rating)
17.5	14±0.4	13±0.6	1.06±0.37	257	60	6
25	19±0.1	23±1.7	0.36±0.13	273	80	9
30	24±0.1	24±0.0	0.29±0.01	305	80	9
35	35±1.5	27±0.2	0.37±0.04	303	48	8
40	56±1.4	15±0.9	1.33±0.67	269	30	7

Table A.4 Physical and mechanical properties at different pigment/binder ratios.

Pigment / Binder Ratio	Film Thickness (μ)	Gloss (20°)	Roughness (μ) (Ra 4.8 mm)	Pendulum Hardness (Persöz)	Impact Res. (Inch-Pounds)	Stone Chip Res. (Rating)
0.05	30±0.9	33±1.5	0.59±0.14	225	80	6
0.15	22±0.3	20±1.4	0.22±0.02	305	80	9
0.25	25±0.6	13±0.6	0.30±0.05	323	80	8

Table A.5 Physical and mechanical properties at different solid content ratios.

Solid Ratio (%)	Film Thickness (μ)	Gloss (20°)	Roughness (μ) (Ra 4.8 mm)	Pendulum Hardness (Persöz)	Impact Res. (Inch-Pounds)	Stone Chip Res. (Rating)
15	19±0.5	19±1.3	0.23±0.02	240	80	7
21	22±0.3	31±1.5	0.22±0.02	305	80	9
27	24±0.8	24±1.2	0.23±0.02	338	80	8

Table A.6 Physical and mechanical properties at different organic solvent ratios.

O. Solvent Ratio (%)	Film Thickness (μ)	Gloss (20°)	Roughness (μ) (Ra 4.8 mm)	Pendulum Hardness (Persöz)	Impact Res. (Inch-Pounds)	Stone Chip Res. (Rating)
2.47	29±0.3	31±1.5	0.21±0.02	305	80	9
4.85	37±0.9	19±1.3	0.41±0.10	350	80	4
7.11	48±1.8	12±1.5	0.47±0.13	333	34	3

Table A.7 Physical and mechanical properties at different baking temperatures.

Baking Temperature (°C)	Film Thickness (μ)	Gloss (20°)	Roughness (μ) (Ra 4.8mm)	Pendulum Hardness (Persöz)	Impact Res. (Inch-Pounds)	Stone Chip Res. (Rating)
135	23±1.4	78±4.5	0.14±0.06	189	80	4
175	22±0.3	20±1.5	0.22±0.02	305	80	9
195	22±0.4	15±0.3	0.23±0.02	265	80	10

B. Summary of Thermal Properties of Preliminary Assessments

Table A.8 Glass transition temperature and residue percentage obtained by DSC and TGA at different deposition voltages.

Specimens	T_g (°C)	Residue (%) at 900°C
200 V	73	14.4
300 V	66	23.9
400 V	68	17.0

Table A.9 Glass transition temperature and residue percentage obtained by DSC and TGA at different induction times.

Specimens	T_g (°C)	Residue (%) at 900°C
100 sec	76	27.2
135 sec	76	24.6
170 sec	76	24.5
200 sec	78	14.1

Table A.10 Glass transition temperature and residue percentage obtained by DSC and TGA at different bath temperatures.

Specimens	T_g (°C)	Residue (%) at 900°C
17.5 °C	66	25.3
25 °C	75	25.1
30 °C	76	24.6
35 °C	78	25.9
40 °C	74	27.2

Table A.11 Glass transition temperature and residue percentage obtained by DSC and TGA at different pigment/binder ratios.

Specimens	T_g (°C)	Residue (%) at 900°C
0.05	80	17.6
0.15	76	24.6
0.25	66	30.9

Table A.12 Glass transition temperature and residue percentage obtained by DSC and TGA at different solid content ratios.

Specimens	T_g ($^{\circ}\text{C}$)	Residue (%) at 900°C
15%	80	18.6
21%	76	24.6
27%	72	25.3

Table A.13 Glass transition temperature and residue percentage obtained by DSC and TGA at different organic solvent ratios.

Specimens	T_g ($^{\circ}\text{C}$)	Residue (%) at 900°C
2.47%	76	24.6
4.85%	75	24.4
7.11%	75	24.3

Table A.14 Glass transition temperature and residue percentage obtained by DSC and TGA at different baking temperatures.

Specimens	T_g ($^{\circ}\text{C}$)	Residue (%) at 900°C
135 $^{\circ}\text{C}$	65	18.9
175 $^{\circ}\text{C}$	76	19.1
195 $^{\circ}\text{C}$	107	27.4

C. Minitab™ 17 Software Outputs for DOE Studies

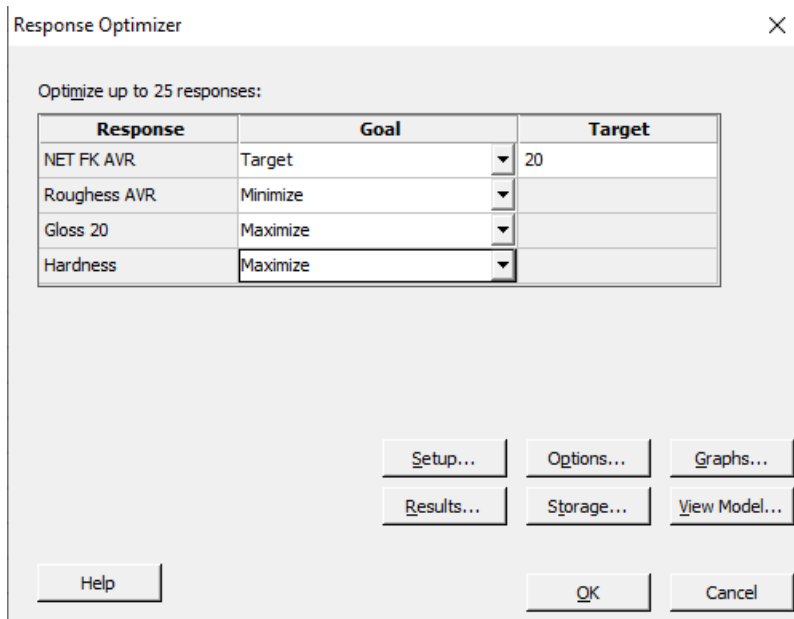


Figure A.1 Response Optimizer Interface of Minitab™ 17.

Model Summary

S	R-sq	R-sq (adj)	R-sq (pred)
0,0279861	90,25%	85,68%	78,06%

Term	Effect	Coef	SE Coef	T-Value	P-Value	VIF
Constant		0,26097	0,00404	64,60	0,000	
p/b ratio	-0,12118	-0,06059	0,00404	-15,00	0,000	1,00
voltage	-0,01893	-0,00947	0,00404	-2,34	0,025	1,00
time	-0,04068	-0,02034	0,00404	-5,04	0,000	1,00
temp	-0,03665	-0,01833	0,00404	-4,54	0,000	1,00
p/b ratio*voltage		0,00690	0,00345	0,85	0,399	1,00
p/b ratio*time		0,01810	0,00905	2,24	0,032	1,00
p/b ratio*temp		0,00712	0,00356	0,88	0,384	1,00
voltage*time		0,00451	0,00226	0,56	0,580	1,00
voltage*temp		-0,02274	-0,01137	-2,81	0,008	1,00
time*temp		-0,00599	-0,00299	-0,74	0,464	1,00
p/b ratio*voltage*time		-0,00110	-0,00055	-0,14	0,893	1,00
p/b ratio*voltage*temp		0,00432	0,00216	0,53	0,597	1,00
p/b ratio*time*temp		0,01046	0,00523	1,29	0,205	1,00
voltage*time*temp		0,01232	0,00616	1,52	0,137	1,00
p/b ratio*voltage*time*temp		0,00293	0,00147	0,36	0,719	1,00

Figure A.2 Model Summary.

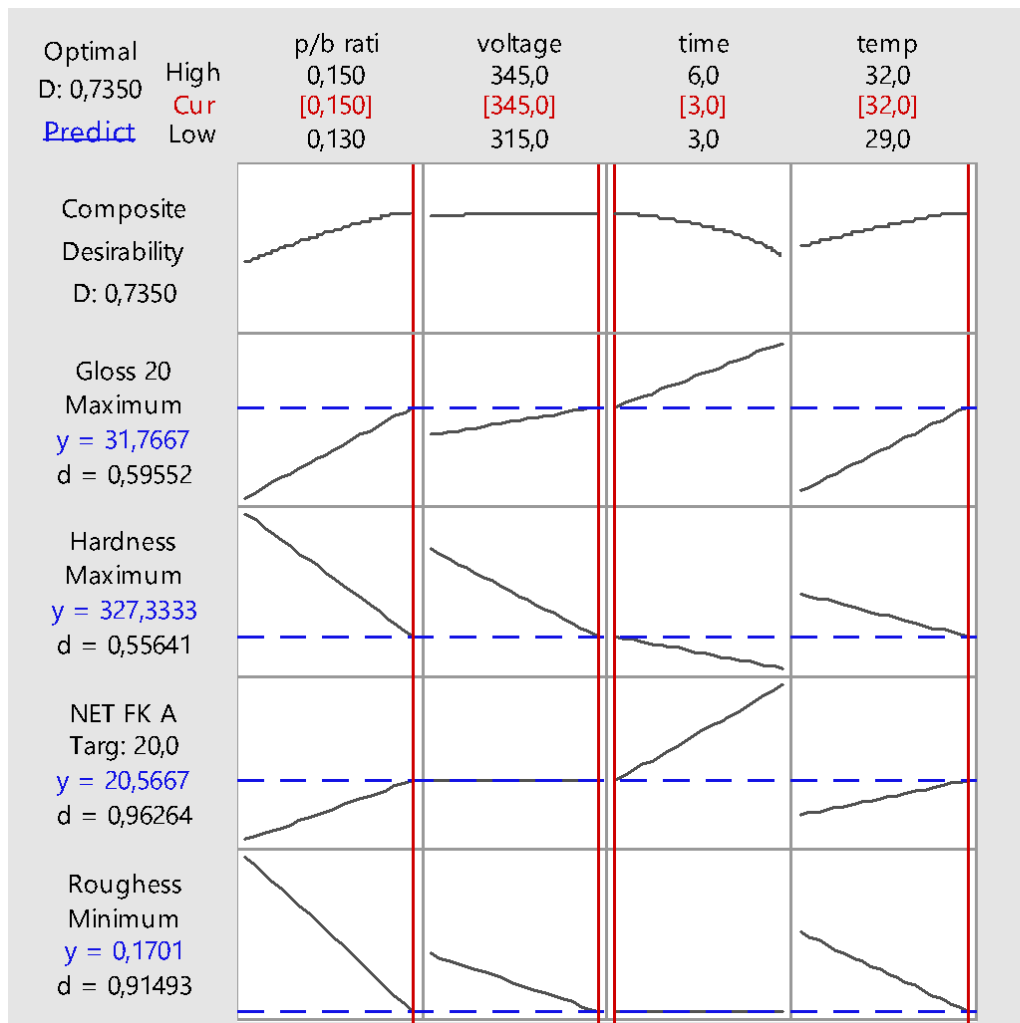


Figure A.3 Response optimizer output of Minitab™ 17 software.

Model Summary			
S	R-sq	R-sq(adj)	R-sq(pred)
0,0897527	93,05%	90,98%	87,64%

Coefficients						
Term	Coef	SE Coef	T-Value	P-Value	VIF	
Constant	3,2083	0,0150	214,48	0,000		
Temperature						
45	-0,1417	0,0212	-6,70	0,000	1,33	
55	-0,1417	0,0212	-6,70	0,000	1,33	
Time						
60	-0,0833	0,0212	-3,94	0,001	1,33	
120	-0,0250	0,0212	-1,18	0,248	1,33	
Temperature*Time						
45 60	0,1917	0,0299	6,41	0,000	1,78	
45 120	0,0583	0,0299	1,95	0,062	1,78	
55 60	0,0417	0,0299	1,39	0,175	1,78	
55 120	0,0583	0,0299	1,95	0,062	1,78	

Regression Equation

$$\text{Coating Weight} = 3,2083 - 0,1417 \text{ Temperature}_{45} - 0,1417 \text{ Temperature}_{55} + 0,2833 \text{ Temperature}_{65} - 0,0833 \text{ Time}_{60} - 0,0250 \text{ Time}_{120} + 0,1083 \text{ Time}_{180} + 0,1917 \text{ Temperature}^* \text{Time}_{45 60} + 0,0583 \text{ Temperature}^* \text{Time}_{45 120} - 0,2500 \text{ Temperature}^* \text{Time}_{45 180} + 0,0417 \text{ Temperature}^* \text{Time}_{55 60} + 0,0583 \text{ Temperature}^* \text{Time}_{55 120} - 0,1000 \text{ Temperature}^* \text{Time}_{55 180} - 0,2333 \text{ Temperature}^* \text{Time}_{65 60} - 0,1167 \text{ Temperature}^* \text{Time}_{65 120} + 0,3500 \text{ Temperature}^* \text{Time}_{65 180}$$

Figure A.4 Model summary and regression equation of coating weight versus temperature and time.

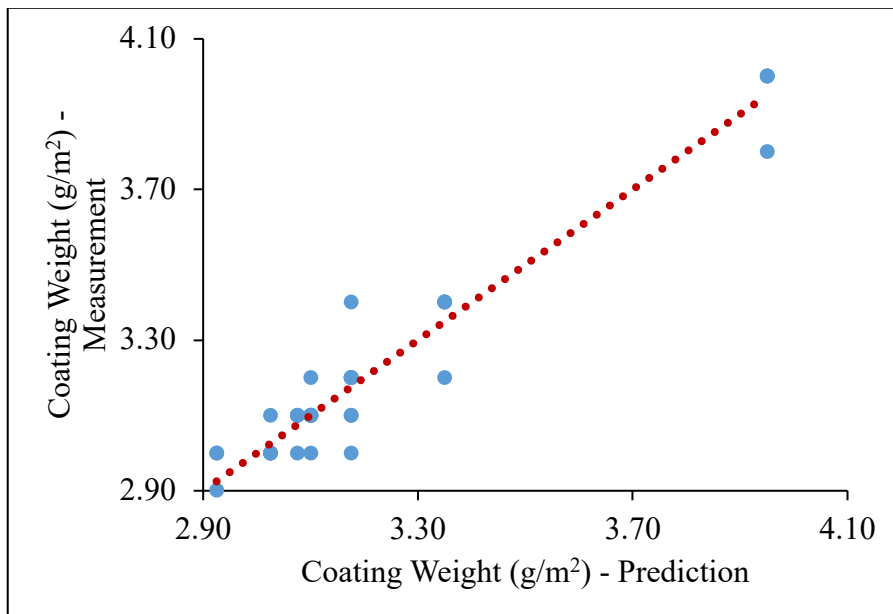


Figure A.5 Measurement vs Minitab Prediction for Coating Weight.

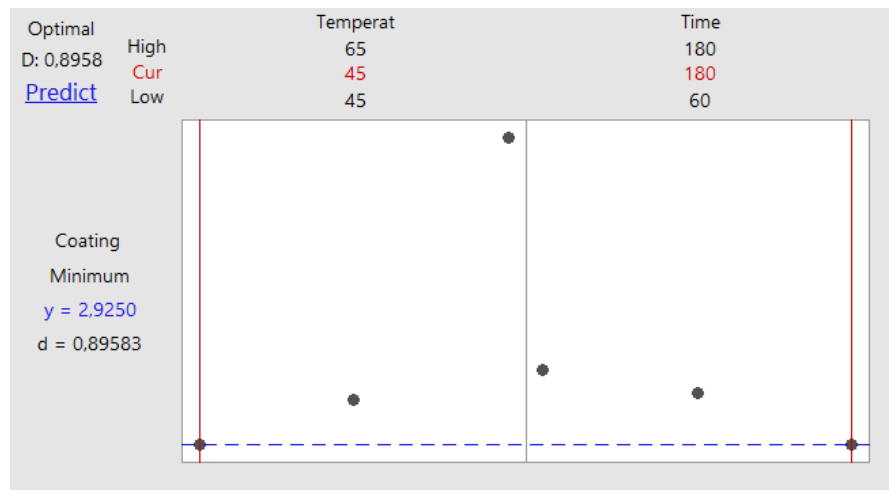


Figure A.6 Response Optimizer Output for Coating Weight versus Temperature and Time.

D. Ford Laboratory Material Specifications and Test Methods

3.5	RESISTANCE PROPERTIES	
3.5.1	Adhesion, max (FLTM BI 106-01, Procedure B)	Coating System I - Grade 0 Coating System II & III - Grade 1
3.5.2	Stone Chip Resistance, max (FLTM BI 157-06)	Coating System I - Grade 9 Coating System II - Grade 7 Coating System III - Grade 5
3.5.3	Water Immersion (FLTM BI 104-01)	240 h
	No blistering, loss of gloss or loss adhesion accepted.	
3.5.4	Salt Spray (FLTM BI 103-01; Coating System I and III; not for Precoated Steel)	960 h
	Perform test on iron and steel substrates only. Scribe panels after painting with two diagonal lines from corner to corner diagonally. Scribe to the bare metal.	
	Failure is blisters, rust or loss of adhesion exceeding 3 mm from scribe line.	

Figure A.7 Ford Motor Company material specification and test methods for electrocoat material.

CURRICULUM VITAE

Surname, Name : Baydağ (Kaykaç), Nalan Gülçin
Date of Birth : Oct 4, 1987
E-mail : nalan.kaykac@metu.edu.tr; nkaykac@ford.com.tr
Phone : 0262 3156513

EDUCATION

Degree	Institution	Graduation
PhD	Middle East Technical University	2022
MS	Gazi University Advanced Technologies	2012
BS	Gazi University Chemical Engineering	2009
High School	Kurtuluş High School, Ankara	2005

FOREIGN LANGUAGES

Advanced English, Fluent German

WORK EXPERIENCE

2022 April – Present	Ford Otosan Otomotiv San.	Paint Process Lead
2017 Mar – 2022 Apr	Ford Otosan Otomotiv San.	Paint Lab. Lead
2013 Nov – 2017 Feb	Taç Boya San. Tic. Ltd. Şti.	R&D Lab. Lead
2011 Oct – 2013 Nov	Taç Boya San. Tic. Ltd. Şti.	QC Lab. Lead
2009 Jul – 2011 Oct	Taç Boya San. Tic. Ltd. Şti.	QC Lab. Engineer

HOBBIES

Spinning, Yoga, Pilates, Ice-Skating, Playing Guitar, Travelling

PUBLICATIONS

1. "Varisli D., Kaykac, N.G., "CO_x free Hydrogen Production over Cobalt Incorporated Silicate Structured Mesoporous Catalysts", Applied Catalysis B: Environmental, 127 (2012) 389– 398, (SCI)."
2. "Varisli D., Kaykac, N.G., "Hydrogen from ammonia over cobalt incorporated silicate structured catalysts prepared using different cobalt salts", International journal of hydrogen energy 41 (2016) 5955-5968

PROCEEDINGS OF INTERNATIONAL CONFERENCES

3. Dilek Varışlı, Nalan Gülçin Kaykaç, 2011. Co-silicate based nanocomposite materials for production of CO_x free hydrogen from ammonia, 8th ECCE, 2011 8th European Congress of Chemical Engineering together with ProcessNet-Annual Meeting, 25-29 September 2011, Berlin-Germany.
4. Dilek Varisli, Nalan Gulcin Kaykac, 2011. The Effects of the Promoter in Cobalt Based mesoporous Silicate Catalysts for Ammonia Decomposition, 12th Mediterranean Congress of Chemical Engineering Barcelona, Spain.
5. Dilek Varışlı, Nalan Gülçin Kaykaç, Co-silicate based nanocomposite materials for production of CO_x free hydrogen from ammonia, NCC4, 2012 4th National Catalyst Congress, 21-24 March 2012, Kocaeli Üniversitesi, Kocaeli, Türkiye.
6. Dilek Varışlı, Nalan Gülçin Kaykaç, Amonyaktan Hidrojen Üretimi için Kobalt Esaslı Silikat Malzemeler, UKMK10, 10. Ulusal Kimya Mühendisliği Kongresi, 4-6 Eylül 2012, Koç Üniversitesi, İstanbul, Türkiye.
7. Dilek Varışlı, Nalan Gülçin Kaykaç, Effects of Precursors on the Performans of Cobalt Based Silicate Catalysts to Produce Hydrogen for Fuel Cell Application, ECCE 9, 9th European Congress of Chemical Engineering, 21 - 25 April 2013, World Forum, The Hague, Netherlands